

Republic of Iraq
Ministry of Higher Education
and Scientific Research
Al-Nahrain University
College of Sciences
Department of Chemistry



Theoretical Spectroscopic Study for a Series of 1,3,4-Oxadiazole Derivatives

A Thesis

Submitted to the College of Sciences / Al-Nahrain University as a Partial Fulfillment of the requirements for the Degree of Master of Science in Chemistry

By

Hassan Fa'ez Hayder

B.Sc. Chemistry / College Science / Baghdad University
(2013)

May 2017

Ramadan 1438

Republic of Iraq
Ministry of Higher Education
and Scientific Research
Al-Nahrain University
College of Sciences
Department of Chemistry



Theoretical Spectroscopic Study for a Series of 1,3,4-Oxadiazole Derivatives

A Thesis

Submitted to the College of Sciences / Al-Nahrain University as a Partial Fulfillment of the requirements for the Degree of Master of Science in Chemistry

By

Hassan Fa'ez Hayder

B.Sc. Chemistry / College Science / Baghdad University
(2013)

Supervised by

Dr. Shatha Fadil AL-Saidi

(Asst. Prof.)

May 2017

Ramadan 1438

بِسْمِ اللَّهِ الرَّحْمَنِ الرَّحِيمِ

وَيَسْأَلُونَكَ عَنِ الرُّوحِ قُلِ الرُّوحُ مِنْ أَمْرِ رَبِّي وَمَا أُوتِيتُمْ مِنَ

الْعِلْمِ إِلَّا قَلِيلًا ﴿٨٥﴾

صَدَقَ اللَّهُ الْعَلِيِّ الْعَظِيمِ

سورة الإسراء

﴿الآية 85﴾

Supervisor Certification

I, certify that this thesis entitled "**Theoretical Spectroscopic Study for a Series of 1,3,4-Oxadiazole Derivatives**" was prepared by "**Hassan Fa'ez Hayder**" under my supervision at the College of Science / Al-Nahrain University as a partial fulfillment of the requirements for the Degree of Master of Science in Chemistry (Physical Chemistry).

Signature:

Name: **Dr. Shatha Fadil AL-Saidi**

Scientific degree: Assistant Professor

Date: / /

In view of the available recommendations, I forward this thesis for debate by Examining Committee.

Signature:

Name: **Dr. Emad Al-Sarraj**

Scientific Degree: Professor

Title: Head of the Department of Chemistry

Date: / /

Committee Certification

We, the examining committee, certify that we have read this thesis entitled "**Theoretical Spectroscopic Study for a Series of 1,3,4-Oxadiazole Derivatives**" and examined the student "**Hassan Fa'ez Hayder**" in its contents and that in our opinion, it is accepted for the Degree of Master of Science, in Physical Chemistry, with (**excellence**) standing.

Signature:

Name: **Dr. Khulood Abid Saleh AL-Saade**

Scientific Degree: professor

Date: / /

(Chairman)

Signature:

Name: **Dr. Hasan R. Obayes**

Scientific Degree: Assistant Professor

Date: / /

(Member)

Signature:

Name: **Dr. Taghried Ali Salman**

Scientific Degree: Assistant Professor

Date: / /

(Member)

Signature:

Name: **Dr. Shatha Fadil AL-Saidi**

Scientific Degree: Assistant Professor

Date: / /

(Member/ **Supervised**)

I, hereby certify upon the decision of the examining committee.

Signature:

Name: **Dr. Hadi M. A. Abood**

Scientific Degree: Professor

Title: Dean of College of Science

Date: / /

Dedication

To My Parents

Thank you for the times you shared with me the suffering and gave me assistance and confidence all times, I'm really grateful that you have been my inspiration.

To my major professor

Thank you for the countless hours of revisions and advice on my thesis and for all the wonderful lessons that he has taught me during the last 2 years of my education.

Acknowledgements

*I wish to express my great thanks to **ALLAH** for uncountable gifts and for helping me to present this thesis. It is a pleasure to express my sincere thanks and appreciation to my supervisor Instructor **Dr. Shatha Fadil AL-Saidi** for suggesting the subject of this thesis and supervision of my work.*

*The study and analysis of the organic compounds would have been much more difficult without the help of **Abeer Shams and Yasser H. Sabah** my great thank to them.*

Thanks to the staff of the Chemistry Department, College of science, AL-Nahrain University.

Also, I am very grateful to all the people who helped me during my work.

Hassan

Summary

In recent years the computational chemistry becomes of great importance in many chemical and pharmaceutical scientific fields. Since many of the oxadiazole derivatives have a wide range in biological, and pharmacological activities. Therefore this work involves a theoretical study for two series of oxadiazole derivatives. Series one contains oxadiazole molecules which are substitute by electron donating or electron with drawing groups [1,3,4-oxadiazole (**OD**), 1,3,4-oxadiazole-2-amine (**ODA**), 1,3,4-oxadiazole-2,5-diamine (**ODDA**), 5-chloro-1,3,4-oxadiazole-2-amine (**CODA**), 2-amino-1,3,4-oxadiazole-5-carbonitrile (**AODCN**), 5-nitro-1,3,4-oxadiazole-2-amine(**NODA**)]. Series two consist the following oxadiazole derivatives which obtain by substituting electron donating or electron with drawing as well as phenyl groups [2-phenyl-1,3,4-oxadiazoles (**POD**), 5-phenyl-1,3,4-oxadiazole-2-thiol (**PODT**), 5-phenyl-1,3,4-oxadiazole-2-amine (**PODA**), 5-(4-chlorophenyl)-1,3,4-oxadiazole-2-amine (**CPODA**), 2,5-diphenyl-1,3,4-oxadiazole (**DPOD**)] molecules.

The theoretical study is done by employing the density functional theory **DFT** with **B3LYP** / high basis set 6-311++G(2d,2p), using Gaussian program 09. In few cases, Avogadro program is used to assist and view the electronic orbitals or molecular electrostatic potentials.

For the above mentioned two series molecules, the calculations are done to evaluate several physical properties such as:- equilibrium optimize geometry, vibrational spectra, electronic properties (electronic absorption spectra, energy of molecular orbital, molecular electrostatic potential [in gas phase and in water solution]), and nuclear magnetic resonance spectra [in gas phase and in Dimethyl sulfoxide solution]. Then a comparison is done between their different states.

Since experimental and theoretical data of the optimized geometry for only **OD**, **POD**, **PODT**, and **PODA** molecules are available, the comparison of this work results reveals a good agreement with them. In **ODDA** molecule the C₂-N₆ bond (between C₂ atom in oxadiazole ring and -NH₂ group) is (1.372 Å). In the other molecules, the C₂-N₆ bond changing in the following sequence **PODA** > **ODA** = **CPODA** > **CODA** > **AODCN** > **NODA**. This may be due to the replacement of the electron withdrawing group or phenyl ring instead of electron donating group in C₅ position.

The vibrational spectra (frequencies, IR, and Raman intensities) with its reliable assignment for each 3N-6 fundamental vibrational of all studied molecules are acquired. The calculated results of **OD**, **POD**, and **PODT** molecules are in a good coincidence with the former experimental and theoretical data.

In series one, the electronic properties (electronic absorption spectra, frontier molecular orbital analysis, molecular electrostatic potential [in gas phase and in water solution]) are computed. The calculated λ max values in gas phase are changed as the following order for **OD** < **ODA** < **CODA** < **ODDA** < **AODCN** < **NODA** (179, 207, 211, 213, 248, and 306 nm respectively). The greater λ max value for **NODA** molecule is attributed to the extra conjugation.

The calculated electronic spectra for series two compounds have two absorption electronic peaks in each phase (water, and gas) except **DPOD** molecule which has only one peak. The λ max (nm) of the strongest peak in gas phase, is changed in the following configuration: **DPOD** (303) > **CPODA** (288) > **PODA** (280) > **PODT** (278) > **POD** (254) nm. In water solvent, λ max of strongest peak changed in the same order: **DPOD** (307) > **CPODA** (295) > **PODA** (285) > **PODT** (283) > **POD** (259). According to these results it can be concluded that the red, and *hyperchromism* shifts occur during the changing from gas phase to the polar solvent (water). This confirmed that the transition is $\pi \rightarrow \pi^*$. The higher value of λ max in **DPOD** spectra may be due to the high conjugation between oxadiazole and

the two phenyl rings, which causes a decreasing the energy gap ΔE_g . The calculated ΔE_g values in two phases for molecules of series two changed according the following manner: **POD > PODT > PODA > CPODA > DPOD**.

The molecular electrostatic potential maps for the oxadiazole derivatives in series one show a negative potential over the electronegative atoms (nitrogen ring atoms), and positive potential over the carbon and hydrogen atoms. From these results, it can be concluded that the carbon atoms indicate the strongest attraction and the nitrogen ring atoms associated with the strongest repulsion. Changing the H atom by NH_2 groups in compounds **ODA**, and **ODDA** show a blue color on NH_2 , this mean that NH_2 have positive potential. When substituted electron with drawing groups such as Cl, NO_2 , and CN the color on the nitrogen ring atoms approach to yellow, this represent moderate negative potential. The molecular electrostatic potential surfaces of series two molecules show a negative potential swings between oxygen and nitrogen atoms, and phenyl ring, which accessing for negative charge (red region). The negative regions of MEP are related to electrophilic reactivity. The carbon oxadiazole atoms and hydrogen atoms bear a positive charge (blue color) which indicate nucleophilic reactivity.

List of Abbreviations and Symbols

<i>Meaning</i>	<i>Abbreviations</i>
A spin angular momentum	$\hbar/2$
A symmetric stretching	ν_{as}
Atomic mass unit	amu
Atomic Orbitals	AOs
Away for hybrid Hartree–Fock/density functional theory introduced by (Becke-Lee-Yang-Parr) or Adiabatic connection method using B exchange and LYP correction functions.	B3LYP
Change in Total Energy	$\Delta E_{tot.}$
Chemical shift	δ
Dimethyl sulfoxide	DMSO
Electron correlation energy	E_{corr}
Electron–Conducting Hole–Blocking	ECHB
Energies in Electron Volts	E(eV)
Energy of the highest occupied molecular orbital	E_{HOMO}
Energy of the lowest unoccupied molecular orbital	E_{LUMO}
Exchange–Correlation potential	V_{xc}
Field strength	\vec{B}_0
Gauge-including atomic orbitals	GIAO
Gaussian Type Orbitals	GTOs
gerade	g
Hartree-Fock	HF
Hessian matrix	H_{ij}
highest occupied molecular orbital	HOMO (H)
Hückel molecular orbital	HMO
Individual gauge for localized orbitals	IGLO
Infrared Radiation Spectra	IR Spectra
In-plane bending	β
kilometer	km
Linear combinations atomic orbitals	LCAOs
lowest unoccupied molecular orbital	LUMO (L)
Magnetic moment for one proton	μ_p
Magnetic moment vector	$\vec{\mu}$
Maximum Absorption wavelengths	λ_{max}

Molecular Electrostatic Potential	MEP
Molecular mechanics	MM
Moller-Plesset perturbation theory second order	MP2
Nanometer	<i>nm</i>
Nuclear magnetic resonance	NMR
Nuclear magneton	μ_N
Nucleus-independent chemical shift	NICS
Organic Light Emitting Diode	OLED
Oscillator strengths	<i>f</i>
Out-of-plane bending	γ
Parts per million	<i>ppm</i>
Quantum mechanics	QM
Ring deformation	Ring def.
Ring puckering	Ring puck.
Rocking	ρ
Scissoring	δ
Self-consistent-field	SCF
Semi-Empirical	SE
Singlet	S
Slater Type Orbitals	STOs
Symmetric stretching	ν_s
Tetramethylsilane	TMS
The energy gap between $E_{LUMO} - E_{HOMO}$	ΔE_g
Time Dependent Density Functional Theory	TD-DFT
Torsion	t
Total energy	$E_{tot.}$
transmittance	T
Triplet	T
Twisting	τ
Ultraviolet Spectra	UV Spectra
ungerade	u
Wagging	ω

The Conversion Coefficient:

1 Hartree (a.u.) = 27.2114 eV

List of Contents

No.	Subjects	Page No.
Chapter One-Introduction		
1.1	General Introduction for oxadiazoles	1
1.1.1	The chemistry of oxadiazole ring	2
1.1.2	Preparation of 1,3,4-oxadiazole ring	2
1.1.3	Reactivity of 1, 3, 4-oxadiazole	3
1.1.4	Applications of 1,3,4-oxadiazole	3
1.2	Molecular spectroscopy	4
1.2.1	Basic Principles of Vibrational Spectroscopy	6
1.2.1.1	Molecular Vibrations	6
1.2.1.2	Selection rules	10
1.2.2	Nuclear magnetic resonance	11
1.2.2.1	Chemical Shift	14
1.2.3	Basic concepts of electronic spectroscopy	15
1.2.3.1	Electronic spectroscopy	15
1.2.3.2	Nature of Electronic Transitions	17
1.2.3.3	Franck–Condon principle	18
1.2.3.4	The intensities of spectral lines	21
1.2.3.5	Selection rules	22
1.2.3.6	Solvent effects	23
1.3	Literature Review	24
1.4	The Aim of the Work	26
Chapter Two-Theoretical Method		
2.1	Computational Chemistry	28
2.2	Quantum mechanics (QM)	28
2.2.1	Molecular Mechanics (MM)	29
2.2.2	Semi-empirical Methods (SE)	30
2.2.3	Ab initio Methods	30
2.2.4	Density functional theory (DFT)	31
2.3	Basis function	32
2.3.1	Slater and Gaussian Type Orbital's	33
2.3.2	Types of basis set	34
2.4	Geometry Optimization	36
2.5	Time-Dependent Density Functional Theory (TD-DFT)	37
2.6	Nuclear Magnetic Resonance (NMR)	39
2.7	Molecular Electrostatic Potential (MEP)	40
Chapter Three-Result and Discussion		

No.	Subjects	Page No.
3.1	Results and Discussion of series one	42
3.1.1	Molecular geometry	42
3.1.2	Vibrational Spectra	46
3.1.3	Electronic properties	52
3.1.3.1	Electronic absorption spectra	52
3.1.3.2	Molecular electrostatic potential (MEP)	63
3.1.4	NMR Spectroscopy	65
3.2	Results and Discussion of series two	71
3.2.1	Molecular geometry	71
3.2.2	The vibrational spectra	77
3.2.3	Electronic properties	86
3.2.3.1	UV–visible spectral analysis	86
3.2.3.2	Molecular electrostatic potential	95
3.2.4	NMR Spectroscopy	96
Chapter Four-Conclusion and Suggestions for Further Research		
4.1	Conclusions	101
4.2	Further work	103
	References	104

List of Figures

Figure No.	Figure Title	Page No.
Chapter One		
1.1	The four isomers of oxadiazole.	1
1.2	The electromagnetic radiation spectrum.	6
1.3	The design of ball and spring for a diatomic molecule.	7
1.4	The infrared electromagnetic spectrum.	8
1.5	The type of molecular vibration.	9
1.6	The energy level diagram of Rayleigh and Raman scattering.	11
1.7	The UV and visible region of the electromagnetic spectrum.	16
1.8	The visible spectrum from higher to lower frequencies.	16
1.9	The energies for the most common orbitals involved in electronic spectroscopy of organic groups.	17
1.10	Represents the vertical electronic transition between the two potential-energy curves for the ground and excited state of a diatomic molecule.	19

1.11	The area under the curve is equal to the integrated absorption coefficient for transition of the molar absorption coefficient versus the wavenumber of the incident radiation.	22
1.12	The coupling of orbital (L) and spin (S) angular momenta in a linear molecule.	23
Chapter Two		
2.1	A) 1s-STO modelled by a linear combination of three GTOs (STO-3G). B) Approximating a STO with several GTOs.	34
Chapter Three		
3.1	The calculated molecular structure for the studied compound along with the atom numbering scheme.	42
3.2	UV-visible spectra of OD molecule in gas phase and water.	54
3.3	Theoretical UV VIS spectra of ODA molecule in gas phase and water.	55
3.4	Theoretical electronic spectra for ODDA molecule in gas phase and water.	56
3.5	UV-visible spectra of CODA molecule in gas phase and water.	57
3.6	Theoretical UV–Vis spectra of AODCN molecule in gas phase and water.	58
3.7	Theoretical electronic spectra for NODA molecule in gas phase and water.	59
3.8	The energy with molecular orbital geometry for the OD , ODA , ODDA , CODA , AODCN , and NODA compounds, in gas phase.	61
3.9	The energy with molecular orbital geometry for the OD , ODA , ODDA , CODA , AODCN , and NODA compounds, in solvent water.	62
3.10	The Molecular Electrostatic Potentials.	64
3.11	NMR spectra of OD molecule in gas phase and DMSO solvent.	65
3.12	NMR spectra of ODA molecule in gas phase and DMSO solvent.	66
3.13	NMR spectra of CODA molecule in gas phase and DMSO solvent.	67
3.14	NMR spectra of ODDA molecule in gas phase and DMSO solvent.	68

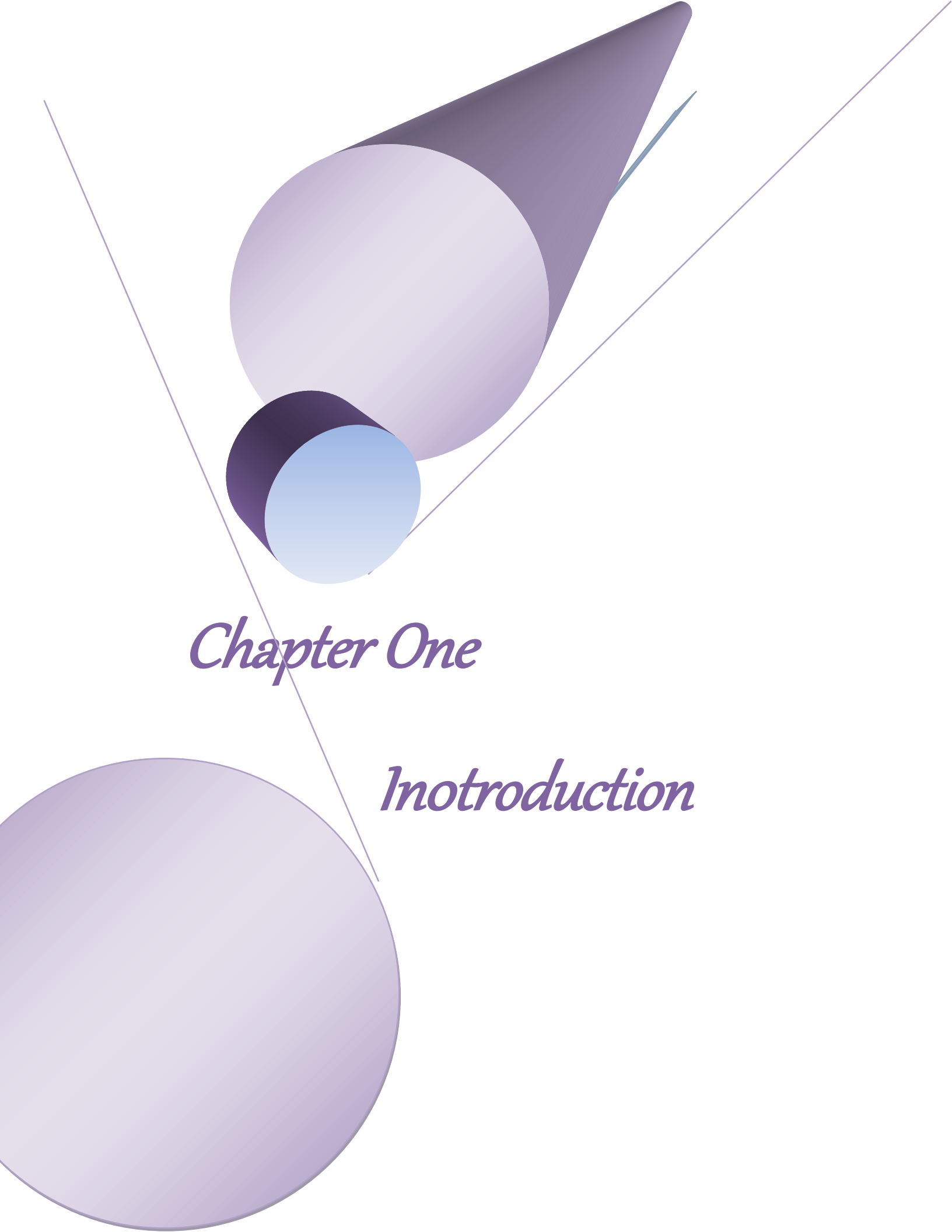
3.15	NMR spectra of AODCN molecule in gas phase and DMSO solvent.	69
3.16	NMR spectra of NODA molecule in gas phase and DMSO solvent.	70
3.17	Optimized structures for the studied compounds (belong to series two) along with its atom numbering scheme. [A= phenyl ring, B= 1, 3, 4-oxadiazole ring].	71
3.18	UV-visible spectra of POD molecule in gas phase and water phase.	87
3.19	Theoretical UV–VIS spectra of PODT molecule in gas phase and water solution.	89
3.20	The theoretical UV absorption spectra of PODA molecule in gas phase and water phase.	90
3.21	UV-visible spectra of CPODA molecule in gas phase and water solvent.	91
3.22	Theoretical UV–VIS spectra of DPOD molecule in gas phase and water Solution.	92
3.23	The energy with molecular orbital geometry for the POD, PODT, PODA, CPODA, and DPOD molecules in gas phase.	93
3.24	The energy with molecular orbital geometry for the POD, PODT, PODA, CPODA, and DPOD molecules in water.	94
3.25	The Molecular Electrostatic Potentials (MEP).	96
3.26	NMR spectra of POD molecule in gas phase and DMSO solvent.	97
3.27	NMR spectra of DPOD molecule in gas phase and DMSO solvent.	98
3.28	NMR spectra of PODA molecule in gas phase and DMSO solvent	99
3.29	NMR spectra of CPODA molecule in gas phase and DMSO solvent.	100
3.30	NMR spectra of PODT molecule in gas phase and DMSO solvent.	100

List of Tables

Table No.	Table Title	Page No.
Chapter One		
1.1	Magnetogyric Ratios, NMR Frequencies (in a 4.7-T	14

	Field), and Natural Abundances of Isotopes.	
Chapter Three		
3.1	The optimized geometry data of OD , ODA , ODDA , CODA , AODCN , and NODA molecules, plus the available theoretical and experimental data.	44
3.2	Theoretical vibrational frequencies and the assignment of the OD molecule compared with other experimental and theoretical data.	46
3.3	Theoretical vibrational frequencies (cm^{-1}), IR intensity, Raman activities and the assignment of the ODA .	47
3.4	The theoretical vibrational frequencies (cm^{-1}), with its assignment for the ODDA molecule.	48
3.5	The theoretical vibrational frequencies, IR intensities and Raman activity with its assignment for the 21 normal modes of the CODA molecule.	49
3.6	Theoretical vibrational frequencies (cm^{-1}), IR intensity, Raman activities and the assignment of the AODCN .	49
3.7	The theoretical vibrational frequencies (cm^{-1}), with its assignment for the NODA molecule.	50
3.8	The absorption wavelength, energies, and oscillator strengths of the OD molecule.	53
3.9	The absorption wavelength, energies, and oscillator strengths of the ODA molecule.	54
3.10	The absorption wavelength, energies, and oscillator strengths of the ODDA molecule.	55
3.11	The absorption wavelength, energies, and oscillator strengths of the CODA molecule.	57
3.12	The absorption wavelength, energies, and oscillator strengths of the AODCN molecule.	58
3.13	The absorption wavelength, energies, and oscillator strengths of the NODA molecule.	59
3.14	The calculated NMR chemical shifts in ppm for OD molecule in (gas phase, and DMSO solvent).	65
3.15	The calculated NMR chemical shifts in ppm for ODA molecule in (gas phase, and DMSO solvent).	66
3.16	The calculated NMR chemical shifts in ppm for CODA molecule in (gas phase, and DMSO solvent).	67
3.17	The calculated NMR chemical shifts in ppm for ODDA molecule in (gas phase, and DMSO solvent).	68
3.18	The calculated NMR chemical shifts in ppm for AODCN molecule in (gas phase, and DMSO solvent).	69

3.19	The calculated NMR chemical shifts in ppm for NODA molecule in (gas phase, and DMSO solvent).	70
3.20	The optimized geometry data of PODT , PODA , CPODA , DPOD , and POD molecules, plus the available theoretical and experimental data.	73
3.21	Theoretical vibrational frequencies and the assignment of the POD molecule compared with other experimental and theoretical data.	77
3.22	Calculated theoretical wavenumbers (cm^{-1}) and assignment of the PODT molecule compare with other experimental and theoretical data.	79
3.23	Theoretical vibrational frequencies (cm^{-1}), IR intensity, Raman activities and the assignment of the PODA molecule.	80
3.24	The theoretical vibrational frequencies (cm^{-1}), with its assignment for the CPODA molecule.	82
3.25	The theoretical vibrational frequencies, IR intensities and Raman activity with assignment for the 75 normal modes of the DPOD molecule.	83
3.26	The absorption wavelength, energies, and oscillator strengths of the POD molecule.	87
3.27	Calculated absorption wavelengths, energies and oscillator strengths of PODT molecule.	88
3.28	The absorption wavelength, energies, and oscillator strengths of the PODA molecule.	89
3.29	Calculated absorption wavelengths, energies and oscillator strengths of CPODA molecule.	90
3.30	The absorption wavelength, energies, and oscillator strengths of the DPOD molecule.	91
3.31	The calculated NMR chemical shifts in ppm of all atoms for POD molecule in (gas phase, and DMSO solvent).	97
3.32	The calculated NMR chemical shifts in ppm for DPOD molecule in (gas phase, and DMSO solvent).	98
3.33	The calculated NMR chemical shifts in ppm for PODA molecule in (gas phase, and DMSO solvent).	99
3.34	The calculated NMR chemical shifts in ppm for CPODA molecule in (gas phase, and DMSO solvent).	100
3.35	The calculated NMR chemical shifts in ppm for PODT molecule in (gas phase, and DMSO solvent).	100



Chapter One

Inotroduction

1.1- General Introduction for oxadiazoles

Heterocycles are important class of compounds. The nature of heterocycles provided a number of biologically important compounds such as carbohydrates, proteins, amino acids, steroids, polymers, etc. These compounds contain one or more heterocyclic rings or chains.

Oxadiazole is a heterocyclic compound containing one oxygen and two nitrogen atoms in the five membered ring. Oxadiazole is available in four isomeric forms, depending upon the position of N- atoms in the heterocyclic ring: (1) 1,2,3-oxadiazole (Diazo-oxides), (2) 1,2,4-oxadiazole (Azoxime), (3) 1,2,5-oxadiazole (Furazan), and (4) 1,3,4-oxadiazole (Biazole) [1], figure 1.1.

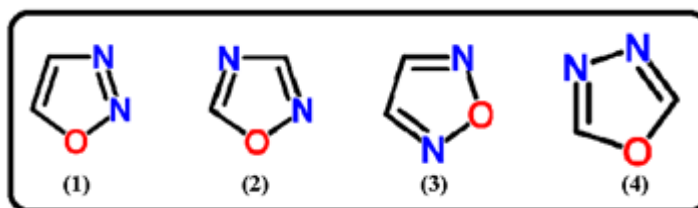


Figure 1.1.The four isomers of oxadiazole [1].

The 1,2,3- oxadiazole isomer is unstable, and it return back to the diazoketone tautomer [2].

However, 1,3,4-oxadiazole and 1,2,4-oxadiazole are known, in a wider scale by researchers related to their important chemical and biological properties. 1,3,4-oxadiazole is attracted the medicinal chemist in developing a new therapeutic compound. Literatures revealed that a minor modification in structure of 1,3,4-oxadiazole can lead to produce a different new derivatives which improved its activity, and with lesser toxicity [3,4].

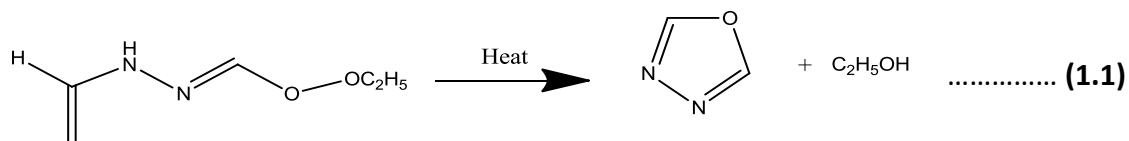
1.1.1- The chemistry of oxadiazole ring

Oxadiazole is a heterocyclic aromatic chemical compounds having molecular formula of $C_2H_2N_2O$. 1,3,4-oxadiazole is a liquid boiled at 150°C . It is a very weak base related to the inductive effect of the additional heteroatom. The replacement of two ($-\text{CH}=\text{)$ groups in furan by two pyridine type nitrogen ($-\text{N}=\text{)$ reduces the aromaticity of the resulting oxadiazole ring to a point that the oxadiazole ring show character of conjugated diene.

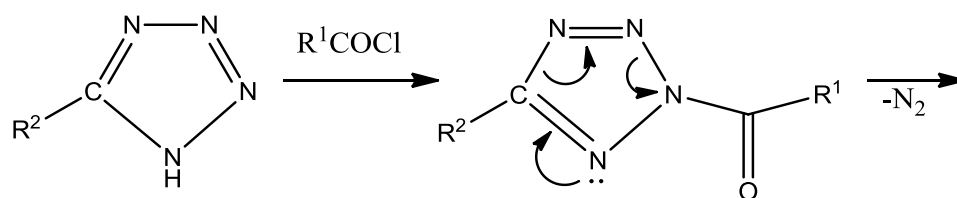
Oxadiazoles subjected to number of reactions like nucleophilic substitution, electrophilic substitution, photochemical, and thermal [5].

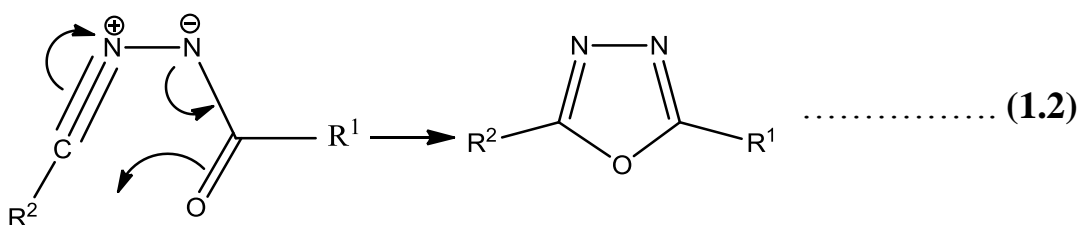
1.1.2- Preparation of 1, 3, 4-oxadiazole ring

In 1965 Ainsworth firstly prepared 1,3,4-oxadiazole by the thermolysis from ethyl formate formly hydrazine at atmospheric pressure, equation(1.1) [2].



Using Huisgen reaction, 2-Acyltetrazoles in solution when subjected to dediazonation at room temperature the acyl nitrilimines cyclize immediately produce derivative of 1,3,4-oxadiazoles, equation (1.2) [6]:





1.1.3- Reactivity of 1, 3, 4-oxadiazole

As 1,3,4-oxadiazole have a relatively low density of electrons at carbon atoms and a high electron density at nitrogen atoms. So alternatively the electrophilic in oxadiazole ring are extremely difficult at carbon atom because of the relatively low electron density. This can be referred to electron withdrawal effect of the pyridine sort (nitrogen atom). However the attack of electrophiles occurs at nitrogen, when the oxadiazole ring is replaced with electron-releasing groups. Therefore the oxadiazole ring is resistant to nucleophilic attack. The major reactions of nucleophilic attack occur at carbon atom, generally followed by ring cleavage and electrophilic attack at nitrogen atom. The interaction towards the nucleophiles, also catalyzed by acid, causes difficulties in reactions, which involve basic or acidic conditions. Oxadiazole ring will be more stable when substituted, from one side or more, by aryl groups [7].

1.1.4- Applications of 1, 3, 4-oxadiazole

1,3,4-oxadiazole derivatives have been attracted special attention due to its large number of uses in various areas, drug synthesis, scintillation material and the dye stuffs industry [8,3]. These compounds are widely employed in organic chemistry as intermediate compounds for the synthesis of different heterocyclic compounds [9].

Many of them have a wide range of pharmacological activities such as antihypertensive, antiamoebic, muscle relaxant, antifungal and antibacterial,

anticonvulsant, antiviral (especially anti- HIV-1), antimycobacterial, anticancer, antiobesity, anti-inflammatory and analgesic [10-13].

Since the delocalized π -electronic planar of the molecule is required to design a new organic compound. Much attention was paid for the use of rigid electron-withdrawing 1,3,4-oxadiazole unit as fundamental elements in the synthesis of synthetic metals, and organic light-emitting diodes materials [14].

The oxadiazole derivatives are the state between crystals and liquid characteristics. Liquid crystals possess properties that are not present in liquids and solids, so they can be classified into two major categories (thermotropic, and lyotropic) liquid crystals [15,16].

Oxadiazole-containing compounds have a considerable interest in the field of organic electronics, related to their electron-deficiency. Electron-deficiency gives them great possibility as electron-conducting hole-blocking (ECHB) layers in organic light emitting diode (OLED). They are also electrochemically active with well documented reversible reduction potentials [17,18].

Due to its highly electron-deficient nature it is a poor hole-acceptor, so 1,3,4-oxadiazole derivatives have been incorporated into compounds enabling them to act as an electron-conducting, hole blocking layer for application in OLEDs [19].

Many works were interested in synthesis of variety oligomers containing oxadiazole ring [17-19].

1.2- Molecular spectroscopy

The two common types of spectra: The **emission spectroscopy**, a molecule undergoes a transition from a level of high energy E_i to lower level of energy E_f emitting the excess energy as a photon. In **absorption spectroscopy**, the incident radiations are monitored as radiation losing a number of frequencies due to the absorption of these frequencies.

The energy of the photon emitted or absorbed, ΔE , is given by [20 a]

$$\Delta E = E_f - E_i = h \cdot \nu = h \cdot \frac{c}{\lambda} = h \cdot c \cdot \bar{\nu} \quad \dots \dots \dots \quad (1.3)$$

where

E_f = final energy level

E_i = initial energy level

h = Planck's constant ($6.62606896 \times 10^{-34}$ J s)

ν = frequency of the radiation

λ = wavelength

$\bar{\nu}$ = wavenumber

c = velocity of light in vacuum (2.997925×10^8 m s⁻¹)

The transitions between electronic energy levels occur at ultraviolet, visible, or near-infrared regions. The direct emission or absorption of infrared radiation can produce changes in vibrational energy levels. The vibrational and rotational energy levels can be evaluated from the frequencies appeared from the scattered radiation in Raman spectroscopy.

Infrared, ultraviolet, and nuclear magnetic resonance spectroscopic are non destructive and involve the interaction of molecules with electromagnetic energy, rather than the mass spectrometry which interact with an ionizing source [20 b].

Information's present from electronic spectroscopy combine with the results obtain from NMR and IR spectral data leads to values structural proposal.

The electromagnetic spectrum ranges from short wavelengths (gamma and X-rays) to longest wavelengths (microwaves and radio waves) [21], was presented in figure 1.2.

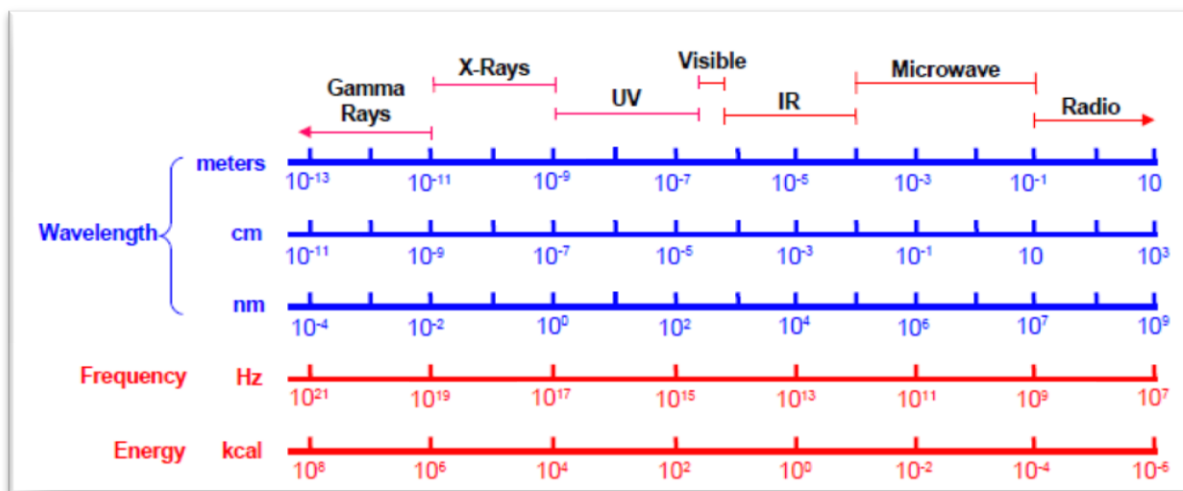


Figure 1.2. The electromagnetic radiation spectrum [21].

1.2.1- Basic Principles of Vibrational Spectroscopy [22]

1.2.1.1- Molecular Vibrations

Atoms in molecule implement vibration motions along the bond, when bond length and bond angle varied periodically. The vibrational motion appeared when atom displaced out from its equilibrium position.

The way providing the molecular vibrations is to imagine the atoms of a molecule as balls, and the bonds as weightless springs, figure 1.3. Where m_1 , m_2 , and f represent the masses of the atoms, and the strength restoring force of bond respectively. The restoring force f of the spring is proportional to the displacement x of the atoms from their equilibrium position.

According to Hooke's law :

$$f = -kx \quad \dots \dots (1.4)$$

Where

f = restoring force

k = force constant of the spring, in N m^{-1}

x = displacement

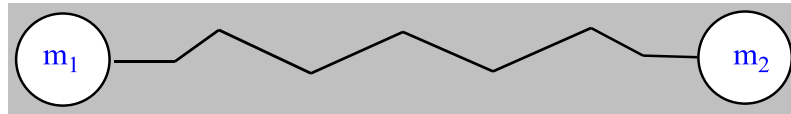


Figure 1.3. The design of ball and spring for a diatomic molecule.

The vibrations of atoms in molecule can be approximately described as a simple harmonic motion, where the vibrational frequency ν_0 (Hz) of this motion can be obtained according to the classic mechanics, equation

$$\nu_0 = \frac{1}{2\pi} \sqrt{\frac{k}{\mu}} \quad \dots \dots \dots (1.5)$$

μ = reduced mass

$$\mu = \frac{m_1 m_2}{m_1 + m_2} \quad \dots \dots \dots (1.6)$$

In quantum mechanics, the harmonic oscillator vibrational energy E_{vib} is represented by equation (1.7)

$$E_{vib} = h\nu_0 \left(n + \frac{1}{2} \right) = \frac{h}{2\pi} \sqrt{\frac{k}{\mu}} \left(n + \frac{1}{2} \right) \quad \dots \dots \dots (1.7)$$

The anharmonic oscillator vibrational energy E_{vib} is approximately given by equation (1.8)

$$E_{vib} = h\nu_0 \left[\left(n + \frac{1}{2} \right) - x_e \left(n + \frac{1}{2} \right)^2 \right] \quad \dots \dots \dots (1.8)$$

Where

n = vibrational quantum number (0, 1, 2, 3.... etc.)

x_e = anharmonicity constant

The vibrations of a polyatomic molecule can be described as a system of coupled anharmonic oscillators.

If the number of atoms in molecule is N , there will be a $3N$ degrees of freedom of motion for all these atoms. When the pure three translations and three rotations motion of the molecule subtracted, this will leaves $(3N-6)$ vibrational degrees of freedom for a nonlinear molecule. But subtract three translations and two rotations motion leaves $(3N-5)$ vibrational degrees of freedom for a linear molecule. These degrees of freedom are appropriate with number of independent normal modes of vibration. The normal modes of vibration define: - when the vibrations of all atoms of molecule have the same frequency and pass through their equilibrium positions simultaneously. Vibrational spectra span with frequency range of $10-4000 \text{ cm}^{-1}$ proportional to the reduced mass and the strength of the bond in the vibrational mode, figure 1.4.

Vibrational spectroscopy: gives information on both dynamics of molecular species and structure, applying Raman and Infrared (IR) spectroscopy.

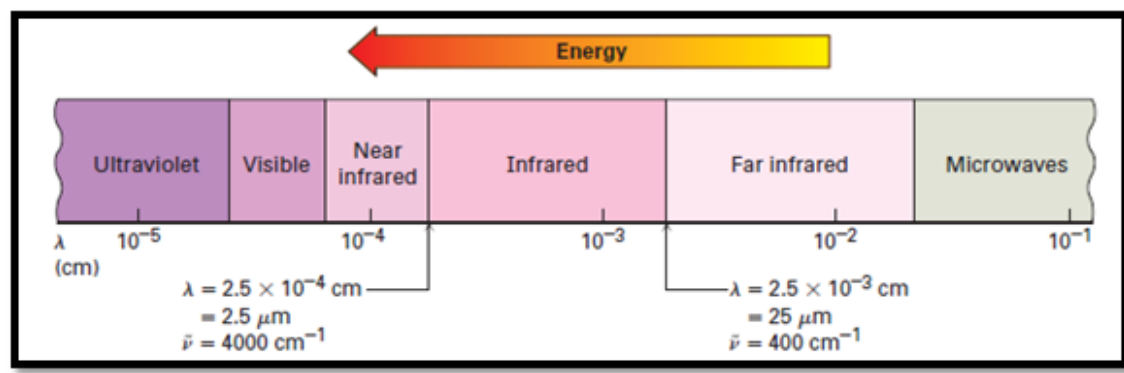


Figure 1.4. The infrared electromagnetic spectrum[22].

Raman and mid-IR spectroscopy are complementary methods, which required completing all the vibrational modes measurements of molecule. Although some vibrations are active in Raman or IR, or in both of them. These techniques of spectroscopy arise from various operations and different selection rules. Usually Raman spectroscopy is best at symmetric vibrations of non-polar groups, but IR spectroscopy is better at the asymmetric vibrations of polar groups.

Infrared spectroscopy is susceptible to changes in the dipole moment as the molecule undergoes vibrations, while Raman spectroscopy sensitive to the changes in polarizability as a function of the vibrational motion [23].

There are different types of the allowable vibrations, figure 1.5.

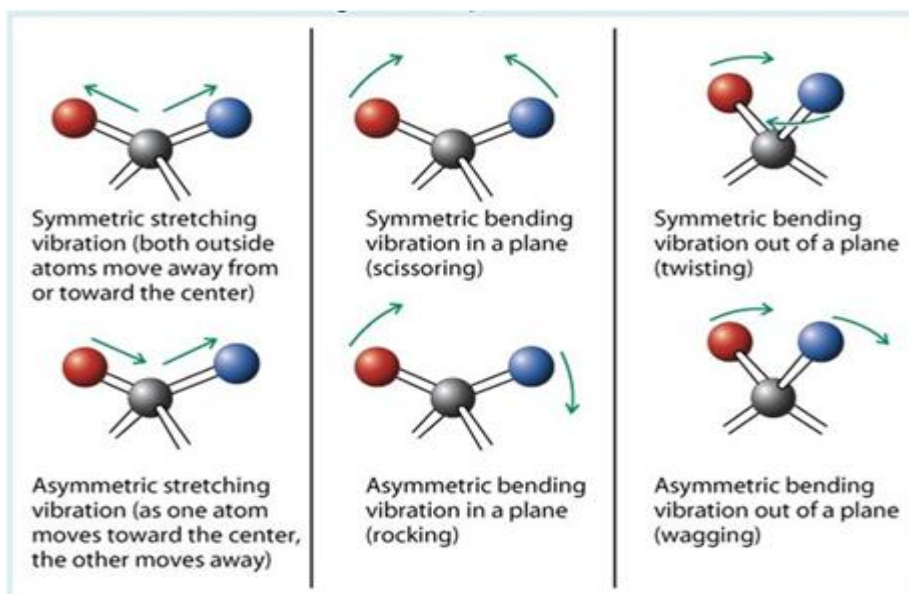


Figure 1.5.The type of molecular vibration [24].

1.2.1.2-Selection rules:

The selection rule is defined as the change in vibrational level response to the change of the electric dipole moment for the molecule (when the atoms are displaced relative to one another). Such vibrations are called **infrared active**.

The selection rule is obtained from the analysis the properties of the integrals over the harmonic oscillator wave functions.

The change in the vibrational quantum number Δn must equal

$$\Delta n = \pm 1 \quad \dots \dots \dots (1.9)$$

Where

$\Delta n = +1$ correspond to absorption, and $\Delta n = -1$ to emission [25].

The group theory aids the determining of vibration types (IR, Raman active) for different symmetry groups. If a molecule has a center of symmetry the **mutual exclusion rule** can be applied, which states that the vibrations active in Raman spectrum are inactive in IR, and vice versa.

In **Raman spectroscopy** the interaction of the electric vector of the electromagnetic wave with the electrons of a compound are leading to the scattering of the incident light. These interactions cause a periodic vibration in the electrons of the compound, inducing oscillation in electrical moments. The oscillating electrons become new sources for emitting radiation (scattered light) [26-28]. Raman scattering occurs when there is an exchange of energy between the molecule and the photon, leading to the emission of another photon with a different frequency than the incident photon.

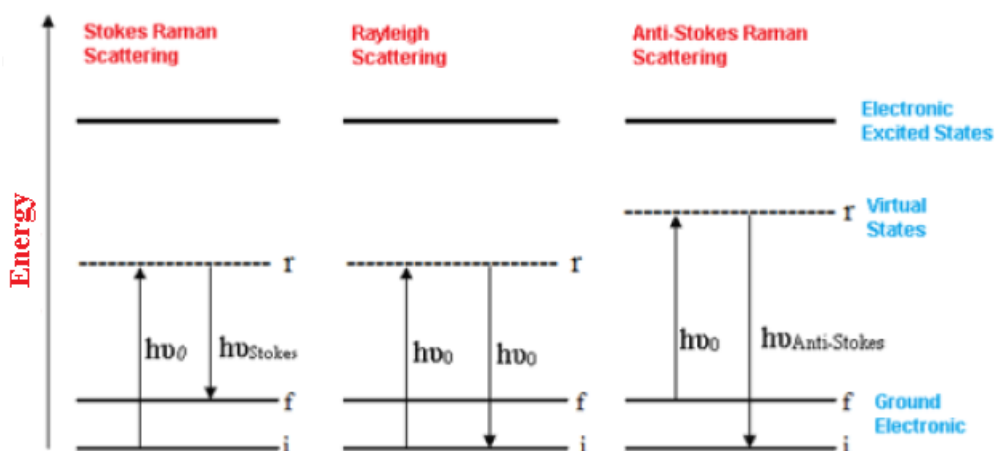


Figure 1.6. The energy level diagram of Rayleigh and Raman scattering[26].

Basically there are two types of scattering, figure 1.6:

- Elastic (Rayleigh scattering); the scattered light has the same frequency (wavelength) as the incident light.
- Inelastic; Stokes, and Anti-Stokes Raman scattering
 - a- Stokes Raman scattering Inelastic ; the scattered light has Lower frequency (longer wavelength) than that of the incident light.
 - b- Anti-Stokes Raman scattering Inelastic; the scattered light has higher frequency (shorter wavelength) than the incident light.

The different energies between incident and scattered photons is due to the change in the vibrational or the rotational state of a molecule. For this reason, the analysis of the Raman spectra provide information about molecular properties and type of vibrations [23, 29].

1.2.2- Nuclear magnetic resonance

Nuclear magnetic resonance (NMR) was discovered by Bloch, Purcell and Pound in 1945 [30], as a development depending on nuclear spins. Initially, was employed to determine accurately the nuclear magnetic moments. However, increases in instrumental accuracy led to the detection of chemical shifts and then

of spin–spin couplings. It can determine the structure, and the conformation for most medium-sized molecules in the solution phase. NMR used in biochemistry to determine the structures of smaller proteins and other biomolecules.

Since atomic nuclei are composed of neutrons and protons, each of them like electrons, has a spin angular momentum ($\hbar/2$). Therefore any proton or neutron produces a tiny magnetic field. The calculations of the magnetic field interactions for proton or netroun, using the magnetic moment vector $\vec{\mu}$, the magnitude of the magnetic moment for one proton μ_p is

$$\mu_p = 2.793 \mu_N = 1.411 \times 10^{-26} \text{ J T}^{-1} \quad \dots\dots\dots (1.10)$$

the nuclear magneton μ_N ,

$$\mu_N = \frac{e\hbar}{2m_p} = 5.051 \times 10^{-27} \text{ J T}^{-1} \quad \dots\dots\dots (1.11)$$

Where

e = charge of electron

$\hbar = h/2\pi$

m_p = mass of proton

The nuclei spinning motion generate nuclear magnetic moment associated with them. The nuclear spin \mathbf{I} may have one of the following values: $\mathbf{I} = 0, 1/2, 1, 3/2, 2$. A nucleus with spin \mathbf{I} can have $(2\mathbf{I} + 1)$ spin orientations, which degenerate without external magnetic field, so the nuclear spin for all the different m_I states of a nucleus have the same energy [30]. Applying any external magnetic field, the energies of the different m_I states will split. NMR spectroscopy involves the flip of the nuclear spin in the presence of a external magnetic field \mathbf{B}_0 . The transitions excite in an NMR change the value of the magnetic nuclear spin quantum number, m_I , by one unit, so $\Delta m_I = \pm 1$. The energy of the interaction between two

magnetic fields is equal to the dot product of the nuclear magnetic moment $\vec{\mu}$ with the field strength \vec{B}_o

$$E = -\mu B_o \quad \dots \dots \dots (1.12)$$

Usually, the strength of the magnetic field is measured in tesla (1T = 10⁴ gauss)

$$E_I = -m_I B_o \frac{\gamma h}{2\pi} = \gamma h B_o \quad \dots \dots \dots (1.13)$$

γ = magnetogyric ratio of the specified nucleus (T⁻¹ s⁻¹)

The energy separation ΔE between the $m_I = +1/2$ (α or \uparrow) and $m_I = -1/2$ (β or \downarrow) states of proton spin in a magnetic field B_o is

$$\Delta E = E_\beta - E_\alpha = \left(\frac{1}{2}\gamma h B_o\right) - \left(-\frac{1}{2}\gamma h B_o\right) \quad \dots \dots \dots (1.14)$$

or
$$\frac{\Delta E}{h} = \frac{\gamma B_o}{2\pi} \quad \dots \dots \dots (1.15)$$

The direction of the nucleus magnetic moments $\pm 1/2$ are not aligned with or against the external magnetic field but they wobble around or precess about the axis of the external field (as spinning top). The angular frequency of this precession (ω (rad s⁻¹)), is given by

$$\omega = \gamma B_o \quad \dots \dots \dots (1.16)$$

Where $\omega = 2\pi\nu$

ν = Larmor or precession frequency

At constant B_o the larger the γ , the easier to detect the NMR signal. Thus the readily studied nuclei are ^1H , ^{19}F , and ^{31}P , (table 1.1). The modern NMR instrumentation, applied high B_o the NMR signal of the ^{13}C nucleus (which has a small γ value and very low natural abundance), can be studied easily [31].

Table 1.1. Magnetogyric Ratios, NMR Frequencies (in a 4.7-T Field), and Natural Abundances of Isotopes [31].

Isotope	I	$\gamma/10^7 \text{ T}^{-1} \text{ s}^{-1}$	ν/MHz	Natural abundance (%)
^1H	1/2	26.75	200	99.985
^2H	1	4.11	30.7	0.015
^{13}C	1/2	6.73	50.3	1.108
^{14}N	1	1.93	14.5	99.63
^{15}N	1/2	2.71	20.3	0.37
^{17}O	5/2	3.63	27.2	0.037
^{19}F	1/2	25.17	188.3	100
^{31}P	1/2	10.83	81.1	100
^{33}S	3/2	2.05	15.3	0.76

1.2.2.1- Chemical Shift

The nucleus magnetic field B is related to the external magnetic field B_o as follows

$$B = B_o(1 - \sigma) \quad \dots\dots\dots (1.17)$$

where σ , is the screening, or shielding, constant. The σ shifts the frequency of the nuclear spin transition

$$\nu = \frac{\gamma B_o(1 - \sigma)}{2\pi} \quad \dots\dots\dots (1.18)$$

Usually the absolute values of σ is not measured but calibrated to the transition frequency of some reference compound ν_o which provides the **chemical shift**, δ (ppm) [32]:

$$\delta = \frac{\nu - \nu_o}{\nu_o} \quad \dots\dots\dots (1.19)$$

1.2.3- Basic concepts of electronic spectroscopy

1.2.3.1- Electronic spectroscopy

Electronic spectroscopy is the field in which the change produced by the photon absorption or emission combined with the rearrangement of the electrons in the system. These changes are interpreted in terms of the quantum theory of electronic structure.

The frequencies or wavelengths of transitions help to distinguish atoms and molecules and provide information's about their energy levels, electronic structure, and bonding. Intensities of absorption or emission determines the concentrations of species. For all previous reasons, the electronic spectroscopy can be considered the most useful tools in physics and chemistry [33].

The electronic spectra of molecules are presented in the range of wavelengths 100-800 nm of the electromagnetic spectrum.

The UV and visible radiation interacts with mater rise an electronic transitions (promotion of electrons from the ground state to a high energy state). The UV region is divided into two regions; (1) UV ranged from 200 - 400 nm is referred to as the near UV region, (2) the region below 200 nm, is called the vacuum or far UV region, figure 1.7 [34].

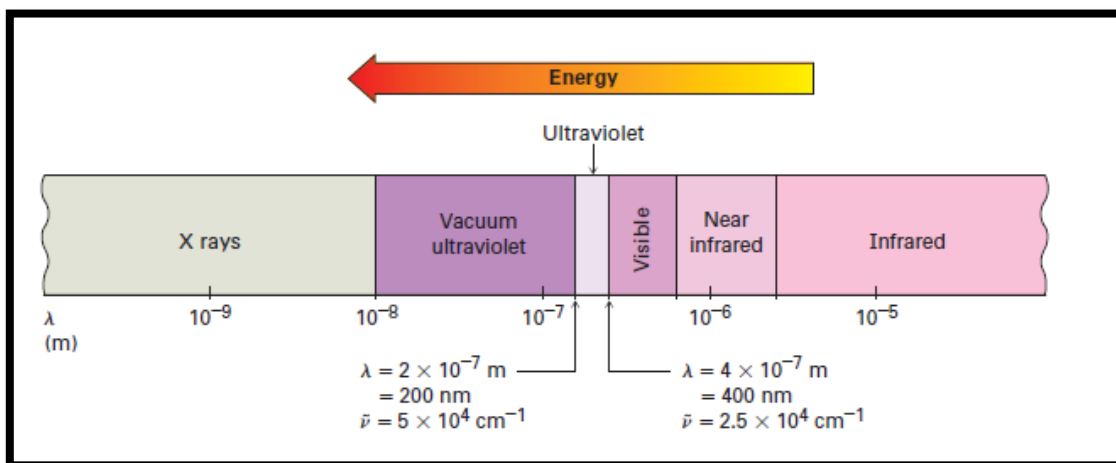


Figure 1.7. The UV and visible region of the electromagnetic spectrum[33].

The visible region, corresponds to the range of wavelength from 400 - 800 nm. The shortest visible is the violet and the longest wavelength is red, figure 1.8.

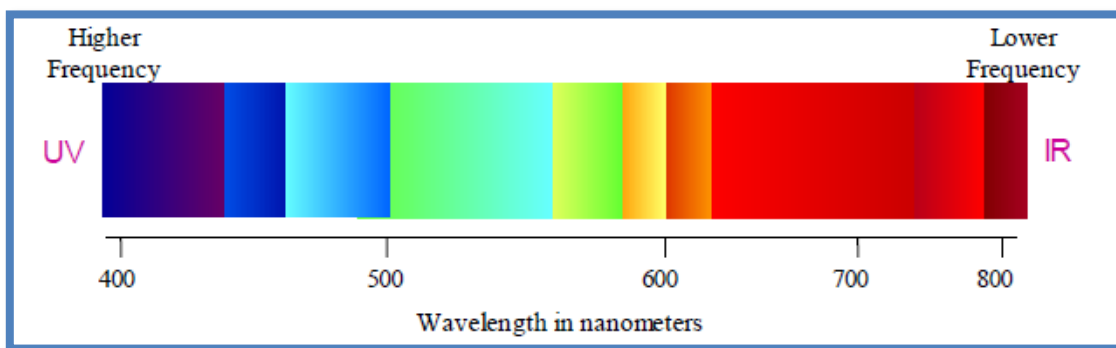


Figure 1.8. The visible spectrum from higher to lower frequencies[34].

There are three types of electronic transition:

- ❖ transition include π , σ , and n electrons, figure 1.9
- ❖ transition include charge-transfer electrons
- ❖ transitions include d and f electrons

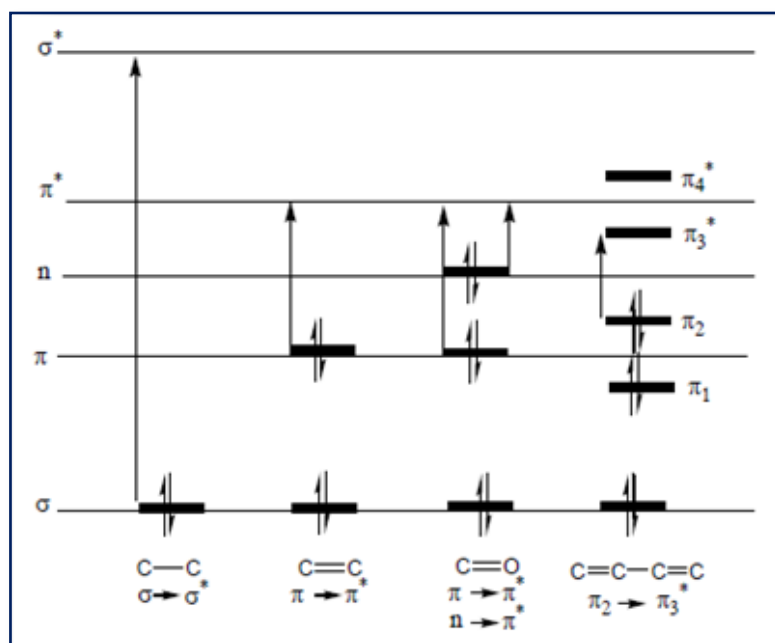


Figure 1.9. The energies for the most common orbitals involved in electronic spectroscopy of organic groups[34].

1.2.3.2- Nature of Electronic Transitions

When a particle absorbs energy, an electron is transferred from occupied molecular orbital (usually a non-bonding n or bonding π orbital) to the greater potential energy unoccupied orbital (an antibonding π^* or σ^* orbital), figure 1.9. From the data of the electronic spectra for organic molecules, the saturated organic molecules (alkanes) do not offer any absorption in the near UV and Visible (200-800 nm), which may be display $\sigma \rightarrow \sigma^*$ in vacuum UV.

Generally, groups conferring color on substances are called *chromophores*. *Auxochromes* is linkage of a certain group of atoms to the *chromophore*. These processes modify *chromophore* ability to absorb light. Examples of *chromophores* would be, C=C, C=O, N=N etc., and of *auxochromes*, C-Br, C-OH, C-NH₂ etc. [35].

The introduction of an *auxochrome* in organic saturated system usually shifts the absorption maximum to a longer wavelength (UV and visible).

1.2.3.3- Franck–Condon principle

The structure of any molecule in the excited electronic state is different from that in the ground state. In general, the anharmonicity constants α_e , force constants k , and moments of inertia I of a molecule are different in its various electronic levels.

$$\bar{\nu} = \bar{\nu}_{el} + \bar{\nu}_v + \bar{\nu}_J \quad \dots \dots \dots (1.20)$$

Where

$\bar{\nu}$ = wave number of radiation (absorbed or emitted)

$\bar{\nu}_{el}$ = wave number of electronic transition

$\bar{\nu}_v$ = wave number of vibrational transition

$\bar{\nu}_J$ = wave number of rotational transition

The transition of an electron from one energy state to another is associated at the same time with the changes in vibrational and rotational states. This causes transitions between different vibrational and rotational levels. Classically, the **Franck–Condon** principle is the approximation stated that electronic transition is almost takes place without changes in the positions of the nuclei in the molecular structure, and its environment. An electron transition happened in very short time ($\sim 10^{-16}$ s) compared to the diatomic nuclei period of vibration ($\sim 10^{-13}$ s). This is due to the large weight difference between electron and nucleus, according to the Born-Oppenheimer approximation. Therefore the positions and the velocities of the nuclei are mostly unchanged during the electronic transition. So such transition can be represented by a *vertical line* drawn between two potential-energy curves, figure 1.10 [36].

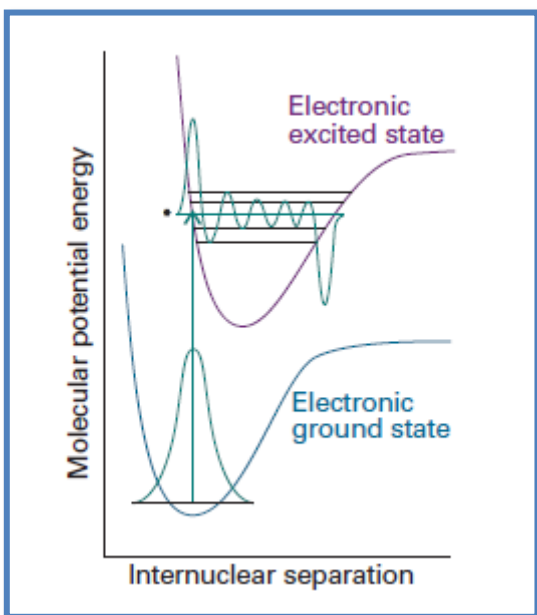


Figure 1.10. Represents the vertical electronic transition between the two potential-energy curves for the ground and excited state of a diatomic molecule[36].

The Franck–Condon principle is obtained from the transition dipole moment μ_{fi} ,

$$\mu_{fi} = \int \Psi_f \hat{\mu} \Psi_i d\tau \quad \dots \dots \dots (1.21)$$

where

Ψ_f = the wavefunctions of the final states

Ψ_i = the wavefunctions of the initial states

$\hat{\mu}$ = dipole moment operator

The dipole moment operator is covering the sum of all nuclei and electrons in the molecule:

$$\hat{\mu} = -e \sum_i r_i + e \sum_I Z_I R_I \quad \dots \dots \dots (1.22)$$

The intensity of transition is related to the square modulus $|\mu_{fi}|^2$ of the transition dipole moment magnitude.

The overlap integral between the vibrational conditions of the initial and final electronic levels $S(\mathbf{v}_f, \mathbf{v}_i)$ is a measure of the match between the vibrational wavefunctions for the excited and ground electronic states : where $S = 1$ referred to a perfect match, and $S = 0$ when there is no similarity.

Since the molecule contains of an electronic part $|\boldsymbol{\varepsilon}\rangle$, and a vibrational part $|\mathbf{v}\rangle$, therefore, within the Born–Oppenheimer approximation, the transition dipole moment equal:

$$\begin{aligned} \boldsymbol{\mu}_{fi} &= \langle \boldsymbol{\varepsilon}_f \mathbf{v}_f | \left\{ -e \sum_i \mathbf{r}_i + e \sum_I \mathbf{Z}_I \mathbf{R}_I \right\} | \boldsymbol{\varepsilon}_i \mathbf{v}_i \rangle \\ &= -e \sum_i \langle \boldsymbol{\varepsilon}_f | \mathbf{r}_i | \boldsymbol{\varepsilon}_i \rangle \langle \mathbf{v}_f | \mathbf{v}_i \rangle + e \sum_i \mathbf{Z}_i \langle \boldsymbol{\varepsilon}_f | \boldsymbol{\varepsilon}_i \rangle \langle \mathbf{v}_f | \mathbf{R}_I | \mathbf{v}_i \rangle \quad \dots \dots (1.23) \end{aligned}$$

The term $e \sum_i \mathbf{Z}_i \langle \boldsymbol{\varepsilon}_f | \boldsymbol{\varepsilon}_i \rangle \langle \mathbf{v}_f | \mathbf{R}_I | \mathbf{v}_i \rangle$ is zero, because $\langle \boldsymbol{\varepsilon}_f | \boldsymbol{\varepsilon}_i \rangle = 0$ (they are orthogonal). Therefore, for the two different electronic levels

$$\boldsymbol{\mu}_{fi} = -e \sum_i \langle \boldsymbol{\varepsilon}_f | \mathbf{r}_i | \boldsymbol{\varepsilon}_i \rangle \langle \mathbf{v}_f | \mathbf{v}_i \rangle = \boldsymbol{\mu}_{\boldsymbol{\varepsilon}_f, \boldsymbol{\varepsilon}_i} S(\mathbf{v}_f, \mathbf{v}_i) \quad \dots \dots \dots (1.24)$$

Where

$$\boldsymbol{\mu}_{\boldsymbol{\varepsilon}_f, \boldsymbol{\varepsilon}_i} = -e \sum_i \langle \boldsymbol{\varepsilon}_f | \mathbf{r}_i | \boldsymbol{\varepsilon}_i \rangle \quad S(\mathbf{v}_f, \mathbf{v}_i) = \langle \mathbf{v}_f | \mathbf{v}_i \rangle \quad \dots \dots (1.25)$$

Where

$\boldsymbol{\mu}_{\boldsymbol{\varepsilon}_f, \boldsymbol{\varepsilon}_i}$ = the electric-dipole transition moment, arising from the redistribution of electrons.

$S(\mathbf{v}_f, \mathbf{v}_i)$ = the overlap integral between the vibrational for initial ($|\mathbf{v}_i\rangle$), and final ($|\mathbf{v}_f\rangle$) levels.

Since the transition intensity is proportional to the square of the transition dipole moment magnitude [37]. Therefore the intensity of the absorption is proportional to **Franck–Condon factor** for the transition $\{ |S(\mathbf{v}_f, \mathbf{v}_i)|^2 \}$. So the greater value of

$S(\nu_f, \nu_i)$ the greater the absorption intensity of that particular synchronous electronic and vibrational transition. Figure 1.10, demonstrated the vibrational wavefunction of the ground state which have the highest overlap with the vibrational levels related to the peaks at similar bond lengths in the upper electronic state.

1.2.3.4- The intensities of spectral lines

The **transmittance** T is the ratio of the transmitted intensity I to the incident intensity I_o for a given frequency.

$$T = \frac{I}{I_o} \quad \dots \dots \dots (1.26)$$

Beer–Lambert law:- the transmitted density changes with the sample length l , and the molar concentration $[J]$ of the absorbing species J

$$I = I_o 10^{-\epsilon[J]l} \quad \dots \dots \dots (1.27)$$

ϵ = molar absorption coefficient

$$A = \log \frac{I_o}{I} \quad \text{or} \quad A = -\log T \quad \dots \dots \dots (1.28)$$

A = absorbance

$$A = \epsilon[J]l \quad \dots \dots \dots (1.29)$$

The area under the curve E is equal to the integral of ϵ over the entire absorption band, figure 1.11.

$$E = \int \epsilon(\nu) d\nu \quad \dots \dots \dots (1.30)$$

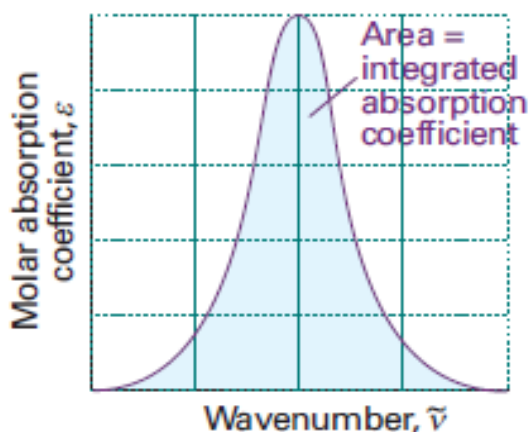


Figure 1.11. The area under the curve is equal to the integrated absorption coefficient for transition of the molar absorption coefficient versus the wavenumber of the incident radiation [37].

E is proportional to a dimensionless quantity called the *oscillator strength* f of the absorption band. The *oscillator strength* f expresses the probability of absorption or emission of electromagnetic radiation in transitions between energy levels of molecule.

$$f = (1.441 \times 10^{-18} \text{ mol s m}^{-2})E \quad \dots \dots \dots (1.31)$$

The f of an absorption band is directly proportional to the transition moment

$$\mu_{fi}^2 = \frac{3}{8\pi^2} \frac{he^2}{m_e \nu} f_{fi} \quad \dots \dots \dots (1.32)$$

Where

ν = the frequency of the maximum absorption

The **oscillator strength** range from 10^{-3} (for very weak absorption bands due to *forbidden* transition) to a maximum of ~ 2 for the *allowed* transition [38,39].

1.2.3.5- Selection rules

The **selection rules** of electronic transition are:

1- **Spin selection rule:** during the electronic transition, no change in spin inversion ($\Delta S=0$ transition allowed). So, T \rightarrow T, S \rightarrow S, are allowed, but T \rightarrow S, S \rightarrow T, are *forbidden* transition.

The selection rules is systematically changed with the angular momentum as follow:

$$\Delta\Lambda=0,\pm 1 \quad \Delta S=0 \quad \Delta\Sigma=0 \quad \Delta\Omega=0,\pm 1$$

Λ = the component of the total orbital angular momentum

Σ = the component of the total spin angular momentum

$\Omega = \Lambda + \Sigma$ = the quantum number of the total angular momentum (orbital and spin) around the inter nuclear axis, figure 1.12.

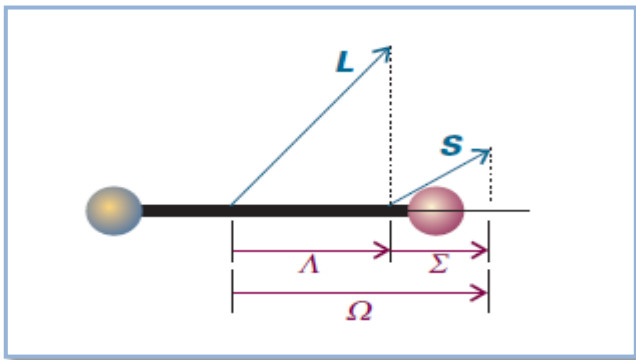


Figure 1.12. The coupling of orbital (L) and spin (S) angular momenta in a linear molecule[38].

2- **symmetry are:**

a- Σ terms, the transitions $\Sigma^+ \leftrightarrow \Sigma^+$ and $\Sigma^+ \leftrightarrow \Sigma^-$ are allowed.

b- **Laporte selection rule**, related to molecules that have a centre of symmetry.

Where, the allowed transitions are $u \rightarrow g$ and $g \rightarrow u$, while the forbidden transitions $g \rightarrow g$ and $u \rightarrow u$ [37,40].

1.2.3.6- Solvent effects

The wavelength and intensity of absorption are affected when a molecule transferred from a gas phase to a solvent environment. This is related to an unequal perturbation of the excited and ground states of the molecule. This depends on the nature of the interactions between solvent and solute at these states. But the absorption spectra in highly non-polar solvents keep almost the same characters of the gas phase spectra.

Kasha [41] suggestion solvent effects as a standardization in distinguishing the $n \rightarrow \pi^*$ and the $\pi \rightarrow \pi^*$ transitions. He specified the shift bands as *red* or *blue* according to their displacement in the solvent. McConnel [42] and other authors have assigned that all the $n \rightarrow \pi^*$ transitions give blue shift bands, but all transitions of $\pi \rightarrow \pi^*$ do not generate red shift bands.

Later, Bayliss and McRae [43] expressed through how the solvent influence the absorption spectra, which can explain qualitatively in terms of dipole-polarization and hydrogen bonding forces between the solvent and the solute.

Generally, terms presenting electronic absorption spectra are:

1. **Chromophores:** functional groups that produce electronic transitions.
2. **Auxochromes:** replacing unshared pair electrons like OH, SH, NH,.... when bound to π chromophore they generally shift absorption maximum toward a longer wavelength (red).
3. **Bathochromic shift:** shift to longer wavelength (red shift).
4. **Hypsochromic shift:** shift to shorter wavelength (blue shift).
5. **Hyperchromism:** increasing in ϵ of a band.
6. **Hypochromism:** decreasing in ϵ of a band.

1.3- Literature Review:

The **OD** structure was studied experimentally in 1972 by microwave [44]. Since the equilibrium structure of **OD** cannot be accurately determined by the microwave technique only. Therefore a quantum chemical calculation (with appropriate uncertainties) fitted with the moments of inertia, using the mixed estimation of the internal coordinates approach, gives more accurate result. Their calculations were confirmed by the extrapolation technique [45].

Many workers were investigated the experimental and theoretical vibrational spectra for **OD** molecule [45-48]. A theoretical studied for the molecular structure and the harmonic vibrational spectra of this molecule employed the followings methods (1) DFT, (2) MP2, and (3) HF with the same basis set 6-31G^{**}. The worker concluded that the scaled calculated spectra by the DFT/6-31G^{**} method revealed good agreement results with experimental spectral data than those calculated by the MP2/6-31G^{**} or HF/6-31G^{**} [47]. Then Kwiatkowski et al [48] obtained a scaled ab initio calculations of vibrational frequencies based on both the DFT and MP2 methods with the standard 6-31G (d,p) basis set. Hegelund with coworker [49] studied the High-resolution of the IR spectra for the four fundamental bands of 1,3,4-oxadiazole in gaseous phase (ranging between 800 and 1600 cm⁻¹), plus the theoretical calculations of optimize geometry, and the complete set of anharmonic frequencies using DFT method. Palmer [50] calculations were done using the B3LYP density functional (with both the TZ2P and cc-pVTZ basis set), and MP2 ab initio techniques (with one basis set cc-pVTZ only). He concluded that the results of the MP2 show less correlations with the experimental data. While the TZ2P basis set is faster than cc-pVTZ, but it is more practicable for larger molecules, therefore its favorable.

The **2-phenyl-1,3,4-oxadiazoles (POD)** was theoretically studied. The geometrical parameters and vibrational frequencies in the ground state were carried out by the HF, and DFT (B3LYP) methods with 6-31G(d), 6-311G(d), 6-31G(d,p), and 6-311G(d,p) basis sets. The scaling theoretical results were in agreement with the experimental results [51].

The **2,5-diphenyl-1,3,4-oxadiazole (DPOD)** molecule produce fluorescence emission of two different wavelengths near 380 and 760 nm [52]. This phenomenon has many applications in the biomedical and chemical sciences. The derivatives (**POD, PODA, DPOD**) of **2-R-5-phenyl-1,3,4-oxadiazole** molecule obtained by the replacement (**R= H, amino, phenyl**) consequently. The molecular structure was checked experimentally by absorption of fluorescence spectra, and theoretically by time dependent density functional theory (TD-DFT) methods [53].

The **5-phenyl-1,3,4-oxadiazol-2-amines (PODA)** molecule was synthesized by many researchers. The optimize geometry of **PODA** molecule, calculated employing (DFT) 6-311G** [54].

In 2012 the structural and vibrational spectra were examined for **5-phenyl-1,3,4-oxadiazole-2-thiol (PODT)** molecule. The complete assignment of the IR spectrum, plus the DFT calculations together with Pulay's scaled quantum mechanical force field method were used to reach an agreement between the theoretical wavenumber and the experimental data. Furthermore, the frontier molecular orbitals (HOMO and LUMO) were computed, and compared with the calculated oxadiazole molecule results [55].

1.4- The Aim of the Work

Molecules studied in this work are divided in two categorized series one, and two. Series one consist the oxadiazole derivatives in which substituting in position 2 or in 5 or in both 2, and 5 by -NH₂, -Cl, -NO₂ and -CN groups. Series one molecules are: 1,3,4-oxadiazole (**OD**), 1,3,4-oxadiazole-2-amine (**ODA**), 1,3,4-oxadiazole-2,5-diamine (**ODDA**), 5-chloro-1,3,4-oxadiazole-2-amine (**CODA**), 2-

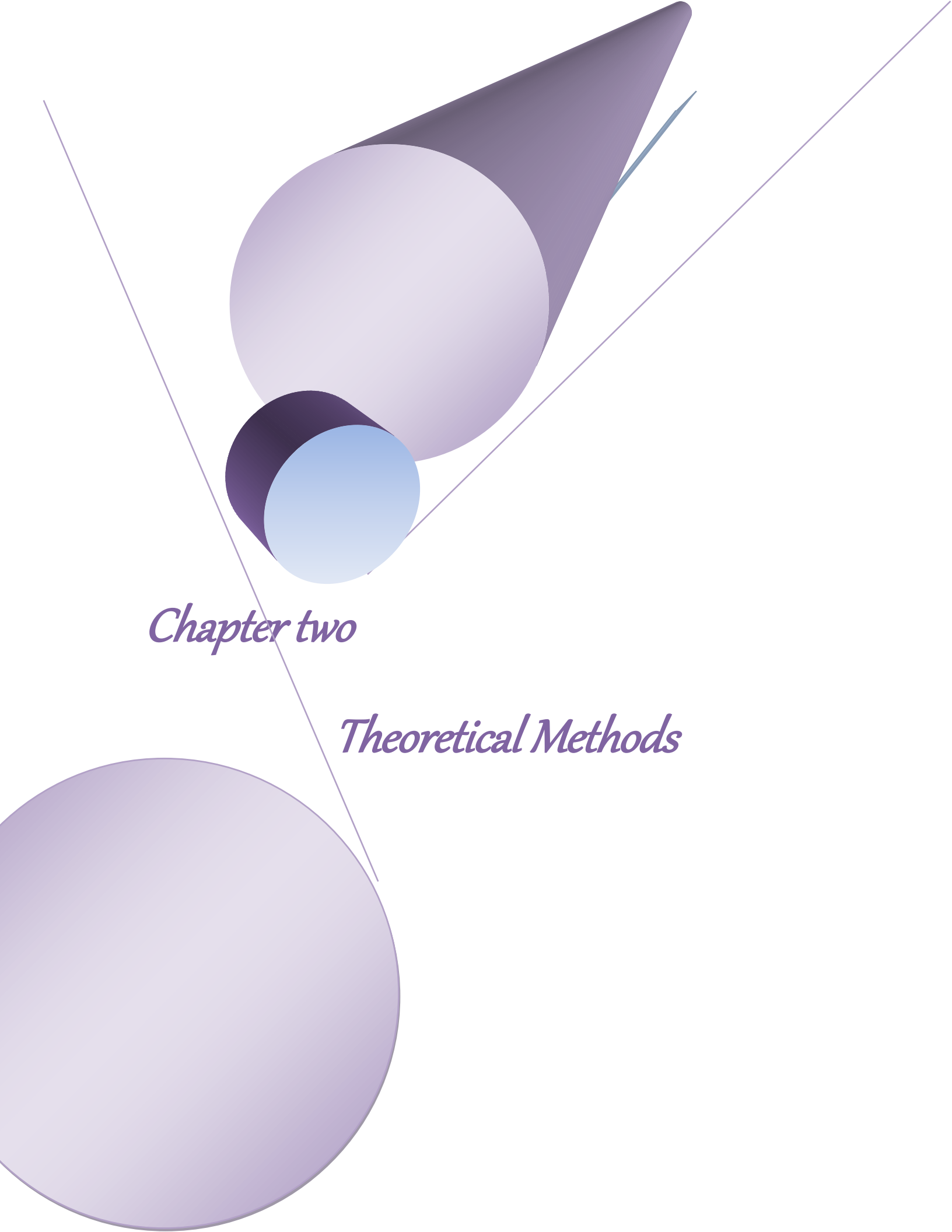
amino-1,3,4-oxadiazole-5-carbonitrile (**AODCN**), 5-nitro-1,3,4-oxadiazole-2-amine (**NODA**).

Series two consist the oxadiazole derivatives by which substituting are done by -NH₂, -Cl, -SH and phenyl groups. So this series contains the following molecules 2-phenyl-1,3,4-oxadiazoles (**POD**), 5-phenyl-1,3,4-oxadiazole-2-thiol (**PODT**), (5-phenyl-1,3,4-oxadiazole-2-amine) (**PODA**), 5-(4-chlorophenyl)-1,3,4-oxadiazole-2-amine (**CPODA**) 2,5-diphenyl-1,3,4-oxadiazole (**DPOD**).

Since there is no available theoretical and experimental data in literature for the most molecules in these two series.

The main objective of this theoretical treatment is to calculate the optimized molecular geometry, vibrational spectra, electronic properties (absorption electronic spectra, frontier molecular orbital analysis, molecular electrostatic potential [in gas phase and in water solution]), and nuclear magnetic resonance spectra [in gas phase and in Dimethyl sulfoxide solution] for the oxadiazole derivatives molecules. Comparison was done between their different states.

All the theoretical treatments are done by employing Gaussian program 09, with the Density Function Theory **DFT** method/B3LYP /basis set 6-311++G (2d,2p) selection. In few cases, using the Avogadro program which assist to view the electronic orbitals or molecular electrostatic potentials.



Chapter two

Theoretical Methods

2.1- Computational Chemistry

Computational chemistry (molecular modeling) is a theoretical calculations technique allowing the investigations of chemical problems by a computer, such as: molecular geometries, reactivities, spectra, and other properties.

- Molecular geometry: is the calculation for the forms of particles, bond lengths, bond angles, and dihedral angles. Plus energies of molecules and its transition states: showing, which isomer is more stable. Also from the transition state and reactant energies the appropriate reaction can be confirmed.
- Chemical interaction: is the knowledge about where the electrons are concentrating (nucleophilic sites), and the way where to go (electrophilic sites), and which to predict types of reagents will attack a molecule.
- NMR, IR, and UV spectra: from its calculated results, workers trying to make molecule to be knows.

The chemical calculations are used in pharmaceutical industry looking for the interactions of valuable drugs with bio molecules to utilize a suitable drug at the active site of enzyme. Plus it is employed to study the properties of solids in materials science [56].

In this study all the theoretical treatments are done by employing Gaussian program 09 [57]. In few cases, using the Avogadro program which assist to view the electronic orbitals or molecular electrostatic potentials [58].

2.2- Quantum mechanics (QM)

Quantum mechanics is a mathematical approach describing particles behavior. It can predict the property of atom or molecule. But in practice, the QM equations can be used to solve only one electron systems. Different approximation

methods have been employed to solve multiple electron systems. These approximations are useful, but it requires knowing when each approximation is valid, and gives accurate results. Two methods were available Schrödinger and Heisenberg. The Schrödinger form was used since it is the basis for the most computational chemistry methods. The Schrödinger equation is:

$$\hat{H}\Psi = E\Psi \quad \dots\dots\dots (2.1)$$

Where

\hat{H} = the Hamiltonian operator.

Ψ = the wave function or Eigen function.

E = the energy or Eigen value.

The wave function Ψ is a function of the electron and nuclear positions, which describing an electron behavior as a wave. It can describe the probability of electrons being in certain locations, but it cannot predict exactly where electrons are located.

The most common methods of computational chemistry are the molecular mechanics, ab initio, semiempirical and density functional theory.

2.2.1- Molecular Mechanics (MM)

Molecular mechanics used the classic mechanics to explain the molecular geometry on the base of a ball-and-springs model. Where the balls represent atoms link together by springs in molecules. Plus there are a number of force fields required to stretch or bend the strings for modeling compounds. These approximations are used to predict the geometry of molecules and their relative energies of conformers.

2.2.2- Semi-empirical Methods (SE)

Semi-empirical methods based on approximate solutions of the Schrödinger equation, combining theoretical values with the experiment data (using parameterization).

2.2.3- Ab initio Methods

Ab initio methods were applicable to the largest group of property. Many typical organic molecules can now be modeled with ab initio methods.

Ab initio calculations based on solving the Schrödinger equation with a necessary approximations, which determines the level of the calculation. The simplest approach was the Hartree–Fock (HF) method, in which the total molecular wavefunction Ψ is approximated to the Slater determinant considering spin orbitals. Where the most important approximation is the central field approximation. Always the calculated energies from HF are greater than the exact energy. This limitation called the Hartree–Fock limit. The second approximation in HF calculations is related to linear combinations for one-electron systems of Gaussian-type orbitals (**GTO**), (e^{-ar^2}) .

The self-consistent field method (SCF) [iterative method] in which the calculation continue iteratively till the energy unchanged from one iteration to the next, reaching to the converge state. The energy difference between the true energy (E) and the energy in the HF limit E_{HF} is called the electron correlation energy (E_{corr}), equation (2.2).

$$E_{\text{corr}} = E - E_{\text{HF}} \dots\dots\dots (2.2)$$

Commercial packages are available for *ab initio* calculations. In ab initio to reach the efficiently as possible a thousands of integrals are used. This is greatly

helped by using the atomic orbitals as LCAOs (linear combinations atomic orbitals) like the linear combinations of Gaussian orbitals [59].

2.2.4- Density functional theory (DFT)

Density functional theory is depending on electron probability density function or electron density function. So it's called the charge density or the electron density, and specified by $\rho(x, y, z)$. Recently the density functional theory becomes popular, since it gives the same accuracy with less computational work than other methods. Therefore in this study the DFT was adopted.

The base of DFT is the electron density ρ , instead of the wavefunction ψ ; where the electron density is a function of position, $\rho(\mathbf{r})$. The ground-state energy $E[\rho]$ of n -electron in a molecule is

$$E[\rho] = E_K + E_{P;e,e} + E_{P;e,N} + E_{\chi C}[\rho] \quad \dots \dots \dots (2.3)$$

Where

E_K = the total electron kinetic energy

$E_{P;e,e}$ = the electron–electron potential energy

$E_{P;e,N}$ = the electron–nucleus potential energy

$E_{\chi C}[\rho]$ = the **exchange–correlation energy**

In DFT the orbitals are employed as a structure for the electron density, equation (2.4):

$$\rho(\mathbf{r}) = \sum_{i=1}^N |\Psi_i(\mathbf{r})|^2 \quad \dots \dots \dots (2.4)$$

While using **Kohn–Sham equations**, which are like the Hartree–Fock equations except the **exchange–correlation potential** $v_{\chi C}$:

$$\left\{ \begin{array}{l} \text{kinetic} \\ \text{energy} \\ \frac{\hbar^2}{2m_e} \nabla_1^2 \\ \text{electron-electron} \\ \text{repulsion} \\ \int \frac{\rho(r_2)e^2}{4\pi\epsilon_0 r_{12}} dr_2 \\ \text{electron-nucleus} \\ \text{attraction} \\ - \sum_{j=1}^N \frac{Z_j e^2}{4\pi\epsilon_0 r_{j1}} \\ \text{exchange-} \\ \text{correlation} \\ + V_{xc}(r_1) \end{array} \right\} \Psi_i(r_1) = \epsilon_i \Psi_i(r_1) \dots \dots (2.5)$$

Where the V_{xc} is the derivative of the exchange–relationship energy:

$$V_{xc}[\rho] = \frac{\delta E_{xc}[\rho]}{\delta \rho} \dots \dots \dots (2.6)$$

Using the iterative technique with the self-consistent-field SCF to solve the Kohn–Sham equations by the speculation the electron density. The exchange–correlation potential is calculated depending on approximate form of the exchange–correlation energy on the electron density $E_{xc}[\rho]$. The simplest approximation is the local-density approximation, equation (2.7):

$$E_{xc}[\rho] = \int \rho(r) \epsilon_{xc}[\rho(r)] dr \dots \dots \dots (2.7)$$

Where

ϵ_{xc} = the exchange–correlation energy of electron in a homogeneous and constant gas density

The Semi-empirical calculations are slower than MM but much faster than ab initio and DFT calculations. Generally the DFT method is faster than ab initio and gives more accurate results [60].

2.3- Basis function

One of the approximations in all QM methods is the introduction of a basis set. The expansion of an unknown function, as a MO, in a set of known functions it cannot be considered approximation when the basis set is completed. The complete basis set meaning the using of an infinite number of functions, which is impossible to accounts. The molecular orbital's can be concluded as functions in the infinite

coordinate system extend by the complete basis set. When a finite basis set is employed, the components of the MO only along with these coordinate axes which related to the selected basis functions can be created. The smaller the basis set, provide poor accuracy.

2.3.1- Slater and Gaussian Type Orbital's

There are two types of basis functions [*Atomic Orbitals* (AO)] which are not generated from the to an atomic Schrödinger equation solutions:

1-*Slater Type Orbitals* (STO)

2-*Gaussian Type Orbitals* (GTO)

1- Slater type orbitals, represented by equation (2.8)

$$\chi_{\zeta,n,l,m}(r, \theta, \varphi) = NY_{l,m}(\theta, \varphi)r^{n-1}e^{-\zeta r} \quad \dots \dots \dots (2.8)$$

Where

ζ = the effective nuclear charge

N = normalization constant

$Y_{l,m}$ = spherical harmonic functions

n, l, m , are the quantum numbers

The STO do not have any radial nodes, which described by linear combinations of STOs.

2- Gaussian type orbitals can be characterized in terms of polar coordinates, equation (2.9)

$$\chi_{\zeta,n,l,m}(r, \theta, \varphi) = NY_{l,m}(\theta, \varphi)r^{2n-2-l}e^{-\zeta r^2} \quad \dots \dots \dots (2.9)$$

The GTO near the nucleus has a zero slope, while the STO has a "tip" (intermittent derivative). Therefore the GTOs have a problems representing suitable behavior near the nucleus. Figure 2.1 shows how a 1s-STO can be modeled by a linear combination of three GTOs, will reveal good calculation results.

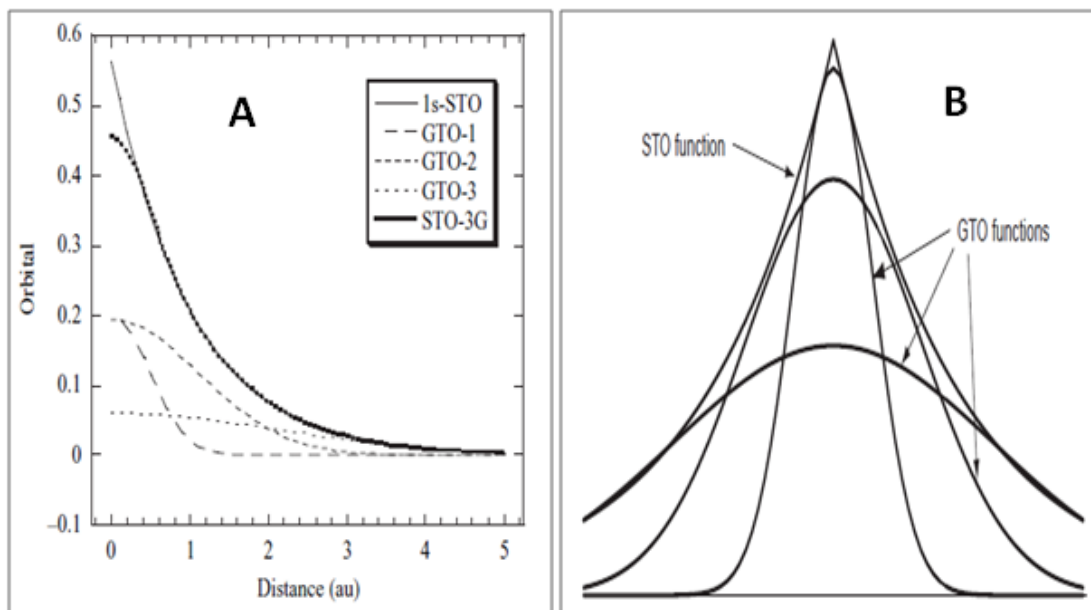


Figure 2.1: A) 1s-STO modelled by a linear combination of three GTOs (STO-3G).
B) Approximating a STO with several GTOs [61].

Increasing the number of GTO basis functions compensated more computational efficiency. Therefore GTOs are favorite as a basis functions in electronic structure calculations.

2.3.2-Types of basis set

The aims of using different basis sets are

- (1) give predictable chemical accuracy in results.
- (2) the cost consideration of calculations.
- (3) the transferable and the flexible used for atoms in various bonding environments.

The common fundamental core and valence basis, in constructing an atomic orbital are:-

1- Minimal basis

Minimal bases which have the number of STO or GTO orbitals equal to the number of the core and valence AOs in the atom. Each of the **STO-3G basis set** functions is formed by the expansion in terms of three Gaussian functions. Where the values of the Gaussian exponents and the linear coefficient can be evaluated by least squares, as the best fits to Slater-type functions.

The STO-3G are replaced by more efficient basis sets: - split-valence basis sets, and polarization basis sets.

2- Split-Valence Basis Sets

The first short coming of a minimal basis set, namely, a bias toward atoms with spherical environments. This basis sets can be provided by two sets of valence basis functions: The inner set is tightly held and the outer one is loosely held. The iterative process of this basis sets reveal a solution for the Roothaan–Hall equations. In which adjusting the balance of the two mentioned parts independently in the three Cartesian coordinates, by adjusting the individual MO coefficients.

The inner AOs represents by one set of functions, and valence AOs by two sets of functions. The simple split-valence basis sets are 3-21G and 6-31G. In 3-21G basis set, each core AOs is expanded to three Gaussians. The inner and outer valence atomic orbitals components are extended in terms of two and one Gaussians, consequently. In 6-31G basis sets of the core orbitals are expressed by six Gaussians and the valence orbitals split into three and one Gaussian components. The Gaussian exponents and the expansion coefficients for 3-21G and 6-31G basis sets have been calculated from Hartree–Fock energy minimization (ground states).

3- Polarization Basis Sets

This basis set can be described in terms of hybrid orbitals (pd and sp hybrids) or in Taylor series expansion. Taylor series expansion adds a further improvement using the second and third derivatives (in terms of d functions which are the derivatives of p functions, and p functions is the derivatives of s functions).

The simplest polarization basis sets of 6-31G is 6-31G*, which build by adding a set of d -type polarization functions in terms of a single Gaussian for a heavy atom (non-hydrogen). A six of second-order Gaussians set is introduced in the basis set of 6-31G*. But for an accurate presentation of the bonding in many H atoms, the Polarization of the s orbitals is required. The 6-31G** basis set is identical to 6-31G*, except that it provides three p -type polarization functions for hydrogen. Gaussian exponents for polarization functions have been chosen to give the lowest energies for the representative molecules [30].

2.4- Geometry Optimization

In order to obtain the geometry of the molecule, it is required to start with a guess of the molecular geometry. Then a systematic changes for all atoms coordinates combined by energy decreases, using SCF. This procedure is continued until the minimum energy is achieved. The efficient geometry optimization requires the first and second derivatives of the energies which are relative to the atomic coordinate's q_i .

The gathering of all the second derivatives H_{ij} in a matrix is called Hessian matrix.

Each element of H_{ij} is

$$H_{ij} = \frac{\partial^2 E}{\partial q_1 \partial q_2} \dots \dots \dots (2.10)$$

The optimization procedure can be summarized in the computational chemistry programs as follows:

- 1- The guess of the geometry of the molecule.
- 2 - Calculate the energy and the gradients of the molecule structure, then obtain the Hessian matrix.
- 3 - The equilibrium optimize geometry is selecting in reaching the optimization criteria.
- 4 - If the optimization criteria are not reached, then repeating Step 2, with the addition option of possessing a new Hessian matrix with the updating of the old one [37].

2.5- Time-Dependent Density Functional Theory (TD-DFT)

Time-dependent density functional theory (TD-DFT) is evaluated the dynamics and properties of many-body systems involving time-dependent potentials, such as magnetic or electric fields. Its employed to study the effects of these fields on molecules in order to obtain features:- such as excitation energies, photo absorption spectra, and frequency-dependent response properties [62,63].

The TD-DFT computational basis is the exchanging of the time-dependent wave function to the time-dependent electronic density. In order to develop a useful method, the imaginary non-interacting system which having the same density like the interacting system of interest, according to Runge-Gross (RG) theorem. This is called the (time-dependent) Kohn-Sham system in DFT [64-66].

The process of RG considers a single-component system in the time-dependent field for which the Hamiltonian holds the following form:-

$$\hat{H}(t) = \hat{T} + \hat{V}_{ext}(t) + \hat{W} \dots \dots \dots (2.11)$$

where

\hat{T} = the kinetic energy operator

\hat{W} = the electron-electron interaction

$\hat{V}_{ext}(\mathbf{r}, t)$ = the external potential (the external potential described the electrons interaction with the nuclei in the system)

Therefore many-body wavefunction formulates relative to the time-dependent Schrödinger equation is:-

$$\hat{H}(t)\Psi(t) = i\hbar \frac{\partial}{\partial t} \Psi(t) \quad \dots \dots \dots (2.12)$$

Using the Schrödinger equation as starting point, the RG theorem indicates that at any time, the density uniquely defines the external potential.

In Kohn-Sham (KS) method chooses a non-interacting system (which its interaction potential is zero) in which the density equal to the interacting system. Then the non-interacting systems can be solved, where the wave function represented by Slater determinant of single-particle orbitals. Each are determined by a single partial differential equation in three variable, therefore the kinetic energy of the non-interacting system can be described in terms of these orbitals. To calculate a potential, presented as $V_s(\mathbf{r}, t)$ or $V_{KS}(\mathbf{r}, t)$, using a non-interacting Hamiltonian H_s , equation (2.13) is

$$\hat{H}_s(\mathbf{r}, t) = \hat{T} + \hat{V}_s(\mathbf{r}, t) \quad \dots \dots \dots (2.13)$$

Where

\hat{T} = the operator of kinetic energy

\hat{V}_s = the operator of potential energy for non – interacting system

So the time dependent equation can be written as:

$$\hat{H}_s(t)\Psi(t) = i\hbar \frac{\partial}{\partial t} \Psi(t) \quad \dots \dots \dots (2.14)$$

The construction for a set of N orbitals will be presented in equation (2.15), which creates the time-dependent density equation (2.16).

$$\left(-\frac{1}{2}\nabla^2 + \hat{V}_s(\mathbf{r}, t) \right) \varphi_i(\mathbf{r}, t) = i\hbar \frac{\partial}{\partial t} \varphi_i(\mathbf{r}, t) \quad \dots \dots \dots (2.15)$$

$$\rho_s(\mathbf{r}, t) = \sum_{i=1}^N |\varphi_i(\mathbf{r}, t)|^2 \quad \dots \dots \dots (2.16)$$

ρ_s = the density of the interacting system at all times

$$\rho_s(\mathbf{r}, t) = \rho(\mathbf{r}, t) \quad \dots \dots \dots (2.17)$$

2.6- Nuclear Magnetic Resonance (NMR) [30]

NMR spectroscopy describes the energy necessary to flip a nuclear spin under the effect of external magnetic field as mentioned in chapter (1). Computation of this phenomenon requires the definition of the origin of the system coordinate, known as “gauge origin”. The magnetic are independent of the gauge origin, while this is necessary when an exact wavefunction is applied. But this is not a practical choice, therefore the selection of gauge origin is desired. Generally there are two commonly methods:

- 1- Individual gauge for localized orbitals (IGLO) [67].
- 2- Gauge-including atomic orbitals (GIAO) [68,69].

Both methods when applied in computer programs will provide good results.

To assess the computed NMR properties, especially the chemical shifts (the magnetic influence related to the electron distribution obtained not just at nuclei but at any point, which is called the “nucleus-independent chemical shift” (NICS))[71]. Rablen [70] investigated the HNMR shifts for 80 organic molecules applied DFT method with different basis sets. A good agreement was found with a systematic difference between the computed and experimental chemical shifts. Therefore he proposed two computational models including linear scaling for the chemical shifts calculations: a high-level model setup on the computed shift at [GIAO/B3LYP/6-311G(2df,p) // B3LYP/6-31G(d)] and the more economical one [GIAO/B3LYP/6-311G(d,p) // B3LYP/6-31G(d)]. The root mean square error is lower than 0.15 ppm for tow models.

In this work the GIAO/B3LYP was adopted with the basis set 6-311G++(2d,2p).

2.7- Molecular Electrostatic Potential (MEP)

Electrostatic potential is a physical property. It is measured experimentally by X-ray diffraction. When a positive charge (unit H^+) set at distance r from a molecule constructed from A nuclei and N electrons undergoes to two types of effects: nuclear repulsion and attraction. The electrostatic potential $V(\mathbf{r})$ is defined by equation (2.18)

$$V(\mathbf{r}) = \sum_A^{N_A} \frac{Z_A}{r - R_A} - \int \frac{\rho(\mathbf{r}') d\mathbf{r}'}{|\mathbf{r} - \mathbf{r}'|} \quad \dots \dots \dots (2.18)$$

where

Z_A = the atomic number

R_A = the position vector of an atom A

$\rho(\mathbf{r}')$ = the continuous electron density at a point \mathbf{r}'

\mathbf{r} = the set of coordinates for the electrons

The electron attraction relate to electron-charge distribution $\rho(\mathbf{r})$, which obtained from the exact normalized solution for the electron Schrödinger equation of the system, equation (2.19)

$$\rho(\mathbf{r}') = \int |\Psi(\mathbf{r})|^2 d\mathbf{r} \quad \dots \dots \dots (2.19)$$

Therefore the wavefunction of the system having nth state, $\Psi(\mathbf{r})$ is approximated by an antisymmetric product of molecular orbitals φ_k 's (SCF approximation). These can be presented as a linear combination of atomic orbitals χ_l 's (LCAO-MO approximation) or a linear combination of another basis set (as STO or GTO).

$$\varphi_k = \sum_l c_k^l \cdot \chi_l \quad \dots \dots \dots (2.20)$$

According to equation (2.18), the MEP of the molecule at a point \mathbf{r} near the molecule can be approximated by

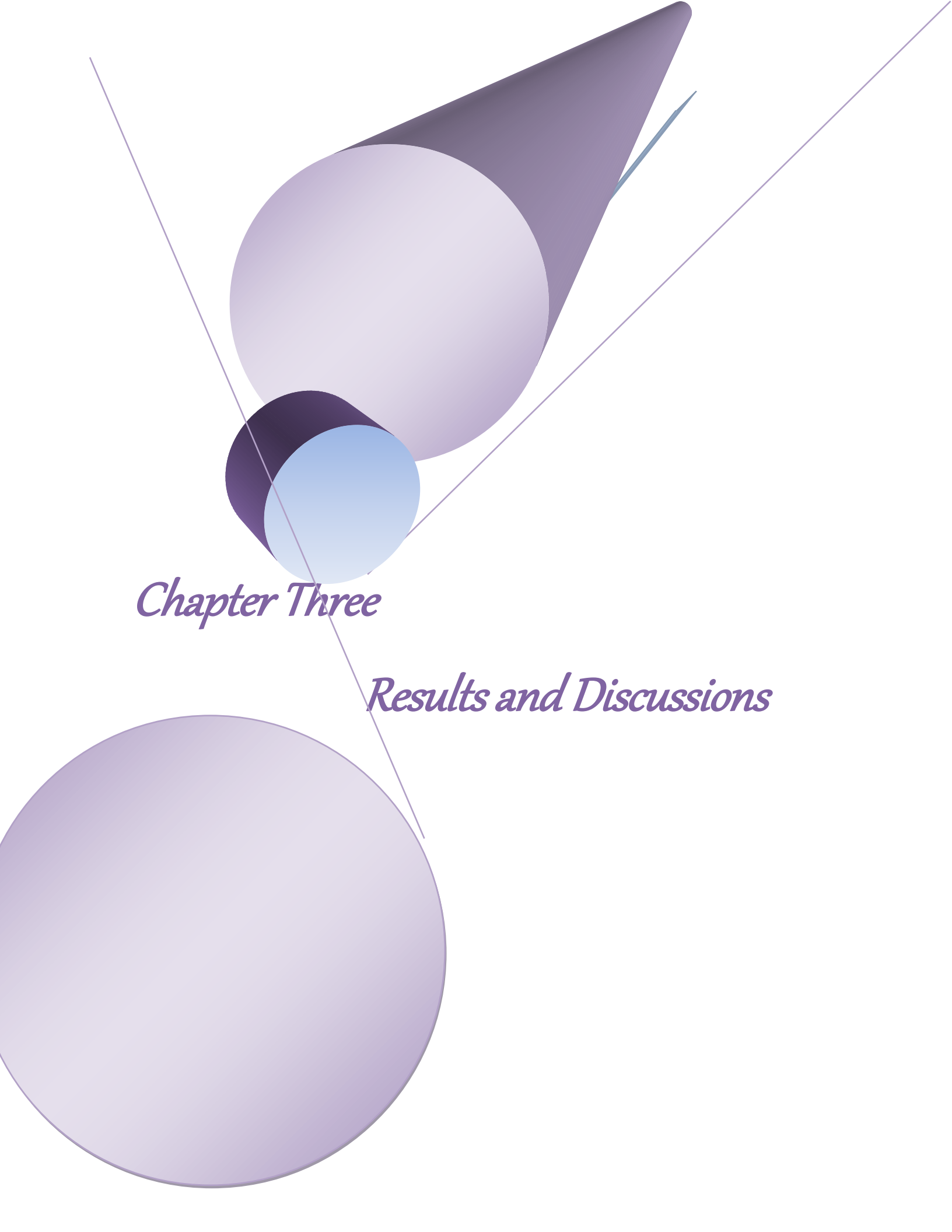
$$V(\mathbf{r}) = \sum_A^{N_A} \frac{Z_A}{r - R_A} - \sum_{ij} p_{ij} \int \frac{\chi_i(\mathbf{r}') \cdot \chi_j(\mathbf{r}')}{|\mathbf{r} - \mathbf{r}'|} d\mathbf{r}' \quad \dots \dots \dots (2.21)$$

Where

p_{ij} = elements density matrix

$$p_{ij} = \sum_r 2 * c_{ir} * c_{jr} \quad \dots \dots \dots (2.22)$$

The repulsion is resulted from the positive nuclear charges, which equal to the difference between electrostatic potential and the electron-density distribution function [72].



Chapter Three

Results and Discussions

3.1- Results and Discussion of series one

Series one consist the following molecules **OD**, **ODA**, **ODDA**, **CODA**, **AODCN**, and **NODA**.

3.1.1- Molecular geometry

The computed optimized geometric of the molecules under study are presented in figure 3.1. The optimized structural parameters such as bond length, bond angle, and dihedral angle are listed in **table 3.1**.

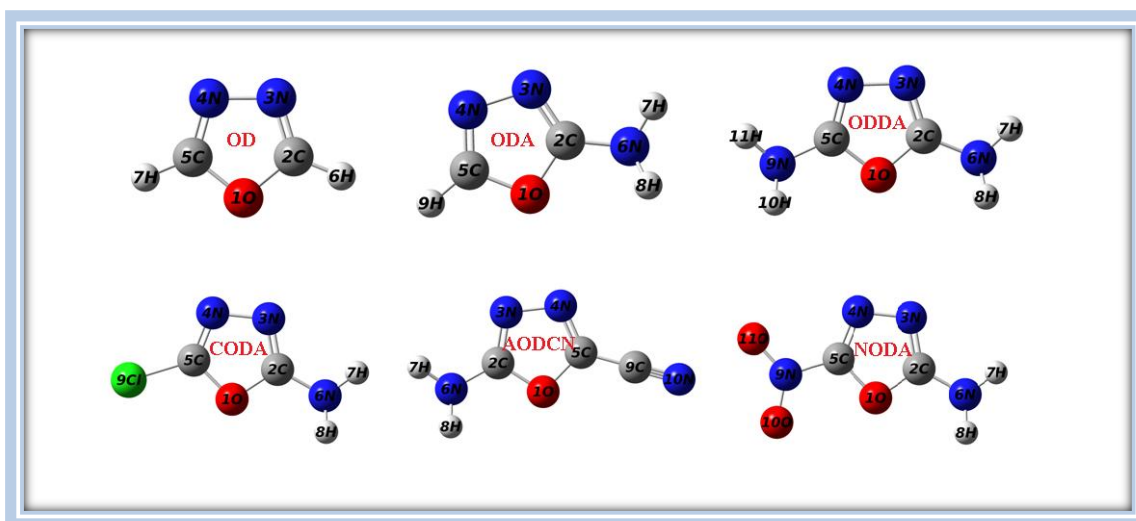


Figure 3.1.The calculated molecular structure for the studied compound along with the atom numbering scheme.

The **1,3,4-oxadiazole (OD)** is belong to C_{2v} point group symmetry. **Table 3.1** is revealed that the molecule structure in a good agreement with the previous experimental and theoretical data [45, 47, 49].

The **ODA**, **CODA**, **AODCN**, and **NODA** molecules belong to C_1 point group, while **ODDA** is related to C_s point group.

The bond length O_1-C_2 is 1.359 \AA in **OD** molecule. When NH_2 (the electron donating group) is substituted in position **2** at **OD** ring, it can be seen a very small shortening (0.02 \AA) in this bond. While the O_1-C_5 bond become longer (1.374 \AA) in **ODA** molecule. These two bonds become longer in **ODDA** compound. In **ODA**

molecule when CN (the electron withdrawing group) is replaced instead of H atom at position **5**, the **AODCN** molecule is obtained. So in **AODCN**, the **O₁-C₅** bond is appeared longer (1.379 Å), and the bond length **O₁-C₂** shorter (1.352 Å). In substitution of **NO₂** (the electron withdrawing group) in position **5** in **ODA**, the **NODA** compound will be formed. **O₁-C₂** and **O₁-C₅** bonds become shorter.

The following two bonds **C₂=N₃** and **C₅=N₄** are 1.284 Å in **OD** molecule. In **ODA** molecule **C₂=N₃** bond is elongated (1.294 Å), while **C₅=N₄** is shorter (1.278 Å). These bonds in **ODDA** and **AODCN** molecules are longer. But the elongation is more in **AODCN** molecule (1.304, 1.289 Å respectively). In **NODA** compound only **C₂=N₃** bond become longer.

The C-Cl bond length show a considerable decrease when substituted in the place of C-H, this is occurred in **CODA** molecule, where the C-Cl bond length is 1.702 Å. This substitution trend to shorting the **C₅=N₄** (1.276 Å) bond adjacent to the substituent, and cause elongation in **C₂=N₃** (1.293 Å). Furthermore **O₁-C₅** bond (1.371 Å) is longer than **O₁-C₂** bond (1.362 Å).

In the **OD** molecule the bond angles around the **C₂** atom (**O₁-C₂-H₆**, **O₁-C₂-N₃** and **N₃-C₂-H₆**) are 118.2, 113.3, and 128.6 degree respectively. Where the total sum equal to 360.1 degree, and the total sum for the three angles around the **C₅** atom is equal 360.1 degree. This indicates that the **C₂**, and **C₅** atoms are related to **sp²** hybridization type. The same results are obtained for all the oxadiazole derivatives, **table 3.1**.

Table 3.1. The optimized geometry data of OD, ODA, ODDA, CODA, AODCN, and NODA molecules, plus the available theoretical and experimental data.

Structural parameter	Exp. [45]	Exp. [49]	DFT 6-311+G (3df,2d) other work [45]	DFT 6-31 G** other work [47]	DFT/6-311++G(2d,2p) This work					
					OD	ODA	CODA	ODDA	AODCN	NODA
<i>Bond length in (Å)</i>										
O ₁ -C ₂	1.354	1.357	1.356	1.360	1.359	1.357	1.362	1.371	1.352	1.353
O ₁ -C ₅						1.374	1.371	1.371	1.379	1.363
C ₂ =N ₃	1.285	1.284	1.283	1.291	1.284	1.294	1.293	1.284	1.304	1.308
C ₅ =N ₄						1.278	1.276	1.284	1.289	1.282
C ₂ -N ₆						1.365	1.363	1.372	1.353	1.348
C ₂ -H ₆	1.074	1.075	1.075	1.079	1.075					
N ₃ -N ₄	1.406		1.401	1.405	1.405	1.406	1.409	1.419	1.385	1.384
C ₅ -N ₉										1.443
C ₅ -C ₉									1.414	
C ₅ -Cl							1.702			
C ₅ -H ₉						1.075				
N ₆ -H ₇						1.007	1.008	1.008	1.007	1.006
N ₆ -H ₈						1.007	1.008	1.009	1.006	1.226
N ₉ -O ₁₀										1.226
N ₉ -O ₁₁										1.219
C ₉ ≡N ₁₀									1.152	
<i>Bond angle in degree</i>										
C ₂ -O ₁ -C ₅	101.4	101.6	101.8	101.5	101.7	101.5	101.0	101.3	101.5	101.0
O ₁ -C ₂ =N ₃	113.8	113.3	113.2	113.4	113.3	113.5	113.4	113.5	113.3	113.2
O ₁ -C ₂ -N ₆						117.7	117.5	116.9	118.2	118.3
N ₃ =C ₂ -N ₆						128.7	128.9	129.5	128.4	128.4
O ₁ -C ₂ -H ₆	118.1		118.2	118.0	118.2					
N ₃ =C ₂ -H ₆	128.2		128.6	128.6	128.6					
C ₂ =N ₃ -N ₄	105.6	105.8	105.9	105.8	105.9	105.4	105.7	105.8	105.8	105.7
N ₃ -N ₄ =C ₅						106.6	105.9	105.8	106.9	106.2
O ₁ -C ₅ =N ₄						113.0	113.9	113.5	112.5	113.9
O ₁ -C ₅ -N ₉										117.9
N ₄ =C ₅ -N ₉										128.1
O ₁ -C ₅ -C ₉									118.8	
N ₄ =C ₅ -C ₉									128.7	
O ₁ -C ₅ -Cl							117.3			
N ₄ =C ₅ -Cl							128.8			
O ₁ -C ₅ -H ₉						117.8				
N ₄ =C ₅ -H ₉						129.2				
C ₂ -N ₆ -H ₇						113.5	113.5	112.4	115.2	115.8
C ₂ -N ₆ -H ₈						115.7	115.9	114.8	117.4	117.9
H ₇ -N ₆ -H ₈						114.1	114.2	112.9	116.0	116.7
C ₅ -N ₉ -O ₁₀										116.3
C ₅ -N ₉ -O ₁₁										116.7
O ₁₀ -N ₉ -O ₁₁										127.0
<i>Dihedral angle in degree</i>										
C ₅ -C ₉ ≡N ₁₀ -O ₁									179.6	

C ₅ -O ₁ -C ₂ =N ₃					0.0	0.2	0.2	0.0	-0.2	0.2
C ₅ -O ₁ -C ₂ -N ₆						-176.6	-176.5	-176.6	177.1	-177.2
C ₅ -O ₁ -C ₂ -H ₆					180.0					
C ₂ -O ₁ -C ₅ =N ₄					0.0	0.1	0.2	0.0	-0.1	-0.0
C ₂ -O ₁ -C ₅ -C ₉									179.6	
C ₂ -O ₁ -C ₅ -H ₇					180.0					
C ₂ -O ₁ -C ₅ -Cl							-179.4			
C ₂ -O ₁ -C ₅ -N ₉								176.6		-179.4
C ₂ -O ₁ -C ₅ -H ₉						-179.6				
O ₁ -C ₂ =N ₃ -N ₄					0.0	-0.4	-0.5	0.0	0.3	-0.3
H ₆ -C ₂ =N ₃ -N ₄					180.0					
N ₆ -C ₂ =N ₃ -N ₄						175.9	175.7	176.0	-176.6	176.8
O ₁ -C ₂ -N ₆ -H ₇						-167.0	-168.1	-168.7	167.4	-168.0
O ₁ -C ₂ -N ₆ -H ₈						-32.3	-33.0	-37.8	25.3	-22.8
N ₃ =C ₂ -N ₆ -H ₇						16.7	15.8	15.4	-15.8	14.9
N ₃ =C ₂ -N ₆ -H ₈						151.4	150.9	146.2	-157.9	160.2
C ₂ =N ₃ -N ₄ =C ₅					0.0	0.5	0.6	0.0	-0.3	0.3
N ₃ -N ₄ =C ₅ -O ₁									0.2	-0.2
N ₃ -N ₄ =C ₅ -C ₉									-179.4	
N ₃ -N ₄ =C ₅ -H ₉						179.3				
N ₃ -N ₄ =C ₅ -Cl							179.1			
N ₃ -N ₄ =C ₅ -N ₉								-176.0		179.2
O ₁ -C ₅ -N ₉ -O ₁₀										0.9
O ₁ -C ₅ -N ₉ -O ₁₁										-179.1
N ₄ -C ₅ -N ₉ -O ₁₀										-178.4
N ₄ -C ₅ -N ₉ -O ₁₁										1.6
O ₁ -C ₅ -N ₉ -H ₁₀								37.8		
O ₁ -C ₅ -N ₉ -H ₁₁								168.7		
N ₄ =C ₅ -N ₉ -H ₁₀								-146.2		
N ₄ =C ₅ -N ₉ -H ₁₁								-15.4		

The calculated $\text{C}\equiv\text{N}$ bond length is (1.152 \AA) in **AODCN** molecule, on the contrary the experimental value in aromatic compound (phenyl nitrile) is (1.136 \AA) [73]. The bond lengths for two bonds **N₉-O₁₀** and **N₉-O₁₁** belong to the **NO₂** group in **NODA** molecule are (1.226 and 1.219 \AA consequently). The experimental X-ray study for nitro aromatic derivative (2-chloro-4-nitroaniline) result are indicated that the N-O bond equal to 1.310 \AA . While its theoretical value employing B3LYP/6-311G (d,p) equal 1.226 \AA [74].

3.1.2- Vibrational Spectra

The computed harmonic vibrational frequencies with its complete assignment for all molecules (**OD**, **ODA**, **ODDA**, **CODA**, **AODCN**, and **NODA**) are presented in **tables 3.2, 3.3, 3.4, 3.5, 3.6, 3.7** respectively.

The **OD** molecule is planar has 7 atoms with 15 normal modes of vibrations. The fundamental modes are distributed as: $\Gamma \text{ vib} = 6A_1 + 2A_2 + 2B_1 + 5B_2$. All these vibrations are active in both Infrared and Raman except the A_2 species which is active in Raman only. This work results show reasonable agreement with experimental, and the theoretical scaling harmonic frequencies data [47], and anharmonic frequencies [49].

Table 3.2. Theoretical vibrational frequencies and the assignment of the **OD** molecule compared with other experimental and theoretical data.

No.	Sym.	Freq. (cm ⁻¹)	IR intensity (km mol ⁻¹)	Raman activity (A ⁴ amu ⁻¹)	Freq. (cm ⁻¹) ab initio [49]	DFT 6-31G** other work [45]	Freq. (cm ⁻¹) Exp.[45]	Assignment
ν_1	A ₁	3291	0.61	135.18	3150	3180	3169	$\nu_s \text{ CH}$
ν_2		1558	46.76	34.84	1527	1529	1534	$\nu_s \text{ C=N} + \beta_s \text{ CH}$
ν_3		1300	0.30	20.22	1275	1275	1272	$\beta_s \text{ CH} + \beta \text{ ring (ring def.)}$
ν_4		1104	37.14	6.59	1085	1093	1092	$\beta_s \text{ CH} + \nu_s \text{ COC}$
ν_5		974	4.17	4.96	948	952	951	$\beta \text{ ring } (\nu_s \text{ NN} + \nu_s \text{ COC})$
ν_6		946	35.73	0.07	926	923	920	$\beta_s \text{ CH} + \beta \text{ ring} (\nu_s \text{ NN} + \nu_s \text{ COC})$
ν_7	A ₂	841	0.00	0.17	825	823	825	$\gamma_{as} \text{ CH}$
ν_8		675	0.00	0.33	666	655	653	$\gamma_{as} \text{ CH} + \gamma \text{ ring (ring puck.)}$
ν_9	B ₁	872	21.62	0.45	854	849	852	$\gamma_s \text{ CH}$
ν_{10}		644	35.75	0.39	633	633	625	$\gamma \text{ HCOCH}$
ν_{11}	B ₂	3285	3.35	28.53	3144	3147	3167	$\nu_{as} \text{ CH}$
ν_{12}		1534	4.56	0.17	1494	1500	1541	$\nu_{as} \text{ C=N} + \beta_{as} \text{ CH}$
ν_{13}		1239	1.47	5.11	1215	1217	1215	$\beta_{as} \text{ CH}$
ν_{14}		1083	45.00	1.10	1044	1081	1078	$\nu_{as} \text{ COC} + \beta \text{ CH}$
ν_{15}		951	0.00	0.38	935	935	925	$\beta \text{ CH} + \beta \text{ ring (ring def.)}$

The frequencies 1104 and 1083 cm^{-1} for the **OD** can be characterized as COC symmetric and asymmetric stretching mixed with the CH in-plane-bending vibration. Also the frequencies of 974 and 946 cm^{-1} are belonged to the ring deformation (NN associated with COC stretching motions). In **ODA** molecule the ν_{10} mode (1080 cm^{-1}) is analyzed as CO stretching plus CH in-plane-bending vibration. The two modes at 968, and 957 cm^{-1} consist different motions, one of them is ring deformation, **table 3.3**.

Table 3.3. Theoretical vibrational frequencies (cm^{-1}), IR intensity, Raman activities and the assignment of the **ODA**.

No.	Sym.	Freq. (cm^{-1})	IR intensity (km mol^{-1})	Raman activity ($\text{A}^4 \text{amu}^{-1}$)	Assignment
ν_1	A	3681	54.26	45.26	$\nu_{\text{as}} \text{NH}_2$
ν_2		3580	50.34	145.75	$\nu_{\text{s}} \text{NH}_2$
ν_3		3290	1.72	89.38	νCH
ν_4		1673	347.05	34.04	$\delta \text{NH}_2 + \nu_{\text{as}} \text{N}=\text{CN}$
ν_5		1612	52.17	11.81	$\delta \text{NH}_2 + \nu_{\text{s}} \text{C}=\text{N}$
ν_6		1561	19.09	17.11	$\nu_{\text{as}} \text{C}=\text{N} + \delta \text{NH}_2$
ν_7		1428	47.49	1.51	$\rho \text{NH}_2 + \nu_{\text{s}} \text{COC} + \beta \text{CH}$
ν_8		1253	2.94	10.97	βCH
ν_9		1134	1.29	8.91	ρNH_2
ν_{10}		1080	55.82	8.02	$\nu \text{CO} + \beta \text{CH}$
ν_{11}		1000	23.34	5.66	$\nu \text{NN} + \rho \text{NH}_2 + \beta \text{CH}$
ν_{12}		968	16.41	4.62	$\beta \text{CH} + \beta \text{ ring (ring def.)} + \rho \text{NH}_2$
ν_{13}		957	6.91	1.06	$\beta \text{CH} + \beta \text{ ring (ring def.)} + \rho \text{NH}_2$
ν_{14}		812	7.14	1.02	$\gamma \text{CH} + \gamma \text{COC}$
ν_{15}		753	46.80	1.84	$\omega \text{NH}_2 + \text{ring puck.} + \gamma \text{CH}$
ν_{16}		730	2.04	6.29	$\omega \text{NH}_2 + \gamma \text{OCN} + \gamma \text{CH}$
ν_{17}		650	22.62	0.27	$\gamma \text{CH} + \gamma \text{ ring (ring puck.)}$
ν_{18}		583	219.63	0.57	ωNH_2
ν_{19}		412	1.43	1.59	$\tau \text{NH}_2 + \text{ring clock wise } (\beta \text{ ring})$
ν_{20}		312	35.85	0.23	τNH_2
ν_{21}		276	14.88	0.45	$\tau \text{NH}_2 + \gamma \text{ ring}$

The **ODDA** molecule has 11 atoms with 27 fundamental vibrations distributed as $\Gamma_{\text{vib}} = 14\text{A}' + 13\text{A}''$. All these fundamental vibrations are active in both Infrared and Raman.

Table 3.4. The theoretical vibrational frequencies (cm^{-1}), with its assignment for the ODDA molecule.

No.	Sym.	Freq. (cm^{-1})	IR intensity (km mol^{-1})	Raman activity ($\text{A}^4 \text{amu}^{-1}$)	Assignment
ν_1	A'	3664	66.35	40.78	$\nu_{\text{as}} \text{NH}_2$
ν_2		3567	10.83	325.90	$\nu_{\text{s}} \text{NH}_2$
ν_3		1717	183.42	76.00	$\nu_{\text{s}} \text{C=N} + \delta \text{NH}_2$
ν_4		1628	23.35	1.75	δNH_2
ν_5		1455	5.51	1.10	βCNH
ν_6		1156	0.22	23.47	$\rho \text{NH}_2 + \text{ring def.}$
ν_7		1008	27.46	6.79	$\rho \text{NH}_2 + \nu \text{NN}$
ν_8		968	15.17	5.92	$\rho \text{NH}_2 + \beta \text{N=CO}(\text{ring def.})$
ν_9		760	94.73	0.77	$\omega \text{NH}_2 + \text{ring puck.} (\gamma \text{ ring})$
ν_{10}		676	27.37	12.18	$\omega \text{NH}_2 + \nu_{\text{s}} \text{COC}$
ν_{11}		637	193.87	0.23	ωNH_2
ν_{12}		334	5.44	1.74	τNH_2
ν_{13}		264	66.74	0.92	τNH_2
ν_{14}		208	10.80	0.27	$\tau \text{NH}_2 + \gamma \text{COC}$
ν_{15}	A''	3664	24.78	62.99	$\nu_{\text{as}} \text{NH}_2$
ν_{16}		3566	61.26	26.91	$\nu_{\text{s}} \text{NH}_2$
ν_{17}		1658	390.41	8.59	$\delta \text{NH}_2 + \beta \text{ ring}$
ν_{18}		1602	81.27	0.54	$\delta \text{NH}_2 + \nu_{\text{as}} \text{C=N}$
ν_{19}		1339	140.63	0.76	$\rho \text{NH}_2 + \nu_{\text{as}} \text{COC} (\text{ring def.})$
ν_{20}		1145	4.50	3.70	ρNH_2
ν_{21}		981	41.28	0.06	$\nu_{\text{as}} \text{COC} (\beta \text{ ring})$
ν_{22}		786	13.16	3.12	$\omega \text{NH}_2 + \beta \text{ ring} (\text{ring def.})$
ν_{23}		704	26.91	1.06	$\omega \text{NH}_2 + \gamma \text{ ring} (\text{ring puck.})$
ν_{24}		629	179.66	0.43	$\rho \text{NH}_2 + \gamma \text{ ring}$
ν_{25}		483	8.91	0.45	$\rho \text{NH}_2 + \text{ring clock wise} (\beta \text{ ring})$
ν_{26}		357	12.38	0.22	$\gamma \text{NH} + \gamma \text{ ring}$
ν_{27}		222	0.05	0.29	τNH_2

The ODA, CODA molecules have a non-planar structure. Both molecules have 9 atoms with 21 normal modes of vibrations. AODCN, NODA molecules are non-planar, having 10, 11 atoms with 24, 27 normal modes of vibrations respectively. All these vibrations are active in Infrared and Raman.

Table 3.5. The theoretical vibrational frequencies, IR intensities and Raman activity with its assignment for the 21 normal modes of the CODA molecule.

No.	Sym.	Freq. (cm ⁻¹)	IR intensity (km mol ⁻¹)	Raman activity (A ⁴ amu ⁻¹)	Assignment
ν_1	A	3680	58.11	49.18	$\nu_{as} \text{NH}_2$
ν_2		3578	61.91	164.96	$\nu_s \text{NH}_2$
ν_3		1677	352.72	45.68	$\delta \text{NH}_2 + \nu_{as} \text{N}=\text{CN}$
ν_4		1614	37.28	13.15	$\delta \text{NH}_2 + \nu_s \text{C}=\text{N}$
ν_5		1551	145.90	19.41	$\nu_{as} \text{C}=\text{N} + \delta \text{NH}_2$
ν_6		1426	21.81	0.62	$\rho \text{NH}_2 + \nu_s \text{COC}$
ν_7		1167	182.49	3.37	$\nu \text{OC}=\text{N} + \rho \text{NH}_2$
ν_8		1138	0.03	16.51	ρNH_2
ν_9		1032	30.48	9.99	$\rho \text{NH}_2 + \nu \text{NN} + \beta \text{COC}$
ν_{10}		973	12.51	3.86	$\beta \text{ring} (\beta \text{N}=\text{CO})$
ν_{11}		969	14.53	5.17	$\rho \text{NH}_2 + \nu \text{CO} + \beta \text{C}=\text{NN}$
ν_{12}		758	25.87	2.95	$\omega \text{NH}_2 + \beta \text{ring} (\text{ring def.})$
ν_{13}		738	7.43	3.00	(ring pucker $\equiv \gamma \text{ring}$) + ωNH_2
ν_{14}		668	0.30	0.35	(ring pucker $\equiv \gamma \text{ring}$) + τNH_2
ν_{15}		582	247.26	0.71	ωNH_2
ν_{16}		490	2.07	6.30	$\nu \text{CCl} + \beta \text{ring}$
ν_{17}		459	2.23	2.39	$\tau \text{NH}_2 + \text{ring clock wise} (\beta \text{ring})$
ν_{18}		347	19.29	0.41	$\tau \text{NH}_2 + \gamma \text{ring}$
ν_{19}		287	13.46	0.57	τNH_2
ν_{20}		244	13.95	2.30	$\rho \text{NH}_2 + \beta \text{CICO}$
ν_{21}		182	1.58	0.20	$\omega \text{NH}_2 + \gamma \text{CICO}$

In ODDA molecule the normal following modes ν_{10} , ν_{19} , and ν_{21} (at frequencies 676, 1339, 981 cm⁻¹ respectively) are assigned as COC stretching vibration combined with many other different motions, **table 3.4**. The COC stretching vibration ν_6 , and ν_{11} modes in CODA molecule are mixed with other various motions, **table 3.5**.

Table 3.6. Theoretical vibrational frequencies (cm⁻¹), IR intensity, Raman activities and the assignment of the AODCN.

No.	Sym.	Freq. (cm ⁻¹)	IR intensity (km mol ⁻¹)	Raman activity (A ⁴ amu ⁻¹)	Assignment
ν_1	A	3703	73.15	45.96	$\nu_{as} \text{NH}_2$
ν_2		3594	101.19	180.31	$\nu_s \text{NH}_2$
ν_3		2339	20.39	527.38	$\nu \text{CC}=\text{N}$
ν_4		1670	478.99	54.41	$\delta \text{NH}_2 + \nu \text{C}=\text{N}$

ν_5		1595	133.43	38.27	$\delta \text{NH}_2 + \nu \text{C}=\text{N}$
ν_6		1554	1.40	152.28	$\nu_{\text{as}} \text{C}=\text{N}(\beta \text{ ring})$
ν_7		1435	26.45	10.32	$\rho \text{NH}_2 + \nu_{\text{a}} \text{COC}$
ν_8		1247	61.59	5.87	$\beta \text{ ring} + \rho \text{NH}_2$
ν_9		1122	23.28	51.82	$\rho \text{NH}_2 + \nu_{\text{as}} \text{C}=\text{NN}$
ν_{10}		1065	39.64	28.20	νNN
ν_{11}		988	14.39	17.33	$\beta \text{ ring}$
ν_{12}		983	4.19	12.86	$\rho \text{NH}_2 + \beta \text{ ring}$
ν_{13}		768	9.04	3.26	$\omega \text{NH}_2 + \gamma \text{ ring}$
ν_{14}		751	9.75	1.52	$\omega \text{NH}_2 + \gamma \text{ ring}$
ν_{15}		697	0.91	1.60	$\gamma \text{ ring}$
ν_{16}		579	3.01	4.05	$\beta \text{C}-\text{C}\equiv\text{N} + \text{ring clock wise}$
ν_{17}		568	0.53	2.55	$\beta \text{C}-\text{C}\equiv\text{N} + \tau \text{NH}_2 + \beta \text{ ring}$
ν_{18}		498	128.72	2.80	ωNH_2
ν_{19}		477	135.84	2.20	ωNH_2
ν_{20}		395	4.52	5.58	$\tau \text{NH}_2 + \text{ring clock wise}$
ν_{21}		333	57.03	0.26	τNH_2
ν_{22}		294	7.08	0.09	τNH_2
ν_{23}		161	4.75	4.12	$\rho \text{NH}_2 + \beta \text{CC}\equiv\text{N}$
ν_{24}		142	2.17	0.00	$\gamma \text{CC}\equiv\text{N} + \gamma \text{ ring} + \omega \text{NH}_2$

C-H vibrations: Generally, the C-H stretch vibrations are appeared in the range (3100-3000) cm^{-1} [23]. The data demonstrate that the CH symmetric and asymmetric stretching band values for **OD** are 3291, 3285 cm^{-1} respectively. These are coincidence with experimental results [47]. The CH stretching for **ODA** appears at 3290 cm^{-1} .

The vibrations of C-H out-of-plane bending (symmetric and asymmetric) for **OD** molecule are 872, and 841 cm^{-1} consequently. But the frequency at 1239 cm^{-1} can be assigned as C-H in-plane bending, which is agreed with experimental data. In the **ODA** molecule the same vibration is 1253 cm^{-1} .

Table 3.7. The theoretical vibrational frequencies (cm^{-1}), with its assignment for the **NODA** molecule.

No.	Sym.	Freq. (cm^{-1})	IR intensity (km mol^{-1})	Raman activity ($\text{A}^{\circ 4} \text{amu}^{-1}$)	Assignment
ν_1	A	3709	79.81	43.20	$\nu_{\text{as}} \text{NH}_2$
ν_2		3598	123.92	206.30	$\nu_{\text{s}} \text{NH}_2$
ν_3		1671	497.12	54.37	$\delta \text{NH}_2 + \text{ring def.}$
ν_4		1593	113.03	34.60	$\delta \text{NH}_2 + \nu_{\text{as}} \text{ONO} + \nu_{\text{s}} \text{C}=\text{N}$

ν_5	1590	291.59	20.64	$\delta \text{NH}_2 + \nu_{\text{as}} \text{ONO} + \text{ring def.}$
ν_6	1547	65.54	158.27	$\nu \text{C}=\text{N}$
ν_7	1453	90.51	10.66	$\rho \text{NH}_2 + \text{ring def.}$
ν_8	1360	286.66	294.51	$\nu \text{CN} + \nu_s \text{ONO}$
ν_9	1236	44.99	3.92	$\text{ring def.} + \rho \text{NH}_2 + \nu_s \text{ONO}$
ν_{10}	1111	67.14	105.97	$\rho \text{NH}_2 + \text{ring def.}$
ν_{11}	1065	63.71	59.92	$\rho \text{NH}_2 + \nu \text{N-N}$
ν_{12}	1001	9.55	11.16	$\nu_s \text{OC}=\text{N}$
ν_{13}	980	9.86	33.41	$\text{ring def.} + \rho \text{NH}_2$
ν_{14}	845	56.29	5.31	δONO
ν_{15}	777	0.30	0.86	$\omega \text{ONO} + \text{ring puck.}$
ν_{16}	755	16.01	3.93	ωNH_2
ν_{17}	743	12.11	2.62	$\omega \text{NH}_2 + \text{ring puck.}$
ν_{18}	636	9.23	0.11	$\text{ring puck.} + \tau \text{NH}_2$
ν_{19}	561	0.54	3.00	$\tau \text{NH}_2 + \text{ring clock wise} + \rho \text{ONO}$
ν_{20}	454	189.81	4.57	ρNH_2
ν_{21}	429	47.05	4.51	$\rho \text{NH}_2 + \text{ring def.}$
ν_{22}	389	9.13	10.79	τNH_2
ν_{23}	346	78.82	1.95	$\tau \text{NH}_2 + \text{ring puck.}$
ν_{24}	313	9.92	1.00	$\tau \text{NH}_2 + \text{ring puck.}$
ν_{25}	198	3.53	0.94	$\rho (\text{ONO} + \text{NH}_2)$
ν_{26}	156	1.07	0.41	$\omega (\text{NH}_2 + \text{ONO}) + \text{ring puck.}$
ν_{27}	61	3.21	0.25	$\tau \text{ONO} + \text{ring puck.}$

Ring vibrations: The N-N stretching vibrations for all molecules are not pure (mixed with several other motions), and the higher value is appeared in **NODA** and **AODCN** molecules are presented in **tables 3.7, 3.6** respectively.

The C=N symmetric and asymmetric stretching frequencies for **OD** molecule, are appeared at 1558, and 1534 cm^{-1} consequently. The $\nu_s \text{C}=\text{N}$ increases in oxadiazole derivatives according to the following order: **OD, NODA, ODA, CODA, AODCN, and ODDA**.

NH₂ vibrations: Always, the N-H stretch are located at the range (3500-3220) cm^{-1} [23]. The frequency of 3681 cm^{-1} is assigned as NH₂ asymmetric vibration, but the symmetric vibration is 3580 cm^{-1} in **ODA** molecule. This results are approximately equal to the frequencies of the **CODA** molecule (3680, 3578 cm^{-1}), and higher than the values of the similar vibrations in **ODDA** molecule (3664, and 3567 cm^{-1}). The symmetric and asymmetric stretching NH₂ vibrations are decreased according to

the following arrangement: **NODA**, **AODCN**, **ODA**, **CODA**, and **ODDA** compounds. There are three pure NH₂ twisting vibrations ν_{12} , ν_{13} , ν_{27} appeared at 334, 264, and 222 cm⁻¹ respectively in **ODDA** molecule, **table 3.4**. In **ODA**, and **CODA** molecules there is only one pure NH₂ twisting vibrations occurred at 312, and 287 cm⁻¹ consequently, **tables 3.3**, and **3.5**.

C-Cl vibrations: The C-Cl stretch vibration usually are presented in the region (850 -550) cm⁻¹ [23]. The frequency 490 cm⁻¹ is related to C-Cl stretching and associated with in-plane ring bending motion, **table 3.5**. The C-Cl in-plane bending is combined with rocking NH₂ vibration evaluated at 244 cm⁻¹. But the C-Cl out-of-plane vibration mixing with NH₂ wagging motion occurs at 182 cm⁻¹.

3.1.3- Electronic properties

3.1.3.1- Electronic absorption spectra

In this work six electronic transitions are computed using the Time-Dependent Density Functional Theory method (TD-DFT) [75–78]. These calculations have been performed on the lowest energy optimize structures which obtained from B3LYP/6-311++G (2d,2p) in gas phase and including the solvent water effect.

Quantum chemical computations are employed to investigate the electronic properties for the studied compounds. The calculations contain the electronic absorption spectra (UV-Visible), such as HOMO and LUMO orbital energies. The energy gap ($\Delta E_g = E_{\text{LUMO}} - E_{\text{HOMO}}$), absorption wavelengths (λ_{max}), and oscillator strengths (f) based on the optimized geometry in water, and gas phase with major contributions, **tables 3.8-3.13** and figures 3.2-3.7. The calculations involving the vertical excitation energies perform according to the Frank–Condon principle, which determine the maximum absorption peak (λ_{max}) in an UV–Vis spectrum.

There are no available data for all studied compounds except the **OD** molecule which was obtained by Kakitani using the improved self-consistent HMO theory [79]. Their values for λ max was 203 nm, and $f = 0.173$. It is well known that their method is less accurate than the DFT. In this study the maximum amount of f value with highest intensity is obtained for electronic transitions of **OD** molecule in gas phase at 179 nm, and in water at 178 nm, **table 3.8**. Based on the evident of oscillator strengths f values, the absorption maxima (λ max) can be evaluated, **tables 3.8-3.13**. The λ max (nm) (in gas phase) is decreased in the following configuration: **NODA (306 s)**, **AODCN (248 s)**, **ODDA (213 m)**, **CODA (211 m)**, **ODA (207 m)**, **OD (179 m)**.

The λ max (nm) (in water) decreased according to the following organization: **NODA (342 s)**, **AODCN (264 vs)**, **CODA (218 s)**, **ODDA (213 s)**, **ODA (210 m)**, **OD (178 m)**.

The symbols represent peak intensities ($s \equiv$ strong, $m \equiv$ medium, $w \equiv$ weak, and $vs \equiv$ very strong). The calculations of **ODA** molecule (in water) is predicted two electronic transitions. The highest one is presented at (210 nm) with an oscillator strength $f = 0.1617$, belong to the transition H \rightarrow L (with major contribution 69%).

Table 3.8. The absorption wavelength, energies, and oscillator strengths of the **OD** molecule.

TD-DFT/(B3LYP)/6-311++G(2d,2p) method							
Gas			Major contribution(%)	Water			Major contribution(%)
λ (nm)	E (eV)	f		λ (nm)	E (eV)	f	
210.09	5.9013	0.0000	H \rightarrow L (70%)	199.06	6.2285	0.0000	H-1 \rightarrow L (70%)
181.47	6.8321	0.0141	H-2 \rightarrow L (46%) H \rightarrow L+2 (54%)	178.25	6.9555	0.1449	H \rightarrow L (70%)
178.70	6.9382	0.1262	H-1 \rightarrow L (69%)	175.57	7.0617	0.0186	H-2 \rightarrow L (-43%) H-1 \rightarrow L+1(57%)
177.24	6.9951	0.0005	H-2 \rightarrow L (54%) H \rightarrow L+2(-46%)	171.31	7.2375	0.0004	H-2 \rightarrow L (57%) H-1 \rightarrow L+1(43%)
168.07	7.3771	0.0276	H \rightarrow L +1(70%)	162.89	7.6114	0.0000	H \rightarrow L+2 (70%)
167.59	7.3979	0.0000	H-1 \rightarrow L+1 (70%)	158.78	7.8085	0.0390	H-1 \rightarrow L+2 (69%)

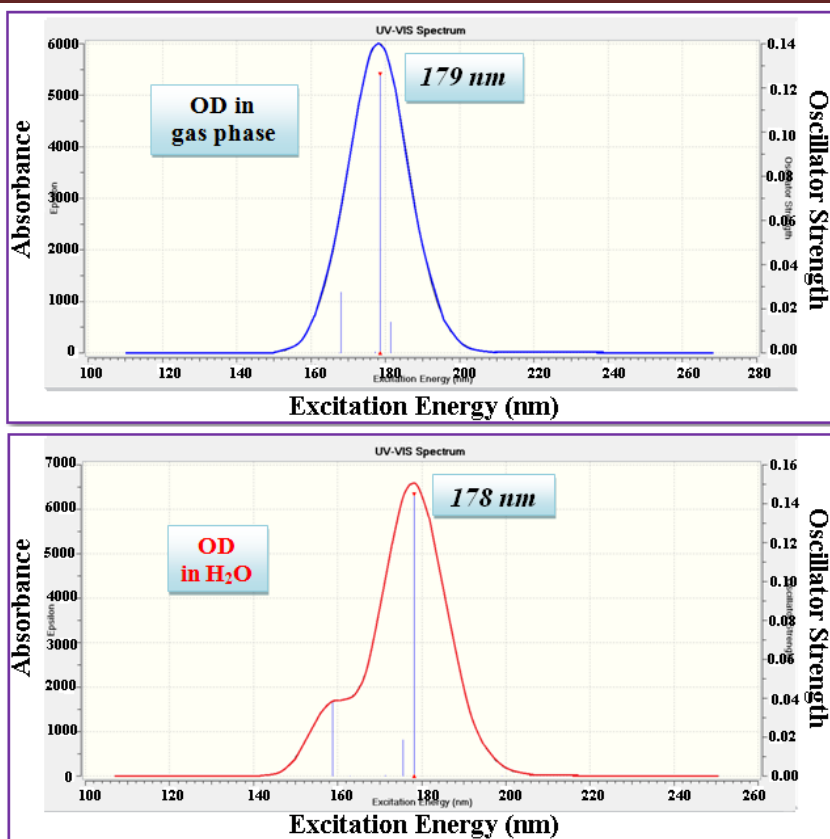


Figure 3.2. UV-visible spectra of OD molecule in gas phase and water.

The lower intense one is occurred at (179 nm) with $f = 0.1327$. But in gas phase only one transition is presented between $H \rightarrow L+1$, at λ_{\max} (207 nm), $f = 0.1437$, with 69% contribution, figure 3.3.

Table 3.9. The absorption wavelength, energies, and oscillator strengths of the ODA molecule.

TD-DFT/(B3LYP)/6-311++G(2d,2p)							
Gas			Major contribution(%)	Water			Major contribution(%)
$\lambda(\text{nm})$	$E(\text{eV})$	f		$\lambda(\text{nm})$	$E(\text{eV})$	f	
228.31	5.4305	0.0108	H \rightarrow L (70%)	211.67	5.8573	0.0103	H \rightarrow L+1(70%)
206.80	5.9954	0.1437	H \rightarrow L+1(69%)	210.22	5.8977	0.1617	H \rightarrow L(69%)
200.47	6.1848	0.0044	H-1 \rightarrow L (-23%) H-1 \rightarrow L+1(77%)	191.29	6.4816	0.0038	H-1 \rightarrow L(70%)
195.47	6.3428	0.0036	H \rightarrow L+2 (70%)	188.36	6.5822	0.0034	H \rightarrow L+2(70%)
188.71	6.5702	0.0096	H-1 \rightarrow L (77%) H-1 \rightarrow L+1(23%)	178.80	6.9343	0.1327	H-3 \rightarrow L(-6%), H-1 \rightarrow L+1(6%) H \rightarrow L+3(32%), H \rightarrow L+4(7%) H \rightarrow L+6(5%)
184.95	6.7038	0.0029	H \rightarrow L+3 (70%)	175.79	7.0531	0.0207	H \rightarrow L+3(-14%) H \rightarrow L+4(86%)

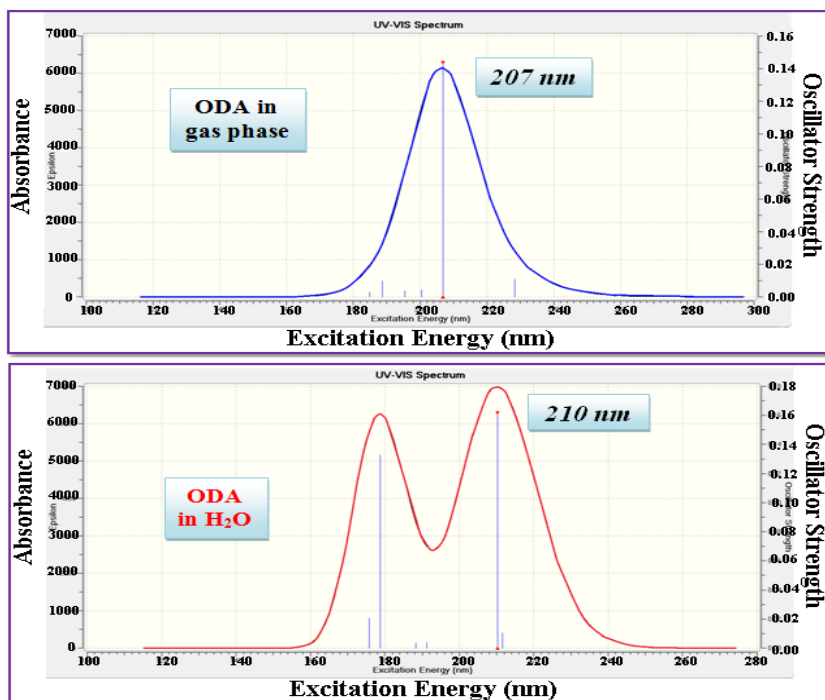


Figure 3.3.Theoretical UV VIS spectra of **ODA** molecule in gas phase and water.

The theoretical absorption bands (in water and gas phase) for **ODDA** both are appeared at the same wavelength (213 nm), with ($f = 0.2446$, $f = 0.1229$), which related to $H \rightarrow L+2$ transition with (70, 79% contribution) respectively. Another lower intense band is noticed in water at 185 nm with an oscillator strengths $f = 0.1160$, figure 3.4, **table 3.10**.

Table 3.10.The absorption wavelength, energies, and oscillator strengths of the **ODDA** molecule.

TD-DFT/(B3LYP)/6-311++G(2d,2p)							
Gas			Major contribution(%)	Water			Major contribution(%)
$\lambda(\text{nm})$	$E(\text{eV})$	f		$\lambda(\text{nm})$	$E(\text{eV})$	f	
263.20	4.7107	0.0046	H \rightarrow L (70%)	240.34	5.1586	0.0004	H \rightarrow L (70%)
247.86	5.0023	0.0091	H \rightarrow L+1(70%)	224.10	5.5325	0.0077	H \rightarrow L+1(70%)
213.05	5.8195	0.1229	H \rightarrow L+2(79%), H \rightarrow L+3(21%)	213.46	5.8082	0.2446	H \rightarrow L+2(70%)
205.70	6.0274	0.0824	H \rightarrow L+2(-20%), H \rightarrow L+3(80%)	195.53	6.3409	0.0128	H \rightarrow L+3 (70%)
198.28	6.2529	0.0043	H \rightarrow L+4 (70%)	186.80	6.6372	0.0056	H \rightarrow L+5 (69%)
195.81	6.3319	0.0135	H-1 \rightarrow L (70%)	185.31	6.6905	0.1160	H-4 \rightarrow L+2 (12%), H \rightarrow L+4(72%), H \rightarrow L+6(16%)

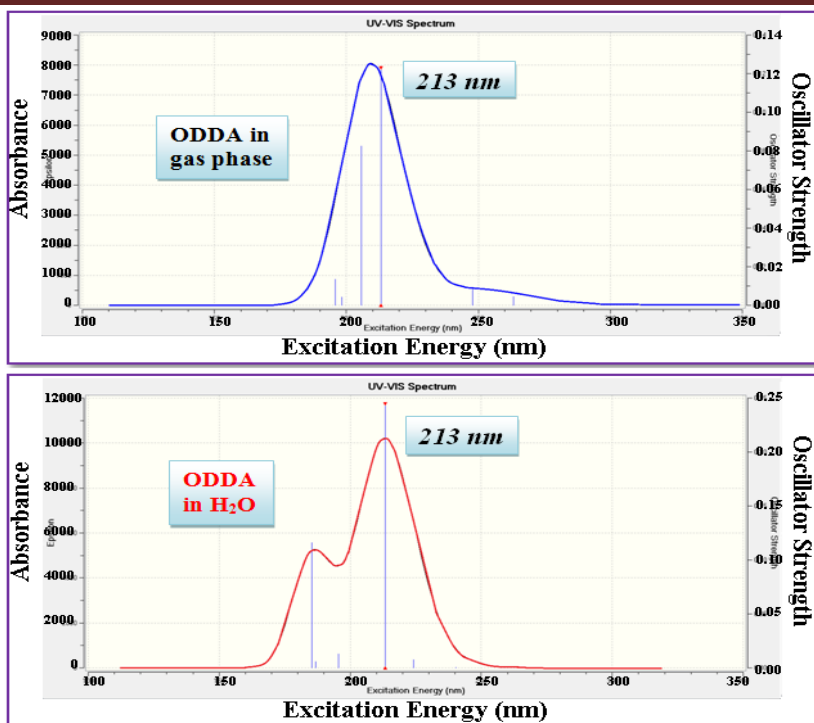
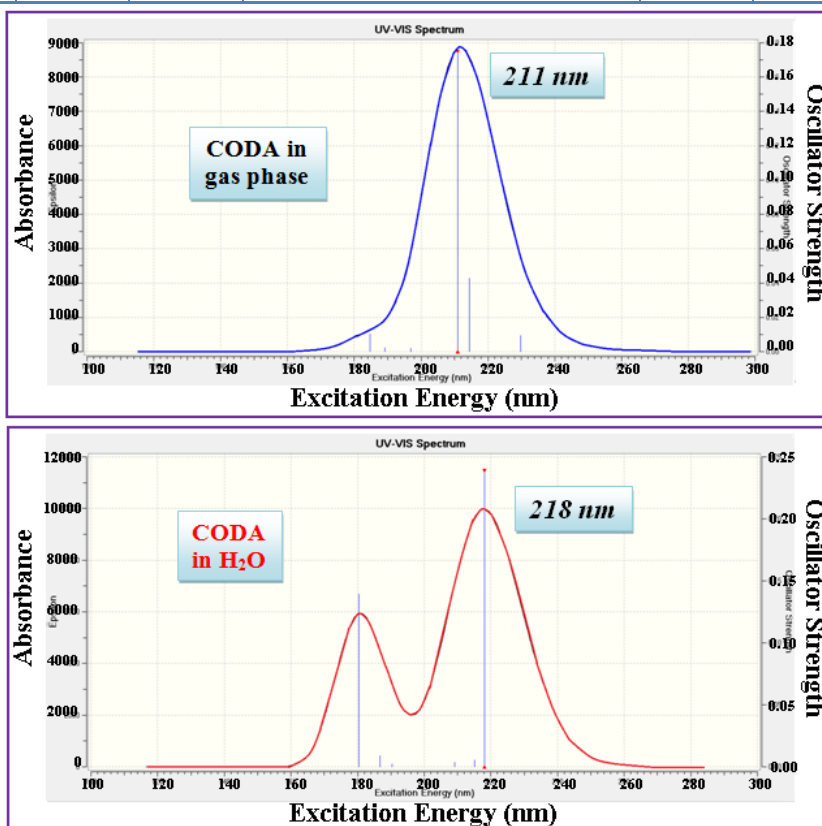


Figure 3.4. Theoretical electronic spectra for **ODDA** molecule in gas phase and water.

The computed electronic spectra in water for **CODA**, **AODCN**, and **NODA** molecules predict two absorption peaks. The most intense one are presented at (218, 264, 342 nm consequently) related to the transition between H→L, with a major contributions of 69, 70, and 71%. In gas phase there is only one absorption band for **CODA** at 211 nm. While the spectra for **AODCN** and **NODA** molecules show two absorption peaks, the high intense one belong to H→L transition, with 69 and 70% contributions respectively, figures 3.6, 3.7. The longest λ max value for **NODA** and **AODCN** molecules in series one molecules may be attributed to the extra conjugation than other compound in this series. A *red shift* of the λ max value with *hyperchromism* is noticed, during the changing from gas phase to the polar solvent (water), when H atoms in **OD** ring are replaced by NH₂, Cl, CN, and -NO₂ groups, **tables 3.9-3.13**. In the H → L transition a red shift take place in spectra of **AODCN** and **NODA** molecules, and the value of ΔE_g decrease when transfer from gas to water solution phase, **tables 3.12, 3.13**, and figures 3.6, 3.7.

Table 3.11. The absorption wavelength, energies, and oscillator strengths of the CODA molecule.

TD-DFT/(B3LYP)/6-311++G(2d,2p)							
Gas			Major contribution(%)	Water			Major contribution(%)
$\lambda(\text{nm})$	$E(\text{eV})$	f		$\lambda(\text{nm})$	$E(\text{eV})$	f	
229.77	5.3961	0.0092	H \rightarrow L (81%), H \rightarrow L+1 (19%)	218.09	5.6850	0.2390	H \rightarrow L (69%)
214.39	5.7830	0.0429	H \rightarrow L+1(37%), H \rightarrow L+2 (63%)	215.12	5.7634	0.0055	H \rightarrow L+1(87%),H \rightarrow L+2(-13%)
211.02	5.8754	0.1747	H \rightarrow L (-12%), H \rightarrow L+1 (55%) H \rightarrow L+2(-34%)	209.21	5.9264	0.0037	H \rightarrow L+1(14%),H \rightarrow L+2(86%)
197.02	6.2929	0.0019	H-1 \rightarrow L(-32%), H-1 \rightarrow L+1(68%)	190.41	6.5113	0.0023	H-1 \rightarrow L (70%)
189.10	6.5565	0.0022	H \rightarrow L+3 (70%), H \rightarrow L+4 (13%) H \rightarrow L+5 (17%)	186.70	6.6408	0.0091	H \rightarrow L+3(46%) H \rightarrow L+4(54%)
184.75	6.7109	0.0103	H-1 \rightarrow L (21%), H-1 \rightarrow L+1 (12%) H \rightarrow L+3 (-22%), H \rightarrow L+4 (50%) H \rightarrow L+5 (45%)	180.46	6.8705	0.1395	H-5 \rightarrow L (-10%), H \rightarrow L+3 (43%) H \rightarrow L+4(-38%), H \rightarrow L+6(9%)

**Figure 3.5.** UV-visible spectra of CODA molecule in gas phase and water.

A higher red shift is seen in AODCN, and NODA respectively. Usually, red shift is noticed in $\pi \rightarrow \pi^*$ transition, which due to the attraction polarisation force between the solvent and the absorber. This lower the energy levels for both the excited and unexcited states, but this effect is greater for the excited state.

Therefore the energy difference between the excited and unexcited state is reduced-causing a red-shift. But the blue shift is occur at the rest of series one molecules (**OD**, **ODA**, **ODDA**, and **CODA**) tables 3.8-3.11. This explain the occurrence of $n \rightarrow \pi^*$ transition in the spectrum for these four molecules, which may be due to the existence of the hydrogen bonding between water and these four molecules. This occurs from the increase solvation of the lone pair, which decrease the energy of the n orbital, then ΔE_g increased.

Table 3.12. The absorption wavelength, energies, and oscillator strengths of the AODCN molecule.

TD-DFT/(B3LYP)/6-311++G(2d,2p)							
Gas			Major contribution(%)	Water			Major contribution(%)
$\lambda(\text{nm})$	$E(\text{eV})$	f		$\lambda(\text{nm})$	$E(\text{eV})$	f	
247.99	4.9996	0.2971	H→L (69%)	264.11	4.6944	0.3322	H→L (70%)
238.67	5.1949	0.0057	H-1→L (70%)	235.65	5.2614	0.0032	H-1→L (75%), H→L+1(25%)
227.13	5.4586	0.0032	H→L+1(78%), H→L+2(22%)	231.44	5.3570	0.0013	H-1→L (-25%),H→L+1(75%)
207.94	5.9626	0.0048	H→L+1(-23%),H→L+2(77%)	197.82	6.2675	0.0065	H→L+2 (68%)
196.09	6.3228	0.0009	H-3→L (-16%), H-2→L(84%)	194.66	6.3694	0.0016	H-3→L(40%),H-2→L(50%) H→L+1(10%)
185.17	6.6957	0.0159	H-1→L+1(71%) H-1→L+2(14%) H→L+3(15%)	182.65	6.7882	0.0647	H-3→L(-16%), H-2→L(12%) H-1→L+1(11%) H→L+3(42%),H→L+4(18%)

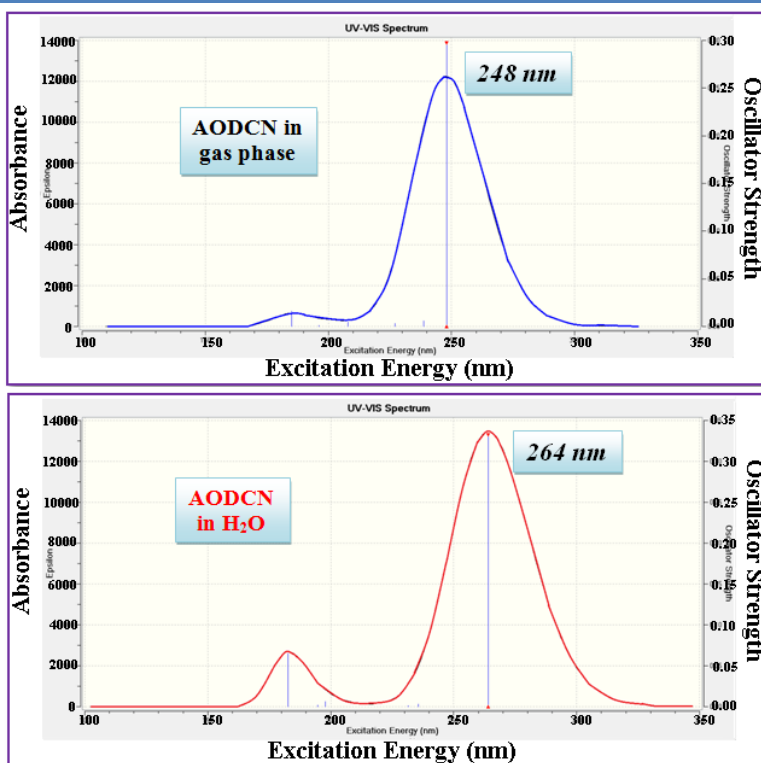
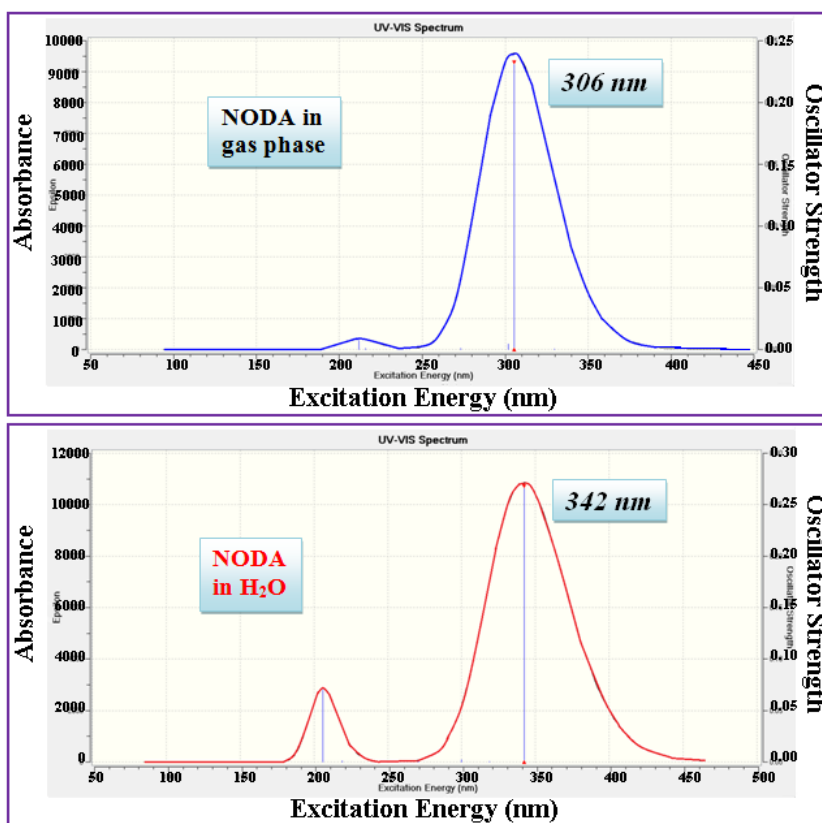


Figure 3.6. Theoretical UV-Vis spectra of AODCN molecule in gas phase and water.

Table 3.13. The absorption wavelength, energies, and oscillator strengths of the NODA molecule.

TD-DFT/(B3LYP)/6-311++G(2d,2p)							
Gas			Major contribution(%)	Water			Major contribution(%)
$\lambda(\text{nm})$	$E(\text{eV})$	f		$\lambda(\text{nm})$	$E(\text{eV})$	f	
329.61	3.7615	0.0003	H-2→L(79%),H-1→L(-21%)	342.27	3.6224	0.2676	H→L (71%)
305.54	4.0578	0.2327	H→L (70%)	318.90	3.8878	0.0007	H-2→L(75%),H-1→L(25%)
301.97	4.1059	0.0043	H-4→L (33%),H-2→L(14%) H-1→L(53%)	299.93	4.1338	0.0020	H-4→L(26%),H-1→L(56%) H-2→L(-18%)
273.12	4.5396	0.0008	H-4→L(57%),H-2→L(-11%) H-1→L(-33%)	270.54	4.5829	0.0004	H-4→L(63%), H-2→L(10%) H-1→L(-27%)
215.66	5.7490	0.0009	H-5→L (69%)	219.15	5.6575	0.0013	H-6→L(21%),H-5→L(79%)
211.91	5.8509	0.0077	H→L+1 (70%)	206.18	6.0133	0.0703	H-7→L(16%),H-6→L(12%) H-3→L(72%)

**Figure 3.7.** Theoretical electronic spectra for NODA molecule in gas phase and water.

Molecular Orbital: The HOMO represents the ability to donate an electron, LUMO as an electron acceptor represents the ability to obtain an electron. The HOMO - LUMO gap energies for all molecules were calculated using DFT/B3LYP method with 6-311++G(2d,2p) level. It is well known that the smaller the ΔE_g express the charge transfer interactions taking place within the molecule [80]. The HOMO and LUMO are the most important orbitals effecting molecular chemical stability [81], The energy gap between them specifies the molecule kinetic stability, chemical reactivity, optical polarizability, and chemical hardness–softness [82,83].

The calculated ΔE_g for all molecules under study in gas phase changing in the following order **NODA < AODCN < ODDA < CODA < ODA < OD** (4.4092, 5.3523, 5.5151, 6.2381, 6.3124, 7.2781 eV respectively), figure 3.8.

The calculated ΔE_g in solvent water changing in the following order **NODA < AODCN < ODDA < CODA < ODA < OD** (3.9842, 5.1161, 6.0139, 6.3241, 6.5422, 7.4868 eV respectively), figure 3.9. The low values mean these molecules are more reactive and less stable. There are the same sequences in the two mentioned progression.

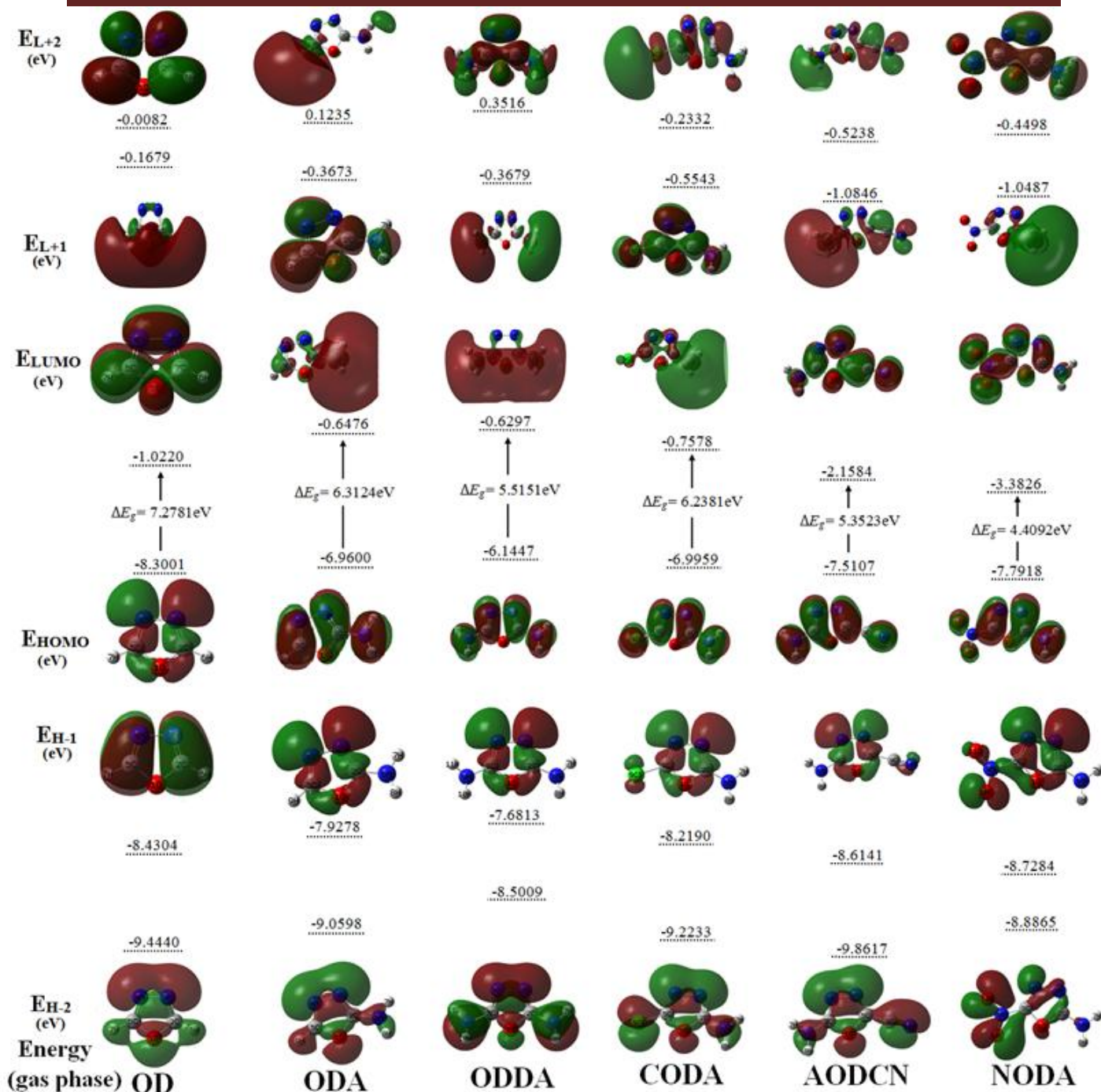


Figure 3.8. The energy with molecular orbital geometry for the OD, ODA, ODDA, CODA, AODCN, and NODA compounds, in gas phase.

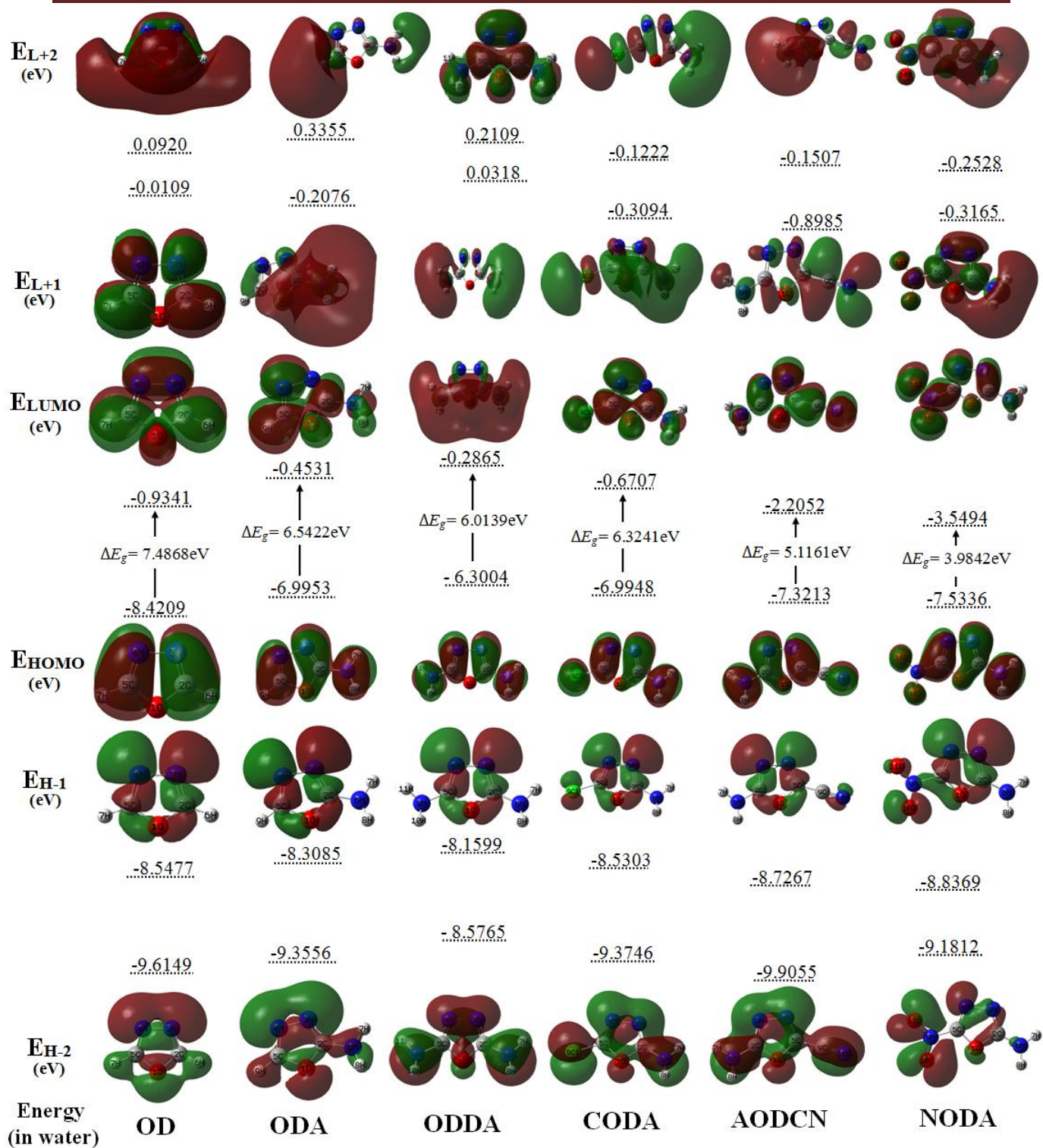


Figure 3.9. The energy with molecular orbital geometry for the OD, ODA, ODDA, CODA, AODCN, and NODA compounds, in solvent water.

3.1.3.2- Molecular electrostatic potential (MEP)

MEP calculations are useful in describing the molecular structure together with its physiochemical properties [84]. It provides knowledge about the net electrostatic effect at any point in space surrounding a molecule, which is generated at that point due to the total charge distribution of the molecule. The electrostatic potential surface electron (density isosurface map) displays molecular size, shape, reactive positions and charge density (positive, negative and neutral zone in terms of colour scaling). The red colour describes the area of maximum negative electrostatic potential, which offers a site for the electrophilic attack. The blue colour indicates the maximum positive area, referred to as the nucleophilic attack. While the green represents the parts close to neutral. The MEP increases according to the following order: red < orange < yellow < green < blue [85]. Furthermore, the MEP aids in determining the reactivity, hydrogen bonding interactions, and the relative polarity for molecules [72] (Luque *et al.*, 2000).

The colours of **OD** maps are ranged between -4.700 (deep red) and $+4.700$ (deep blue), but the rest of the molecules range between the mean value of $(-7$ to $-9)$, and $(+7$ to $+9)$, figure 3.10. Regions of negative $V(r)$ are usually related to the lone pair of electronegative atoms, as seen from the MEP illustration [86]. The MEP maps for all series of molecules show a negative potential over the electronegative atoms (nitrogen ring atoms), and positive potential over the carbon and hydrogen atoms. From these results, it can be concluded that the carbon atoms indicate the strongest attraction and the nitrogen ring atoms are associated with the strongest repulsion. Changing H atoms to NH_2 groups in compounds **ODA**, and **ODDA** shows a blue colour on NH_2 , which means that NH_2 has a positive potential. When substituted with electron-withdrawing groups such as Cl, NO_2 , and CN, the colour on the nitrogen ring atoms approaches yellow, which represents a moderate negative potential.

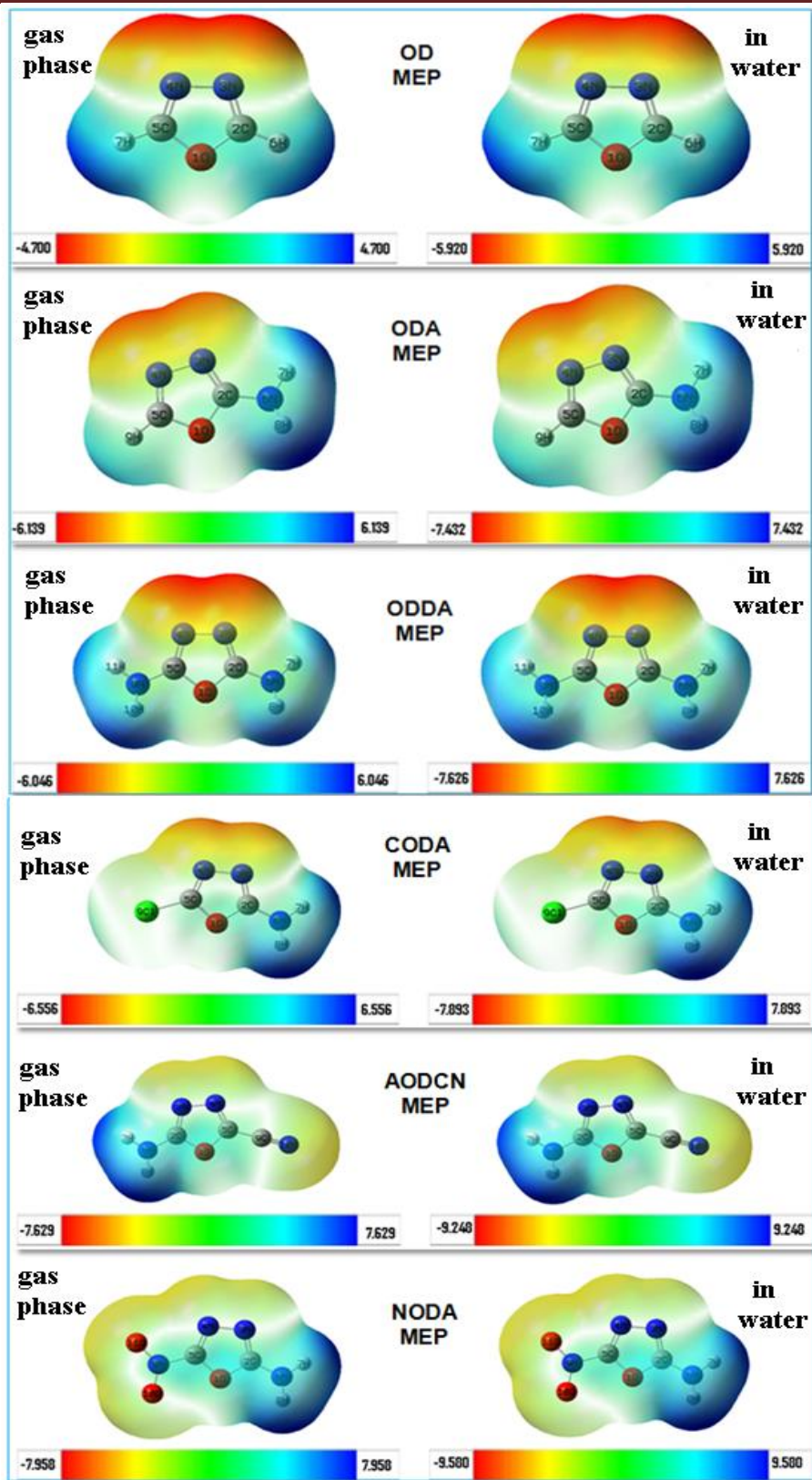


Figure 3.10. The Molecular Electrostatic Potentials.

3.1.4- NMR Spectroscopy

The theoretical NMR results for compounds in series one which are calculated (with the aid of Gaussian program, using the GIAO method [87,88] at the B3LYP/6-311++G(2d,2p) level) from the optimized structures in gas phase, and the DMSO using as a solvent. In order to express the chemical shifts, δ (ppm), the tetramethylsilane (TMS) compound is used as a reference.

Atom	GIAO(B3LYP)/6-311++G (2d,2p)	
	Gas phase	DMSO
O	238.63	247.63
C	104.87	111.17
N	372.53	347.67
H	3.22	3.08

Table 3.14. The calculated NMR chemical shifts in ppm for OD molecule in (gas phase, and DMSO solvent).

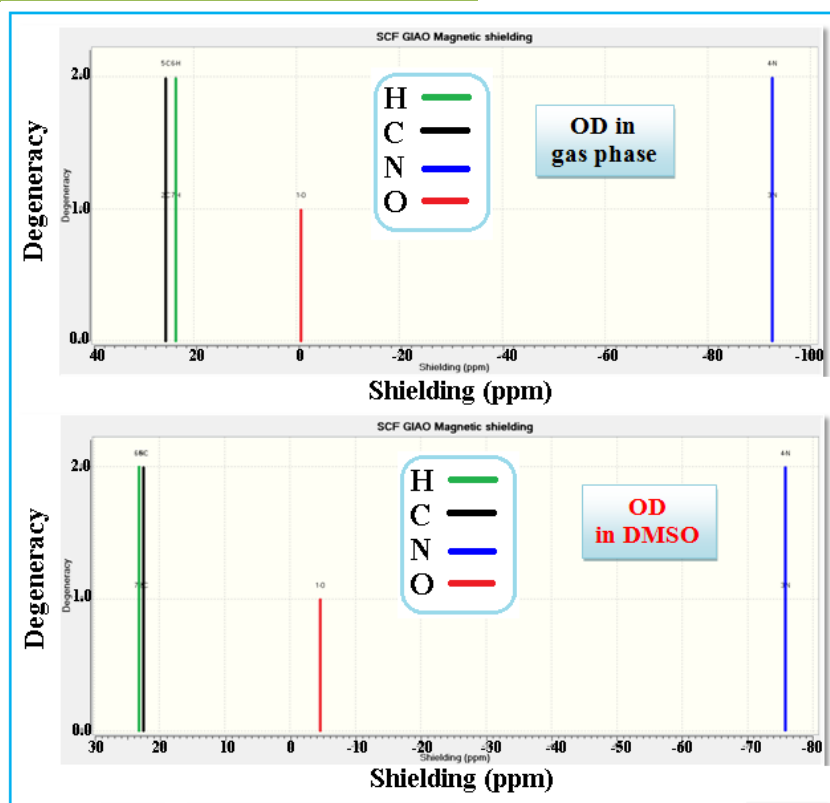


Figure 3.11. NMR spectra of OD molecule in gas phase and DMSO solvent.

The NMR spectra along with the shielding values are presented in figures 3.11 - 3.16, and the predicted chemical shift listed in **tables 3.14 - 3.19**, for all molecules in this series. Since the theoretical calculations are carried out in the isolated gas phase molecule, therefore the theoretical chemical shift values is expected to be slightly deviated from the experimental results. Usually the high shielding electrons show down field, and vice versa.

Atom	GIAO(B3LYP)/6-311++G (2d,2p)	
	Gas phase	DMSO
O(1)	155.41	164.34
C(2)	87.87	91.21
N(3)	257.51	233.35
N(4)	347.31	324.46
C(5)	82.05	88.21
N(6)	74.51	73.85
H(7)	11.88	11.96
H(8)	12.11	12.38
H(9)	2.22	2.07

Table 3.15. The calculated NMR chemical shifts in ppm for ODA molecule in (gas phase, and DMSO solvent).

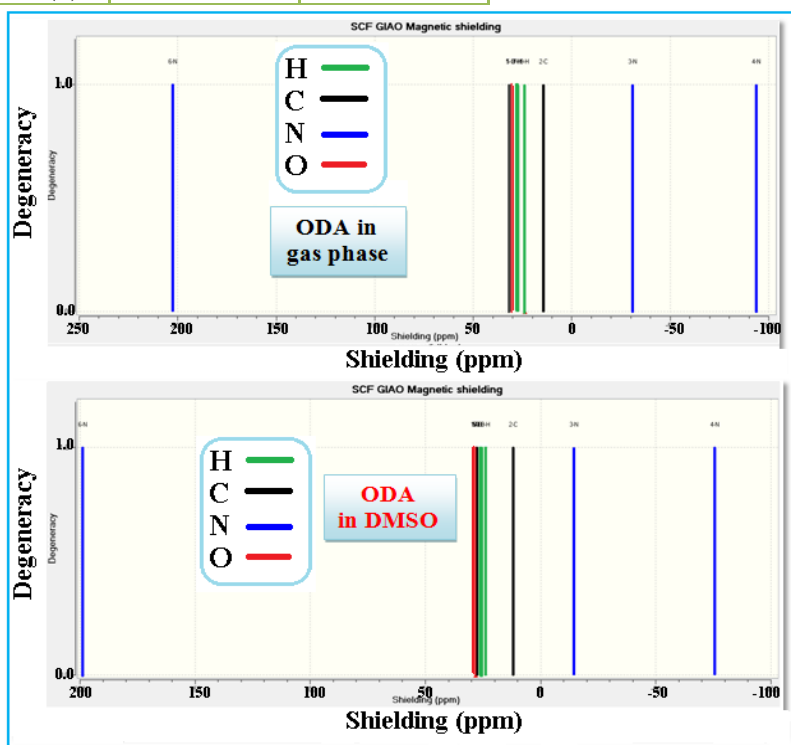


Figure 3.12. NMR spectra of ODA molecule in gas phase and DMSO solvent.

In **OD** molecule the chemical shift values for the two protons bonding with C₂ and C₅ (oxadiazole ring) have the same value (3.22 ppm), this may be associated to the molecular symmetry. While in **ODA** molecule the proton in C₅ position shows lower chemical shift value 2.22 ppm (higher shielding), which due to the substituting –NH₂ group instead of H atom at C₂ position.

Atom	GIAO(B3LYP)/6-311++G (2d,2p)	
	Gas phase	DMSO
O(1)	118.86	126.28
C(2)	84.59	87.13
N(3)	237.10	215.30
N(4)	306.79	289.91
C(5)	105.48	99.28
N(6)	76.20	75.56
H(7)	12.03	12.12
H(8)	11.84	12.10
Cl(9)	487.77	493.53

Table 3.16. The calculated NMR chemical shifts in ppm for CODA molecule in (gas phase, and DMSO solvent).

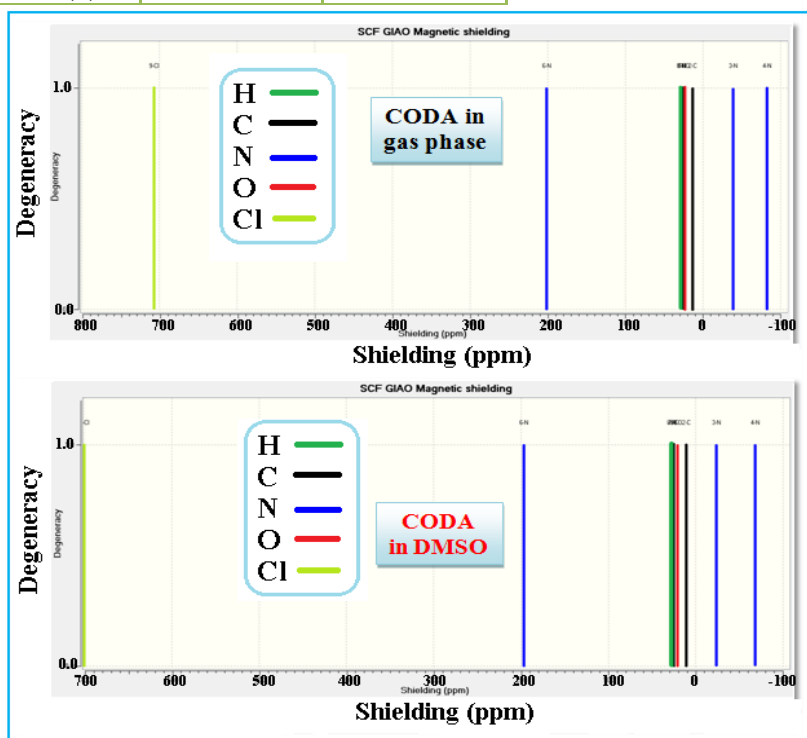


Figure 3.13. NMR spectra of CODA molecule in gas phase and DMSO solvent.

The chemical shift for two protons which belongs to $-\text{NH}_2$ group in series one molecules (except **OD**) is ranged form 11.72 – 12.06 ppm.

The chemical shift values for both carbon atoms (C_2 and C_5 in oxadiazole ring belong to **OD** molecule) is 104.87 ppm. While in **ODA** are 87.87 and 82.05 ppm respectively, this correlated to the $-\text{NH}_2$ group. In **ODDA** molecule the δ value C_2 and C_5 atoms is lower to 71.7 ppm due to present of two $-\text{NH}_2$ groups. The increase in the shielding of electrons is due to the $-\text{NH}_2$ group, which is behaved as an electron donating group. But in **AODCN** molecule the chemical shifts are 84.1 and 77.3 ppm, because the Presence of $-\text{NH}_2$ and $-\text{C} \equiv \text{N}$ groups respectively.

Atom	GIAO(B3LYP)/6-311++G (2d,2p)	
	Gas phase	DMSO
O(1)	91.81	100.65
C(2)	71.76	75.67
N(3)	221.31	198.68
N(6)	75.10	75.20
H(7)	11.91	12.07
H(8)	12.06	12.40

Table 3.17. The calculated NMR chemical shifts in ppm for **ODDA** molecule in (gas phase, and DMSO solvent).

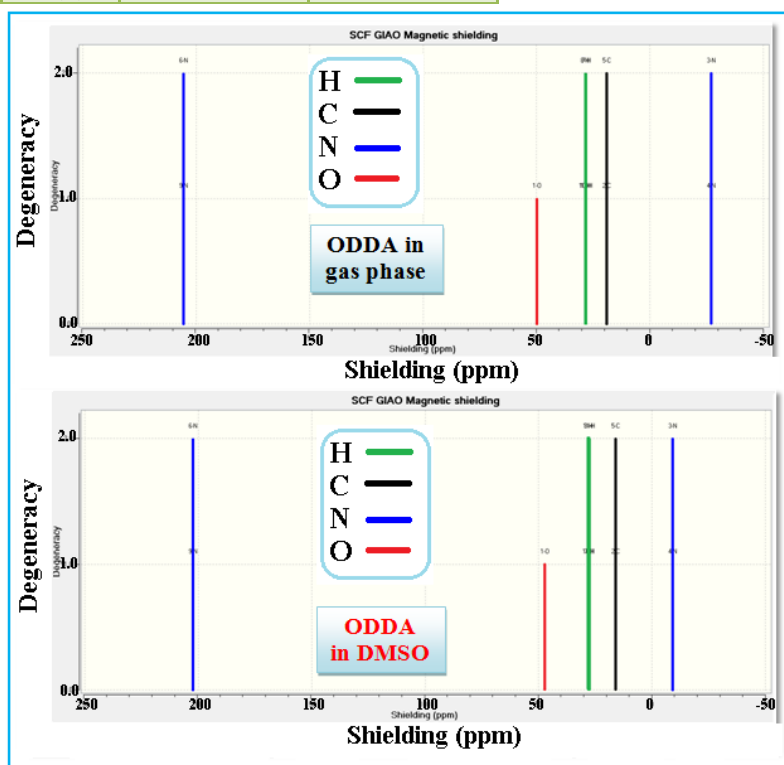


Figure 3.14. NMR spectra of **ODDA** molecule in gas phase and DMSO solvent.

The lowest value of δ , for the C₅ atom due to the direct bonding with the electron withdrawing group ($-C \equiv N$). In **NODA** molecule the δ values belong these two atoms are 80.64 and 80.58 ppm respectively, which related to the presence of $-NH_2$ and $-NO_2$ groups. Generally, the chemical shift for ^{13}C nucleus is much higher than proton because electron clouds surrounding ^{13}C nucleus are denser, therefore the shielding effects are increased [33].

Atom	GIAO(B3LYP)/6-311++G (2d,2p)	
	Gas phase	DMSO
O(1)	152.73	156.60
C(2)	84.17	86.80
N(3)	268.26	253.56
N(4)	412.85	406.54
C(5)	77.32	75.31
N(6)	75.79	74.38
H(7)	11.72	11.65
H(8)	11.87	12.01
C(9)	321.68	322.13
N(10)	443.15	417.77

Table 3.18. The calculated NMR chemical shifts in ppm for AODCN molecule in (gas phase, and DMSO solvent).

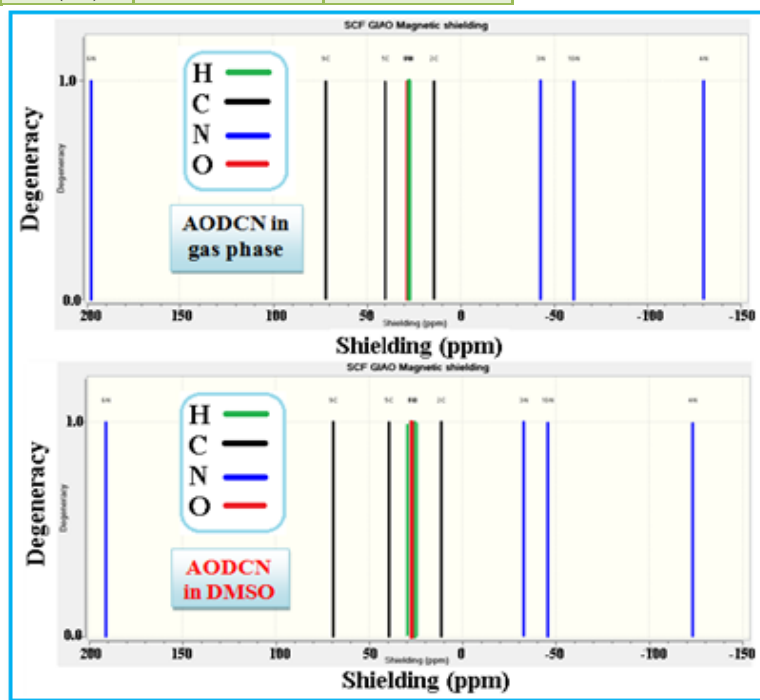


Figure 3.15. NMR spectra of AODCN molecule in gas phase and DMSO solvent.

The oxygen atom O₁ in oxadiazole ring shows higher chemical shift value (239 ppm) of **OD** molecule. The chemical shift for O₁ atom in all molecules under study (in gas phase, and DMSO solvent) increases according to the following order **ODDA**, **CODA**, **AODCN**, **ODA**, **NODA**, and **OD**. The **ODDA** has the lowest value because of the substitution two amine groups in the positions of C₂ and C₅ (electron donating group increase the shielding of electrons). The rest molecules have electron withdrawing groups in these positions.

Atom	GIAO(B3LYP)/6-311++G (2d,2p)	
	Gas phase	DMSO
O(1)	160.31	160.95
C(2)	80.64	82.36
N(3)	252.58	240.83
N(4)	407.50	401.85
C(5)	80.58	74.25
N(6)	75.63	73.29
H(7)	11.54	11.42
H(8)	11.96	11.97
N(9)	228.33	234.17
O(10)	673.17	647.34
O(11)	701.98	652.09

Table 3.19. The calculated NMR chemical shifts in ppm for **NODA** molecule in (gas phase, and DMSO solvent).

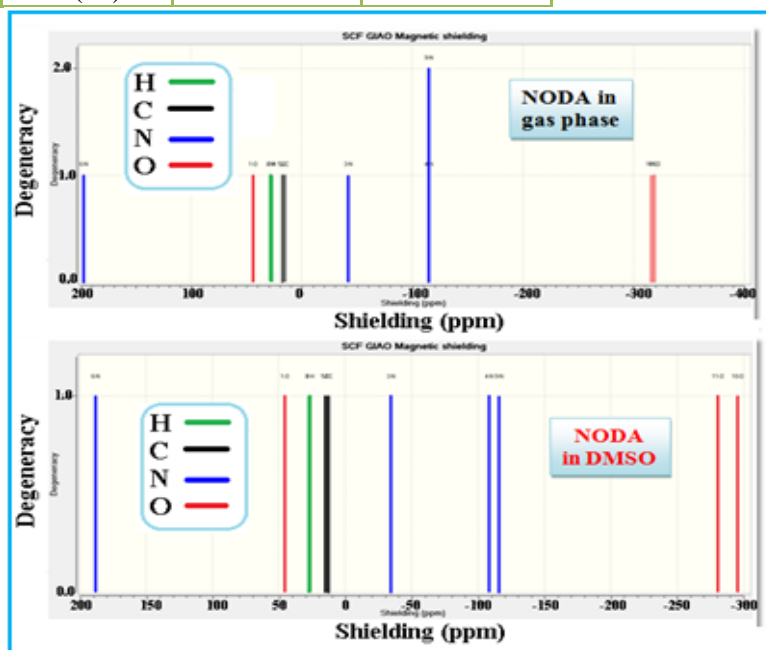


Figure 3.16. NMR spectra of **NODA** molecule in gas phase and DMSO solvent.

3.2- Results and Discussion of series two

Series two consist the following molecules: **POD**, **PODT**, **PODA**, **CPODA**, and **DPOD**.

3.2.1- Molecular geometry

The molecular structure and atom numbering for all molecules belong to series two are presented in figure 3.17.

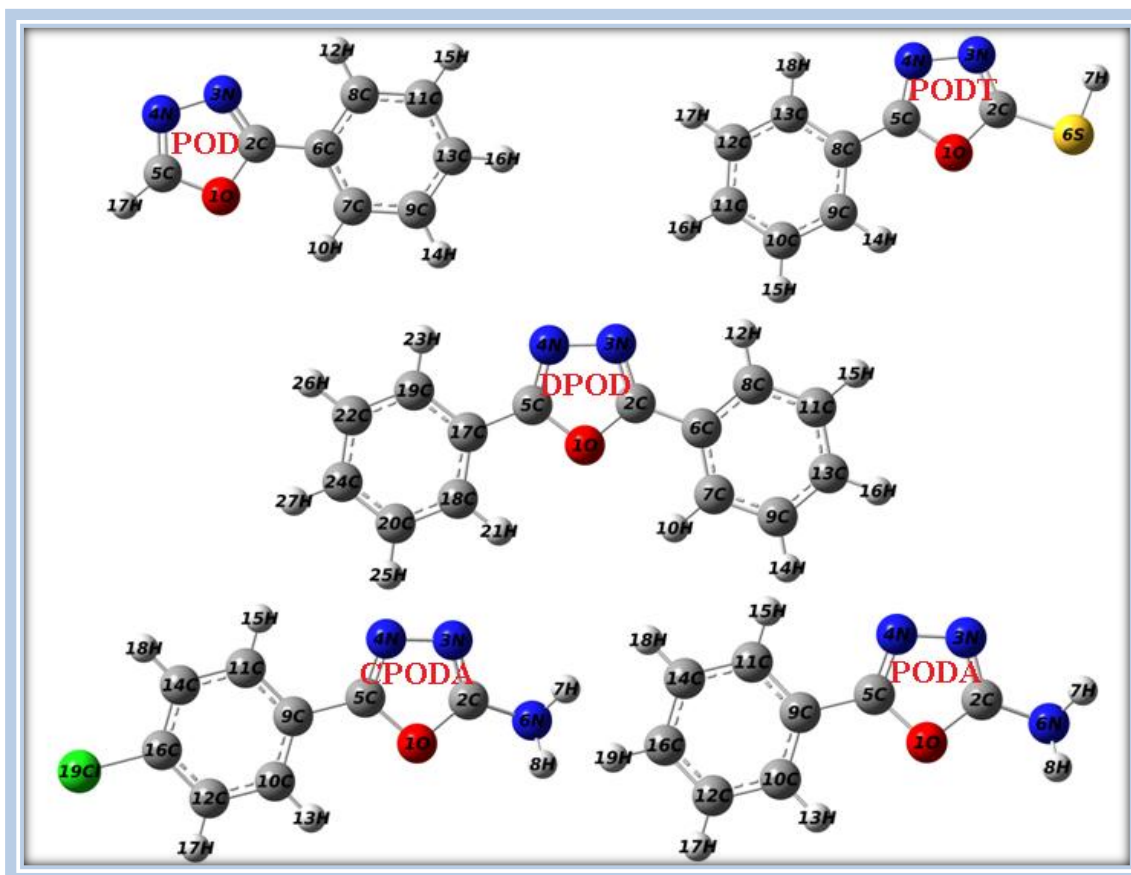


Figure 3.17. Optimized structures for the studied compounds (belong to series two) along with its atom numbering scheme. [A= phenyl ring, B= 1, 3, 4-oxadiazole ring].

Determining the optimized molecular geometry is the first action of the computational work. The optimized geometric parameters such as bond length, bond angles and dihedral angles of the molecules are computed by using DFT and B3LYP method with basis set 6-311++G (2d,2p) levels. The results are

summarized in **table 3.20**. The **PODT**, **PODA**, and **CPODA** molecules are belong to C_1 point group, while **POD**, **DPOD** molecules belongs to C_s , and C_{2v} point group respectively.

The results of optimized bond length and dihedral angles for **PODT** molecule are slightly smaller than the experimental values [89]. This is due to the fact that the theoretical calculation is done for isolated molecule in gaseous state, while the experimental results are determined in solid state. **PODT** results show a good agreement with other theoretical work using DFT methods with the basis set 6-311++G** [55].

In **PODA** molecule, the bond length of $C_2=N_3$ is (1.294 \AA) which is longer than $C_5=N_4$ (1.289 \AA), this may be due to adjacent of $C_5=N_4$ bond to the phenyl ring, which causing conjugation between benzene and oxidiazole ring. The geometrical parameters results of **PODA** molecule are coincidence with other DFT /6-311G** basis set [54].

This work calculations indicate that the bond length of C-Cl in the **CPODA** molecule is (1.754 \AA , **table 3.20**) which is longer than the C-Cl bond in **CODA** molecule (1.702 \AA , **table 3.1**). There are no previous theoretical and experimental data for geometrical parameters about the **DPOD**, and **CPODA** molecules.

A good match is obtained in comparing the **POD** molecule results with other theoretical work using HF and DFT methods / basis set 6-31++G(d,p) [51].

The dihedral angles reveal that the tested molecules are planar except **PODA**, and **CPODA**, due to the presence of NH_2 group.

Table 3.20. The optimized geometry data of **PODT**, **PODA**, **CPODA**, **DPOD**, and **POD** molecules, plus the available theoretical and experimental data.

Structural parameter	Exp. [89]	DFT 6-311 ++G** other work [55]	DFT 6-311 ++G (2d,2p) This work	DFT 6-311 G** other work [54]	DFT/6-311++G(2d,2p) This work				HF 6-31 ++G (d,p) other work [51]	DFT 6-31 ++G (d,p) other work [51]
		PODT		PODA		CPODA	DPOD	POD		
<i>Bond length in (Å)</i>										
O ₁ -C ₂	1.367	1.357	1.356	1.364	1.354	1.355	1.366	1.368	1.338	1.360
O ₁ -C ₅	1.367	1.357	1.376	1.369	1.383	1.382	1.366	1.357	-	-
C ₂ =N ₃	1.328	1.293	1.290	1.289	1.294	1.294	1.296	1.296	1.263	1.292
C ₂ -S ₆	1.657	1.752	1.750							
C ₅ =N ₄	1.285	1.294	1.292	1.285	1.289	1.289	1.296	1.284		
C ₂ -N ₆				1.328	1.366	1.365				
C ₂ -C ₆							1.456	1.457	1.467	1.460
N ₃ -N ₄	1.376	1.396	1.397	1.413	1.399	1.398	1.386	1.397	1.380	1.396
C ₅ -C ₈	1.454	1.457	1.455							
C ₅ -H ₁₇								1.075		
C ₆ -C ₇							1.399	1.398		
C ₆ -C ₈							1.401	1.400		
C ₇ -C ₉							1.389	1.389		
C ₇ -H ₁₀							1.080	1.080	1.075	1.085
C ₈ -C ₁₁							1.386	1.387		
C ₈ -H ₁₂							1.080	1.080		
S ₆ -H ₇			1.342							
C ₈ -C ₉			1.398							
C ₈ -C ₁₃			1.400							
C ₉ -C ₁₀			1.389	1.376	1.399	1.398				
C ₉ -C ₁₁				1.387	1.401	1.401				
C ₁₀ -C ₁₂				1.382	1.390	1.388				
C ₁₀ -H ₁₃				0.930	1.080	1.080				
C ₁₁ -C ₁₄				1.382	1.386	1.385				
C ₁₁ -C ₁₃							1.394	1.393		
C ₁₁ -H ₁₅				0.930	1.080	1.080	1.081	1.081		
C ₁₂ -C ₁₆				1.364	1.391	1.388				
C ₉ -C ₁₃							1.391			
C ₉ -H ₁₄			1.080				1.081	1.081		
C ₁₀ -C ₁₁			1.391							
C ₁₀ -H ₁₅			1.081							
C ₁₁ -C ₁₂			1.393							
C ₁₁ -H ₁₆			1.081							
C ₁₂ -C ₁₃			1.386							
C ₁₂ -H ₁₇			1.081	0.930	1.081	1.079				

C ₁₄ -C ₁₆				1.366	1.394	1.391				
C ₁₄ -H ₁₈				0.930	1.081	1.080				
C ₁₆ -H ₁₉				0.930	1.081					
C ₁₆ -Cl ₁₉						1.754				
C ₁₃ -H ₁₆							1.081	1.081		
C ₁₃ -H ₁₈			1.080							
C ₁₇ -C ₁₈							1.399			
C ₁₇ -C ₁₉							1.401			
C ₁₈ -C ₂₀							1.389			
C ₁₈ -H ₂₁							1.080			
C ₁₉ -C ₂₂							1.386			
C ₁₉ -H ₂₃							1.080			
C ₂₀ -C ₂₄							1.391			
C ₂₀ -H ₂₅							1.081			
C ₂₂ -C ₂₄							1.394			
C ₂₂ -H ₂₆							1.081			
C ₂₄ -H ₂₇							1.081			
C ₅ -C ₉				1.464	1.455	1.454				
N ₆ -H ₇				0.894	1.008	1.008				
N ₆ -H ₈				0.948	1.008	1.007				
<i>Bond angle in degree</i>										
C ₂ -O ₁ -C ₅	106.0	102.2	102.2	102.9	102.1	102.1	102.9	102.3	102.8	102.4
O ₁ -C ₂ =N ₃	104.8	113.3	113.3	112.6	113.5	113.5	111.7	111.8		
O ₁ -C ₂ -C ₆							119.8	119.6	119.6	119.6
O ₁ -C ₂ -S ₆	123.9	117.0	116.9							
N ₃ =C ₂ -C ₆							128.5	128.6	128.6	128.7
N ₃ =C ₂ -S ₆	-	129.7	129.7							
O ₁ -C ₂ -N ₆				117.1	117.8	117.8				
N ₃ =C ₂ -N ₆				130.2	128.6	128.6				
C ₂ =N ₃ -N ₄	113.1	105.7	105.7	105.8	105.5	105.5	106.8	106.7	106.1	106.0
N ₃ -N ₄ =C ₅	103.1	107.2	107.1	107.0	107.4	107.3	106.8	105.9		
O ₁ -C ₅ =N ₄	113.0	111.6	111.6	111.8	111.5	111.6	111.7	113.3	112.7	113.1
O ₁ -C ₅ -C ₉				118.3	119.2	119.3				
O ₁ -C ₅ -C ₁₇							119.8			
O ₁ -C ₅ -H ₁₇								118.2	118.7	118.2
N ₄ =C ₅ -H ₁₇								128.5	128.6	128.7
N ₄ =C ₅ -C ₁₇							128.5			
N ₄ =C ₅ -C ₉				129.9	129.3	129.1				
C ₂ -C ₆ -C ₇							121.2	121.1	120.8	121.1
C ₂ -C ₆ -C ₈							119.2	119.2		
C ₇ -C ₆ -C ₈							119.6	119.7		
C ₆ -C ₇ -C ₉							120.1	120.0		
C ₆ -C ₇ -H ₁₀							119.8	119.8		
C ₉ -C ₇ -H ₁₀							120.1	120.2		
C ₆ -C ₈ -C ₁₁							120.0	119.9		
C ₆ -C ₈ -H ₁₂							119.1	119.2		
C ₁₁ -C ₈ -H ₁₂							120.9	120.8		

C ₇ -C ₉ -C ₁₃							120.2	120.2		
C ₇ -C ₉ -H ₁₄							119.7	119.7		
C ₁₃ -C ₉ -H ₁₄							120.1	120.1		
C ₈ -C ₁₁ -C ₁₃							120.3	120.3	120.0	119.8
C ₈ -C ₁₁ -H ₁₅							119.6	119.7		
C ₁₃ -C ₁₁ -H ₁₅							120.0	120.0		
C ₉ -C ₁₃ -C ₁₁							119.8	119.9		
C ₉ -C ₁₃ -H ₁₆							120.1	120.1		
C ₁₁ -C ₁₃ -H ₁₆							120.1	120.0		
C ₅ -C ₁₇ -C ₁₈							121.2			
C ₅ -C ₁₇ -C ₁₉							119.2			
C ₂ -N ₆ -H ₇				114.6	113.3	113.5				
C ₂ -N ₆ -H ₈				119.2	115.6	115.8				
H ₇ -N ₆ -H ₈				115.3	113.9	114.1				
O ₁ -C ₅ -C ₈	119.9	119.3	119.3							
N ₄ =C ₅ -C ₈	127.1	129.1	129.0							
C ₂ -S ₆ -H ₇			92.8							
C ₅ -C ₉ -C ₁₀				120.3	121.2	121.4				
C ₅ -C ₉ -C ₁₁				120.3	119.3	119.3				
C ₅ -C ₈ -C ₉			121.1							
C ₅ -C ₈ -C ₁₃			119.2							
C ₉ -C ₈ -C ₁₃			119.7							
C ₈ -C ₉ -C ₁₀			120.0							
C ₈ -C ₉ -H ₁₄			119.9							
C ₁₀ -C ₉ -H ₁₄			120.1							
C ₁₀ -C ₉ -C ₁₁				119.5	119.5	119.2				
C ₉ -C ₁₀ -C ₁₂				120.3	120.1	120.5				
C ₉ -C ₁₀ -H ₁₃				119.8	119.8	120.0				
C ₉ -C ₁₀ -C ₁₁			120.2							
C ₉ -C ₁₀ -H ₁₅			119.6							
C ₁₁ -C ₁₀ -H ₁₅			120.1							
C ₁₀ -C ₁₁ -C ₁₂			119.9							
C ₁₀ -C ₁₁ -H ₁₆			120.1							
C ₁₂ -C ₁₀ -H ₁₃				119.8	120.1	119.5				
C ₉ -C ₁₁ -C ₁₄				119.2	120.0	120.5				
C ₉ -C ₁₁ -H ₁₅				120.4	119.1	119.3				
C ₁₄ -C ₁₁ -H ₁₅				120.4	120.8	120.2				
C ₁₀ -C ₁₂ -C ₁₆				120.2	120.3	119.3				
C ₁₀ -C ₁₂ -H ₁₇				119.9	119.6	120.5				
C ₁₆ -C ₁₂ -H ₁₇				119.9	120.1	120.1				
C ₁₁ -C ₁₄ -C ₁₆				121.0	120.4	119.4				
C ₁₁ -C ₁₄ -H ₁₈				119.5	119.6	120.5				
C ₁₆ -C ₁₄ -H ₁₈				119.5	120.0	120.1				
C ₁₂ -C ₁₆ -C ₁₄				119.8	119.8	121.1				
C ₁₂ -C ₁₆ -H ₁₉				120.1	120.1					
C ₁₄ -C ₁₆ -H ₁₉				120.1	120.1					
C ₁₂ -C ₁₆ -Cl ₁₉						119.5				

C ₁₄ -C ₁₆ -Cl ₁₉						119.5				
C ₁₈ -C ₁₇ -C ₁₉							119.6			
C ₁₇ -C ₁₈ -C ₂₀							120.1			
C ₁₇ -C ₁₈ -H ₂₁							119.8			
C ₂₀ -C ₁₈ -H ₂₁							120.1			
C ₁₇ -C ₁₉ -C ₂₂							120.0			
C ₁₇ -C ₁₉ -H ₂₃							119.1			
C ₂₂ -C ₁₉ -H ₂₃							120.9			
C ₁₈ -C ₂₀ -C ₂₄							120.2			
C ₁₈ -C ₂₀ -H ₂₅							119.7			
C ₂₄ -C ₂₀ -H ₂₅							120.1			
C ₁₉ -C ₂₂ -C ₂₄							120.3			
C ₁₉ -C ₂₂ -H ₂₆							119.6			
C ₂₄ -C ₂₂ -H ₂₆							120.0			
C ₂₀ -C ₂₄ -C ₂₂							119.8			
C ₂₀ -C ₂₄ -H ₂₇							120.1			
C ₂₂ -C ₂₄ -H ₂₇							120.1			
C ₁₂ -C ₁₁ -H ₁₆			120.1							
C ₁₁ -C ₁₂ -C ₁₃			120.3							
C ₁₁ -C ₁₂ -H ₁₇			120.1							
C ₁₃ -C ₁₂ -H ₁₇			119.6							
C ₈ -C ₁₃ -C ₁₂			119.9							
C ₈ -C ₁₃ -H ₁₈			119.2							
C ₁₂ -C ₁₃ -H ₁₈			120.8							
<i>Dihedral angle in degree</i>										
C ₅ -O ₁ -C ₂ =N ₃			-0.0	-0.9	0.2	0.2	0.0	0.0		
C ₅ -O ₁ -C ₂ -S ₆	-	-180.0	-180.0							
C ₅ -O ₁ -C ₂ -C ₆							180.0	180.0		
C ₅ -O ₁ -C ₂ -N ₆				176.4	-176.5	-176.5				
C ₂ -O ₁ -C ₅ =N ₄			0.0	0.8	0.2	0.2	0.0	0.0		
C ₂ -O ₁ -C ₅ -H ₁₇								180.0		
C ₂ -O ₁ -C ₅ -C ₁₇							180.0			
C ₂ -O ₁ -C ₅ -C ₈			180.0							
C ₂ -O ₁ -C ₅ -C ₉				-179.6	-179.5	-179.5				
O ₁ -C ₂ =N ₃ -N ₄			0.0	0.7	-0.5	-0.5	0.0	0.0		
S ₆ -C ₂ =N ₃ -N ₄	-	180.0	180.0							
C ₆ -C ₂ =N ₃ -N ₄							180.0	180.0		
O ₁ -C ₂ -C ₆ -C ₇							0.0	0.0		
O ₁ -C ₂ -C ₆ -C ₈							180.0	180.0	180.0	180.0
N ₃ =C ₂ -C ₆ -C ₇							180.0	180.0	180.0	180.0
N ₃ =C ₂ -C ₆ -C ₈							0.0	0.0		
O ₁ -C ₂ -S ₆ -H ₇			-180.0							
N ₃ =C ₂ -S ₆ -H ₇			-0.0							
N ₆ -C ₂ =N ₃ -N ₄				-176.1	175.8	175.8				
O ₁ -C ₂ -N ₆ -H ₇				-	-167.3	-167.5				
O ₁ -C ₂ -N ₆ -H ₈				-	-33.1	-32.8				
N ₃ =C ₂ -N ₆ -H ₇				-	16.6	16.4				

N ₃ =C ₂ -N ₆ -H ₈				-	150.7	151.1				
C ₂ =N ₃ -N ₄ =C ₅			-0.0	-0.2	0.6	0.5	0.0	0.0		
N ₃ -N ₄ =C ₅ -O ₁			0.0	-0.4	-0.5	-0.5	0.0	0.0		

3.2.2- The vibrational spectra

The **POD** molecule has 45 normal modes distributed as $\Gamma_{\text{vib}} = 31A' + 14A''$. All the 45 fundamental vibrations are belong to two irreducible representations, and they are active in both Raman scattering and Infrared absorption, A' (in plane) modes and A'' (out of plane) modes. This work results show a reasonable agreement when compared with experimental and the theoretical scaling frequencies data of Avci and Atalay [51]. The computed vibrational wave numbers, IR intensities, Raman activity, with the complete assignment are summarized in **table 3.21**.

Table 3.21.Theoretical vibrational frequencies and the assignment of the **POD** molecule compared with other experimental and theoretical data.

No.	Sym.	Freq. (cm ⁻¹)	IR intensity (km mol ⁻¹)	Raman activity (A ⁴ amu ⁻¹)	DFT 6-311++ G(d,p) other work [51]	Freq. (cm ⁻¹) Exp. [51]	Assignment
ν_1	A'	3285	1.90	125.88	3273	3677	ν_s CH
ν_2		3209	2.77	163.98	3194	3591	ν_{as} CH ring(A)
ν_3		3205	4.71	82.96	3190	3541	ν_{as} CH ring(A)
ν_4		3195	12.40	125.72	3180	3490	ν_{as} CH ring(A)
ν_5		3185	8.20	109.49	3170	3292	ν_{as} CH ring(A)
ν_6		3175	0.03	43.56	3159	3008	ν_{as} CH ring(A)
ν_7		1645	2.40	396.33	1642	-	(ν_s C-C+ β CH)ring A+ ν_s (C ₂ -C ₆)
ν_8		1623	4.09	52.27	1620	1773	(ν_{as} C-C+ β CH)ring A+ β CCN
ν_9		1580	43.95	448.59	1580	1692	ν_s CCN + β CH ring(A)
ν_{10}		1546	26.44	86.38	1542	1661	ν_s C=N + β CH ring(B)
ν_{11}		1522	38.53	23.24	1512	-	β CH ring(A)
ν_{12}		1483	15.54	60.69	1473	1530	β CH ring(A)
ν_{13}		1369	9.77	40.93	1359	1485	β CH clock wise ring(A)
ν_{14}		1349	2.24	37.87	1347	1370	ν_s CCO + β CH ring(B)+(β CH+ ν_{as} C-C)ring(A)
ν_{15}		1315	3.79	12.37	1315	1313	ν_{as} NCO + β CH ring(A&B)

ν_{16}		1256	4.27	8.58	1248	-	β CH ring(B)
ν_{17}		1205	2.28	14.53	1200	1241	β CH ring(A)
ν_{18}		1187	0.11	8.29	1182	-	β CH ring(A)
ν_{19}		1118	16.15	1.69	1116	-	ν_s CO + β CH ring(A&B)
ν_{20}		1105	13.50	1.14	1102	-	β CH ring(A&B)
ν_{21}		1081	21.13	3.17	1075	-	ν_{as} COC + β CH ring(A&B)
ν_{22}		1046	11.76	6.80	1041	-	β CH ring(A)
ν_{23}		1020	0.47	40.97	1014	-	ring def.(A)
ν_{24}		1001	7.18	81.47	1003	1054	ν_s NN + ring breath(A)
ν_{25}		976	12.08	5.31	974	1016	β OCN
ν_{26}		956	8.26	30.83	953	1008	β ring(B)
ν_{27}		706	7.66	4.21	702	714	ring def.(A)
ν_{28}		634	0.07	5.33	630	616	ring def.(A)
ν_{29}		453	4.94	1.24	451	-	ring clock wise(A&B)
ν_{30}		350	0.17	3.31	-	-	ring elongation(A&B)
ν_{31}		154	2.64	0.17	-	-	ring(A)clock wise + ring(B) anti clock wise
ν_{32}	A''	1015	0.11	0.21	1007	1097	γ CH ring(A)
ν_{33}		999	0.02	0.04	992	-	γ CH ring(A)
ν_{34}		950	2.83	0.02	943	-	γ CH ring(A)
ν_{35}		861	0.04	0.33	858	917	γ CH ring(A)
ν_{36}		844	12.64	0.77	834	853	γ CH ring(B)
ν_{37}		795	7.49	2.57	782	802	t (C ₂ -C ₆) + γ CH ring(A&B)
ν_{38}		729	43.00	0.03	715	-	ring puck.(A&B) + γ CH ring(A&B)
ν_{39}		704	39.56	0.01	702	723	γ CH ring(A)
ν_{40}		658	12.92	0.46	649	-	(ring puck.+ γ CH)ring B
ν_{41}		501	2.52	0.69	493	544	(ring puck.+ γ CH)ring A
ν_{42}		411	0.00	0.00	410	429	(ring puck.+ γ CH)ring A
ν_{43}		286	0.32	2.99	-	-	(γ ring + γ CH) ring (A&B)
ν_{44}		112	0.26	0.38	-	-	Wing ring (A&B)
ν_{45}		51	4.69	0.18	-	-	t (C ₂ -C ₆)

The **PODT** molecule has 18 atoms with 48 normal modes of vibrations. All these vibrations belongs to one class of the C_1 symmetry species A, also all the fundamental vibrations are active in both Infrared and Raman. This work out put results are agreed with theoretical and available experimental results Romano et al.[55], **table 3.22**. The **PODA**, and **CPODA** molecules have a non-planar structure. Both molecules have 19 atoms with 51 normal modes of vibrations. The vibrational frequencies and intensities with the reliable assignment of this work were presented in **table 3.23**, and **table 3.24** respectively. The **DPOD** molecule has 75 normal modes of vibrations distributed as $\Gamma_{3N-6} = 26A_1+12A_2+12B_1+25B_2$.

All the 75 fundamental vibrations are active in Raman scattering, and in Infrared except A_2 species which is active in Raman only. The calculated harmonic vibrational frequencies have been presented in **table 3.25**.

Table 3.22. Calculated theoretical wavenumbers (cm^{-1}) and assignment of the **PODT** molecule compare with other experimental and theoretical data.

No.	Sym.	Freq. (cm^{-1})	IR intensity (km mol^{-1})	Raman activity ($\text{A}^4 \text{amu}^{-1}$)	DFT 6-31G* other work [55]	Freq. (cm^{-1}) Exp.[90]	Assignment
ν_1	A	3208	3.44	210.43	3203	3143	ν_s CH
ν_2		3206	4.13	26.88	3200	-	ν_{as} CH
ν_3		3195	13.64	152.91	3189	3092	ν_{as} CH
ν_4		3185	8.42	116.28	3179	2951	ν_{as} CH
ν_5		3174	0.06	42.21	3168	-	ν_{as} CH
ν_6		2664	7.78	157.07	2674	2364	ν SH
ν_7		1645	0.39	662.21	1646	1609	β CH + ν_s ($\text{C}_9\text{-C}_{10}$)
ν_8		1624	2.32	134.75	1626	1609	ν_s ($\text{C}_{10}\text{-C}_{11}$) + ν_{as} C=N
ν_9		1586	27.68	873.14	1591	1512	ν_{as} N=CC + β CH
ν_{10}		1527	21.50	92.51	1522	1501	β CH
ν_{11}		1508	207.03	142.76	1512	1445	ν C=N + β CH
ν_{12}		1484	3.58	106.97	1478	1350	β CH
ν_{13}		1369	1.41	44.03	1362	1350	β CH (clock wise)
ν_{14}		1347	2.26	45.37	1350	1290	β CH + ν_{as} N=CO + ν_{as} ($\text{C}_9\text{-C}_{10}$)
ν_{15}		1315	1.28	8.88	1319	1290	β CH + ν_{as} ($\text{C}_8\text{-C}_9$) + ν_s COC
ν_{16}		1220	70.63	6.84	1221	1186	β CH + ν CO + β SH
ν_{17}		1205	17.61	33.07	1203	1173	β CH
ν_{18}		1187	0.14	9.74	1185	1173	β CH
ν_{19}		1108	4.07	5.05	1108	1060	β CH
ν_{20}		1080	28.84	25.90	1080	1060	β CH + ν CO
ν_{21}		1048	8.50	23.09	1048	1030	β CH
ν_{22}		1029	21.90	82.39	1029	1030	ν NN + β CH + ν_{as} CH
ν_{23}		1017	4.03	173.24	1015	-	ν_s CH + ring breath (A)
ν_{24}		1016	0.08	0.40	1006	-	γ CH
ν_{25}		999	0.02	0.07	993	-	γ CH
ν_{26}		990	7.95	57.78	992	966	β SH + β ring B
ν_{27}		967	9.18	27.88	967	966	ν_s N=CO
ν_{28}		949	2.57	0.01	943	939	γ CH
ν_{29}		926	17.16	4.68	926	918	β SH
ν_{30}		861	0.02	0.31	860	-	γ CH
ν_{31}		793	15.47	3.07	784	760	γ CH
ν_{32}		724	34.82	0.05	719	696	γ CH
ν_{33}		709	9.54	3.72	708	696	β ring A + β CH
ν_{34}		704	34.42	0.02	700	686	γ CH

ν_{35}	699	3.72	0.10	668	686	γ CH + γ ring B
ν_{36}	634	0.07	5.23	632	627	β ring A
ν_{37}	513	3.01	1.11	514	552	ν CS + β CH (clock wise)
ν_{38}	504	4.11	0.52	498	480	γ CH
ν_{39}	472	2.82	1.95	471	473	β (C ₅ -C ₈) + β SH
ν_{40}	413	0.00	0.00	413	-	γ CH
ν_{41}	329	1.05	1.52	329	-	β CSH + β ring A
ν_{42}	320	0.04	1.25	313	-	γ ring (A&B)
ν_{43}	253	2.75	3.42	253	-	β CSH + β CH
ν_{44}	222	14.55	0.19	215	-	γ SH
ν_{45}	198	2.06	2.04	193	-	γ SH + γ CH
ν_{46}	106	1.13	2.30	105	-	β (CH + ring A)clock wise + β ring B
ν_{47}	94	0.01	0.34	93	-	γ SH + γ CH + γ ring B
ν_{48}	44	1.23	0.99	44	-	γ CH + γ ring B

The discussion of the assignments for the most important groups is presented as follows.

S-H vibrations: The 4000–2000 cm^{-1} region is characteristic as thiol stretching [55]. The calculated band in the IR spectrum for the **PODT** compound is appeared at 2664 cm^{-1} , so it's assigned as a S-H stretching. This frequency value is greater than the experimental by 300 cm^{-1} [90], **table 3.22**. The difference is approximately equal 11% percent. This difference probably related to the existence of S-H...S hydrogen bonding [91].

Table 3.23. Theoretical vibrational frequencies (cm^{-1}), IR intensity, Raman activities and the assignment of the **PODA** molecule.

No.	Sym.	Freq. (cm^{-1})	IR intensity (km mol^{-1})	Raman activity ($\text{A}^{\circ 4} \text{amu}^{-1}$)	Assignment
ν_1	A	3679	51.77	57.33	$\nu_{\text{as}} \text{NH}_2$
ν_2		3578	65.11	255.01	$\nu_{\text{s}} \text{NH}_2$
ν_3		3208	2.94	170.11	$\nu_{\text{s}} \text{CH}$
ν_4		3204	5.78	70.33	$\nu_{\text{as}} \text{CH}$
ν_5		3194	15.20	143.79	$\nu_{\text{as}} \text{CH}$
ν_6		3183	9.24	115.27	$\nu_{\text{as}} \text{CH}$
ν_7		3173	0.24	41.70	$\nu_{\text{as}} \text{CH}$
ν_8		1669	433.19	238.35	$\delta \text{NH}_2 + \nu \text{CN}$
ν_9		1644	2.14	619.09	$\beta \text{CH} + \nu \text{C}=\text{C}$
ν_{10}		1625	2.68	195.79	$\delta \text{NH}_2 + \nu \text{C}=\text{C} + \nu \text{C}=\text{N}$
ν_{11}		1605	81.65	190.25	δNH_2
ν_{12}		1588	45.78	415.51	$\delta \text{NH}_2 + \nu \text{C}=\text{N} + \beta \text{CH}$

ν_{13}	1526	32.94	20.15	β CH
ν_{14}	1486	6.25	44.68	β CH
ν_{15}	1438	27.08	2.87	ν OC + ρ NH ₂ + β CH
ν_{16}	1363	5.74	14.60	β CH (clock wise)
ν_{17}	1326	4.57	29.56	ν C=C (ring def.) + β CH + t (C ₅ -C ₉)
ν_{18}	1301	35.80	61.42	ν_s CCN + β CH
ν_{19}	1205	1.84	28.64	β CH
ν_{20}	1186	0.07	9.31	β CH
ν_{21}	1138	4.20	91.49	ρ NH ₂ + ν_s NCN
ν_{22}	1108	1.12	1.59	β CH
ν_{23}	1074	17.29	6.56	β CH + ρ NH ₂
ν_{24}	1049	18.80	43.62	ρ NH ₂ + ν_s NN + β CH
ν_{25}	1040	57.75	34.93	ρ NH ₂ + ν COC + β CH
ν_{26}	1018	3.52	94.47	ring breath (A)
ν_{27}	1012	0.12	0.33	γ CH
ν_{28}	997	0.02	0.10	γ CH
ν_{29}	987	3.81	49.44	ring def. (B) + ρ NH ₂
ν_{30}	966	13.06	50.79	ring def. (B)
ν_{31}	944	2.71	0.03	γ CH
ν_{32}	859	0.03	0.38	γ CH
ν_{33}	789	8.91	2.35	γ CH
ν_{34}	765	38.19	2.38	ω NH ₂
ν_{35}	743	34.15	1.89	ring puck. (B)
ν_{36}	707	1.27	0.26	γ CH + ring puck. (B)
ν_{37}	703	44.81	0.04	γ CH
ν_{38}	690	8.87	5.25	ω NH ₂ + β ring (A) + β CH
ν_{39}	634	0.07	5.39	β ring (A) + β CH
ν_{40}	593	273.18	12.55	ω NH ₂
ν_{41}	512	3.27	3.45	ρ NH ₂ + β ring (anti clock wise)(A&B)
ν_{42}	505	12.51	0.59	γ CH + ring puck. (A)
ν_{43}	412	0.02	0.00	γ CH
ν_{44}	372	1.59	2.72	τ NH ₂
ν_{45}	347	13.08	1.53	τ NH ₂ + ring puck. (B)
ν_{46}	318	0.75	7.03	τ NH ₂ + t (C ₅ -C ₉)
ν_{47}	287	24.94	0.80	τ NH ₂
ν_{48}	228	1.92	1.78	τ NH ₂ + γ NCO + γ CH
ν_{49}	126	3.84	0.90	β CH-clock wise(A)+ ring anti clock wise(B)+ ρ NH ₂
ν_{50}	97	0.37	0.31	γ ring (A&B) + ω NH ₂
ν_{51}	46	4.91	0.51	γ ring (A&B) + ω NH ₂

C-C/C=C vibrations: The ring C–C stretching vibrations usually extent from 1600–1400 cm⁻¹ [92]. But this vibration in benzene ring occurs around the region 1625-1430 cm⁻¹. Usually, the strongest one being at about 1500 cm⁻¹, while in the ring conjugated condition, the band shifted to about 1580 cm⁻¹. In the present work

the symmetric C-C stretching vibrations are found in the 1649 -1575 cm^{-1} . Socrates mentioned that the symmetric C-C stretching vibrations are observed around 1625-1575 cm^{-1} at the presence of conjugate substituent such as C=C [93].

C=N vibrations: The identification of C=N vibrations is a very difficult since caused by mixing of different bands and many motions is possible in this region. However, theoretical calculations help to assign the C=N stretching vibrations, which identified between 1624 – 1508 cm^{-1} , **tables 3.21-3.25**.

Table 3.24. The theoretical vibrational frequencies (cm^{-1}), with its assignment for the CPODA molecule.

No.	Sym.	Freq. (cm^{-1})	IR intensity (km mol^{-1})	Raman activity ($\text{A}^{\circ 4} \text{amu}^{-1}$)	Assignment
ν_1	A	3681	53.69	59.01	$\nu_{\text{as}} \text{NH}_2$
ν_2		3579	73.46	277.63	$\nu_{\text{s}} \text{NH}_2$
ν_3		3216	0.87	201.36	$\nu_{\text{s}} \text{CH}$
ν_4		3215	1.26	32.83	$\nu_{\text{as}} \text{CH}$
ν_5		3203	0.12	49.12	$\nu_{\text{as}} \text{CH}$
ν_6		3200	1.74	23.43	$\nu_{\text{as}} \text{CH}$
ν_7		1669	477.72	315.80	δNH_2
ν_8		1637	20.48	1157.85	$\beta \text{CH} + \beta \text{ ring A} + \nu (\text{C}_5\text{-C}_9)$
ν_9		1617	18.34	382.89	$\delta \text{NH}_2 + \nu_{\text{s}} \text{C=N}$
ν_{10}		1601	84.17	24.33	$\delta \text{NH}_2 + \nu \text{C=N} + \beta \text{CH}$
ν_{11}		1583	8.27	535.40	$\beta \text{ ring A} + \beta \text{CH} + \nu_{\text{as}} \text{C=N}$
ν_{12}		1521	108.60	49.53	βCH
ν_{13}		1450	9.12	16.52	$\rho \text{NH}_2 + \nu_{\text{s}} \text{COC} + \beta \text{CH}$
ν_{14}		1424	24.02	27.54	$\rho \text{NH}_2 + \beta \text{CH}$
ν_{15}		1335	5.39	25.20	CH clock wise + ring A anti clock wise
ν_{16}		1313	7.25	54.60	ring def. A + $\beta \text{CH} + \rho \text{NH}_2$
ν_{17}		1301	29.71	54.07	ring def. (A&B) + $\beta \text{CH} + \rho \text{NH}_2$
ν_{18}		1203	1.82	67.48	βCH
ν_{19}		1138	5.03	117.76	$\rho \text{NH}_2 + \text{ring def. B}$
ν_{20}		1134	3.77	5.38	βCH
ν_{21}		1102	80.45	53.07	$\nu \text{CCl} + \beta \text{CH} + \text{ring def. A}$
ν_{22}		1072	14.59	9.78	$\rho \text{NH}_2 + \text{ring def. (A&B)} + \beta \text{CH}$
ν_{23}		1045	59.44	150.54	$\rho \text{NH}_2 + \nu \text{N-N}$
ν_{24}		1033	46.23	3.13	ring def. A + βCH
ν_{25}		1002	0.03	0.05	γCH
ν_{26}		986	3.68	46.51	ring def. B + ρNH_2
ν_{27}		983	0.00	0.48	γCH
ν_{28}		967	10.08	70.23	ring def. B

ν_{29}		862	36.08	0.57	γ CH
ν_{30}		842	2.74	0.20	γ CH
ν_{31}		773	16.93	3.08	ω NH ₂ + β ring A + γ ring B
ν_{32}		758	31.19	2.47	γ CH + γ ring B
ν_{33}		742	10.79	3.74	γ CH
ν_{34}		728	1.80	6.41	ω NH ₂
ν_{35}		706	3.02	0.45	γ CH + γ ring B
ν_{36}		646	0.42	6.45	β ring A
ν_{37}		586	271.30	13.26	ω NH ₂
ν_{38}		521	19.51	0.77	γ CH
ν_{39}		518	21.09	1.09	ring (A&B) clock wise + τ NH ₂
ν_{40}		506	26.10	8.13	ν CCl
ν_{41}		419	0.07	0.01	γ CH
ν_{42}		377	5.56	3.10	τ NH ₂ + γ ring (A&B)
ν_{43}		374	0.39	4.85	τ NH ₂ + (ring A&CH)clock wise
ν_{44}		305	23.64	1.44	τ NH ₂
ν_{45}		285	2.07	0.98	β CCl + β CH
ν_{46}		272	7.27	1.27	τ NH ₂
ν_{47}		253	4.92	4.41	ρ NH ₂ + β ring (A&B)
ν_{48}		163	1.24	0.18	γ ring (A&B)
ν_{49}		101	2.71	0.81	ρ NH ₂ + β CH(clock wise)+ring B anti clock wise
ν_{50}		64	1.92	0.02	γ CH + γ ring (A&B)
ν_{51}		46	3.33	0.46	γ CH + γ ring (A&B)

C-Cl vibrations: For the **CPODA** molecule, the C-Cl stretching (mixing with other motions such as CH in-plane-bending, and ring A deformation) computed at 1102 cm⁻¹. Another C-Cl stretching vibration pure one is observed at 506 cm⁻¹.

Table 3.25. The theoretical vibrational frequencies, IR intensities and Raman activity with assignment for the 75 normal modes of the **DPOD** molecule.

No.	Sym.	Freq. (cm ⁻¹)	IR intensity (km mol ⁻¹)	Raman activity (A ^{o4} amu ⁻¹)	Assignment
ν_1	A ₁	3209	0.04	338.64	ν_s CH
ν_2		3205	9.91	113.27	ν_{as} CH
ν_3		3194	0.62	335.83	ν_{as} CH
ν_4		3184	16.00	80.11	ν_{as} CH
ν_5		3174	0.00	52.12	ν_{as} CH
ν_6		1644	0.47	1808.06	β CH + β ring (ring elongation)
ν_7		1624	0.42	415.93	β CH + β ring + ν_s C=N
ν_8		1575	19.13	3210.47	ν_s C=N + ν_s (C ₂ -C ₆) + β CH
ν_9		1523	27.75	300.17	β CH

ν_{10}		1485	2.28	462.58	β CH
ν_{11}		1387	1.55	73.75	ν_s COC + β ring A
ν_{12}		1357	0.45	4.98	β CH
ν_{13}		1317	1.63	4.75	β CH + ν C=C
ν_{14}		1206	0.15	102.54	β CH
ν_{15}		1187	0.12	3.55	β CH
ν_{16}		1135	2.51	114.81	ν_s NN + ν_s COC + β CH
ν_{17}		1100	14.03	12.94	β CH
ν_{18}		1050	0.05	101.36	β CH + ν_s NN
ν_{19}		1034	1.77	341.92	ν_s NN + β ring A
ν_{20}		1014	1.07	764.80	ring breath A + ν_s NN
ν_{21}		985	8.93	57.42	ring elongation B
ν_{22}		695	1.55	11.18	β ring (def.)
ν_{23}		634	0.04	3.31	β ring (def.) + β CH
ν_{24}		401	2.39	5.58	t (C ₂ -C ₆) + β CH
ν_{25}		254	0.19	0.89	β CH
ν_{26}		067	0.72	3.41	β CH
ν_{27}	A ₂	1015	0.00	0.87	γ CH
ν_{28}		998	0.00	0.15	γ CH
ν_{29}		947	0.00	0.01	γ CH
ν_{30}		860	0.00	0.09	γ CH
ν_{31}		790	0.00	7.75	γ CCOCC + γ CH
ν_{32}		717	0.00	0.18	ring puck. B + γ CH
ν_{33}		703	0.00	0.00	γ CH
ν_{34}		518	0.00	1.20	ring puck.(A&B)
ν_{35}		410	0.00	0.00	ring puck. A
ν_{36}		331	0.00	2.26	ring puck.(A&B)
ν_{37}		122	0.00	4.13	ring puck.(A&B)
ν_{38}		031	0.00	0.77	γ CH + ring puck. A
ν_{39}	B ₁	1014	0.16	0.04	γ CH
ν_{40}		999	0.08	0.00	γ CH
ν_{41}		949	4.89	0.00	γ CH
ν_{42}		861	0.05	0.53	γ CH
ν_{43}		801	20.05	0.51	γ CH + γ CCOCC
ν_{44}		731	85.43	0.00	γ CH + γ COC
ν_{45}		703	66.30	0.03	γ CH
ν_{46}		492	8.36	0.01	γ CH + ring puck. A
ν_{47}		411	0.00	0.00	γ CH + ring puck. A
ν_{48}		240	0.29	037	γ CH + γ COC + γ ring A
ν_{49}		090	1.31	0.17	γ ring B
ν_{50}		039	1.22	1.16	γ CH + γ ring (A&B)
ν_{51}	B ₂	3209	7.70	10.49	ν_{as} CH
ν_{52}		3204	0.05	0.04	ν_{as} CH
ν_{53}		3194	31.12	25.50	ν_{as} CH
ν_{54}		3184	0.90	174.23	ν_{as} CH
ν_{55}		3174	0.64	29.39	ν_{as} CH

ν_{56}		1645	0.07	214.37	β CH + ν C=C
ν_{57}		1620	5.61	2.11	β CH + ν C=C
ν_{58}		1574	67.87	135.53	ν_{as} C=N + β CH
ν_{59}		1520	80.16	16.93	β CH + ν_{as} C=N
ν_{60}		1482	35.38	0.49	β CH
ν_{61}		1364	6.92	0.54	β CH (anti clock wise)
ν_{62}		1327	0.32	23.70	ν_{as} C=C + β CH
ν_{63}		1281	5.01	29.07	β CH + ring def. B + ν (C ₂ -C ₆)
ν_{64}		1204	8.29	2.04	β CH
ν_{65}		1186	0.20	15.03	β CH
ν_{66}		1106	0.96	0.13	β CH
ν_{67}		1080	22.06	1.22	ν_{as} COC + γ CH
ν_{68}		1044	31.31	0.15	γ CH + ring def. A
ν_{69}		1019	0.33	3.85	ring def. A
ν_{70}		978	3.98	3.03	ring def. B + β CH
ν_{71}		723	18.74	1.46	ring def. A + β CH
ν_{72}		633	0.01	6.68	ring def. A + β CH
ν_{73}		535	4.56	0.94	t (C ₂ -C ₆) + β CH (anti clock wise)
ν_{74}		408	0.01	0.61	β ring (A&B)
ν_{75}		172	0.75	0.17	β CH+ring clock wise A+ ring anti clock wise B

N-N vibrations: In present study the N-N stretching vibrations for all molecules of series two are observed at the range 1135 – 1001 cm⁻¹. For example, the computed data demonstrate that the four vibrations ν_{16} , ν_{18} , ν_{19} , ν_{20} are assigned as N-N symmetric stretching vibration (combined with other motions) for **DPOD**, their values are 1135, 1050, 1034, and 1014 cm⁻¹ respectively, **table 3.25**. 1095 cm⁻¹ in FTIR and the theoretically computed N-N vibrations in the region 1098 cm⁻¹ by HF method, show a good agreement with available theoretical data in literature [94].

C-H vibrations: The aromatic C–H stretching vibrations are observed in the region of 3100–2800 cm⁻¹ [95] (Sridevi *et al.*, 2012). Accordingly, in the results of **DPOD** molecule, symmetric stretching vibrations of C–H is observed at 3209 cm⁻¹, and the nine asymmetric modes are presented between 3209 -3174 cm⁻¹. In the FT-IR and FT-Raman spectrum, whereas in the symmetric stretching vibrations is observed in 3209 cm⁻¹ in the FT-Raman [95]. All other molecules in series two have one C–H symmetric stretching vibrations is appeared at 3285, 3208, 3208, and

3216 cm^{-1} for **POD**, **PODT**, **PODA**, and **CPODA** consequently. There are four or five C–H asymmetric modes in these molecules are ranged between 3205–3194 cm^{-1} , except in **CPODA** molecule the range is increased (3216– 3200 cm^{-1}). The in-plane and out-of-plane bending vibrations for the aromatic C–H group have also been identified for all molecules in this series. In FT-Raman spectra the vibrations are assigned to C–H in-plane bending vibrations at 1108 cm^{-1} [96]. In this work the C-H in-plane bending vibrations are extent 1523 – 67 cm^{-1} , and the out-of-plane bending are observed around the region 1016 - 413 cm^{-1} . This work results are far away from Sridevi *et al.* results ranging from 1025–1280 cm^{-1} [95].

NH₂ vibrations: Series two consist only two molecules have amine group (**CPODA**, and **PODA**). One fundamental vibration (ν_1) is assigned for the pure NH₂ asymmetric stretching vibrations at 3681, and 3679 cm^{-1} for **CPODA**, and **PODA** molecules respectively. The one pure NH₂ symmetric vibration (ν_2) have been assigned at 3578 cm^{-1} for **PODA**, and at 3579 cm^{-1} for **CPODA**. A pure NH₂ scissoring vibration (ν_7 , and ν_{11}) has also been specified at 1669, 1605 cm^{-1} for **CPODA**, **PODA** molecules respectively. Two pure NH₂ wagging vibrations are assigned for each **PODA**, **CPODA** molecules, (ν_{34} , and ν_{40}) and (ν_{34} , and ν_{37}) respectively, **tables 3.23, 3.24**.

3.2.3- Electronic properties

3.2.3.1- UV–visible spectral analysis

UV–visible spectroscopy is greatly used to identify conjugated systems which having stronger absorptions. These calculations are performed in gas phase and in water as a solvent.

The calculated data involving six electronic transitions [using the TD-DFT/B3LYP/6-311++G(2d,2p) level] : oscillator strength (f), major contributions, and wavelength (λ) are presented in **tables 3.26, 3.27, 3.28, 3.29, 3.30** and figures

3.18, 3.19, 3.20, 3.21, 3.22 for the **POD**, **PODT**, **PODA**, **CPODA**, and **DPOD** molecules respectively. There are no available experimental and theoretical UV-vis. data for all series two compounds except **DPOD** molecule. **DPOD** produce florescence at 380 nm [52] this value is approximated to the calculated value in this work, 303 nm in gas phase and 307 nm in water solution.

Table 3.26.The absorption wavelength, energies, and oscillator strengths of the **POD** molecule.

TD-DFT/(B3LYP)/6-311++G(2d,2p)							
Gas			Major contribution(%)	Water			Major contribution(%)
$\lambda(\text{nm})$	$E(\text{eV})$	f		$\lambda(\text{nm})$	$E(\text{eV})$	f	
256.49	4.8339	0.0940	H-1→L(43%),H→L(27%) H→L+1(30%)	259.28	4.7819	0.4153	H-1→L(-28%),H→L(55%) H→L+1(16%)
253.75	4.8861	0.3959	H-1→L(-24%),H→L(58%) H→L+1(-18%)	257.47	4.8154	0.1744	H-1→L(45%),H→L(30%) H→L+1(-26%)
241.28	5.1385	0.0007	H-2→L (70%)	227.45	5.4511	0.0010	H-2→L (70%)
212.86	5.8246	0.0941	H-1→L(-32%),H-1→L+3(-10%) H→L+1(47%),H→L+3(12%)	213.95	5.7950	0.1074	H-1→L(28%),H-1→L+2(10%) H→L+1(50%),H→L+2(11%)
207.83	5.9656	0.0003	H→L +2(70%)	202.78	6.1141	0.0822	H-1→L(-10%),H-1→L+1(-24%) H-1→L+2(-9%),H→L+2(57%)
202.22	6.1311	0.0480	H-5→L(-11%),H-3→L(-21%) H-1→L(9%),H-1→L+1(13%) H→L+3(56%)	202.67	6.1175	0.0000	H→L+3 (70%)

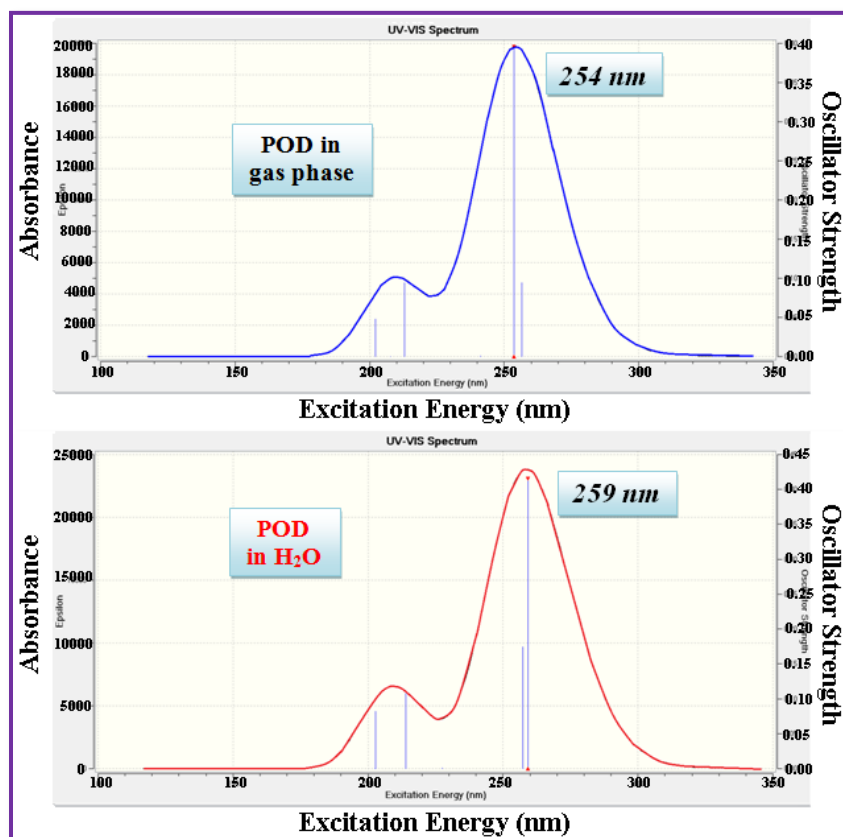


Figure 3.18.UV-visible spectra of **POD** molecule in gas phase and water phase.

The calculated electronic spectra are predicted two electronic peaks in each phase (water, and gas) except the **DPOD** have only one peak. The strongest peak λ_{max} (nm) in gas phase for the series two molecules, is changed in the following configuration: **DPOD (303) > CPODA (288) > PODA (280) > PODT (278) > POD (254)**.

In water solvent, λ_{max} of strongest peak changed in the same order: **DPOD (307) > CPODA (295) > PODA (285) > PODT (283) > POD (259)**. According to these results it can be concluded that the red, and *hyperchromism* shifts occur during the changing from gas phase to the polar solvent (water). The higher value of λ_{max} in **DPOD** spectra may be due to the high conjugation between oxadiazole and the two phenyl rings, which causes a decreasing the energy gap ΔE_g , figure 3.23. The second smaller intense peaks in gas phase and water decrease in the same previous sequence.

Table 3.27. Calculated absorption wavelengths, energies and oscillator strengths of **PODT** molecule.

TD-DFT/(B3LYP)/6-311++G(2d,2p)							
Gas			Major contribution(%)	Water			Major contribution(%)
$\lambda(\text{nm})$	$E(\text{eV})$	f		$\lambda(\text{nm})$	$E(\text{eV})$	f	
278.36	4.4542	0.5224	H→L (70%)	283.29	4.3766	0.6087	H→L (70%)
259.35	4.7806	0.0035	H-2→L+1(-11%) H-1→L(46%),H→L+1(43%)	260.00	4.7686	0.0110	H-2→L+1 (-12%) H-1→L(52%),H→L+1(36%)
247.79	5.0036	0.0006	H-2→L+2(17%) H→L+2(67%),H→L+3(-16%)	238.95	5.1888	0.0009	H-2→L+2(18%) H→L+2(65%),H→L+4(-17%)
236.84	5.2349	0.0008	H-3→L (70%)	226.82	5.4661	0.0779	H-2→L(-23%), H-1→L(-24%) H→L+1(38%), H→L+3(14%)
225.87	5.4893	0.0536	H-2→L+1(14%),H-1→L(-35%) H→L+1(42%), H→L+5(9%)	225.23	5.5047	0.0011	H-3→L (70%)
223.55	5.5462	0.0081	H→L+2 (17%), H→L+3(53%) H→L+4(-30%)	225.01	5.5102	0.0321	H-2→L (46%), H-1→L(-14%) H-1→L+1(10%) H→L+1(21%), H→L+3(-9%)

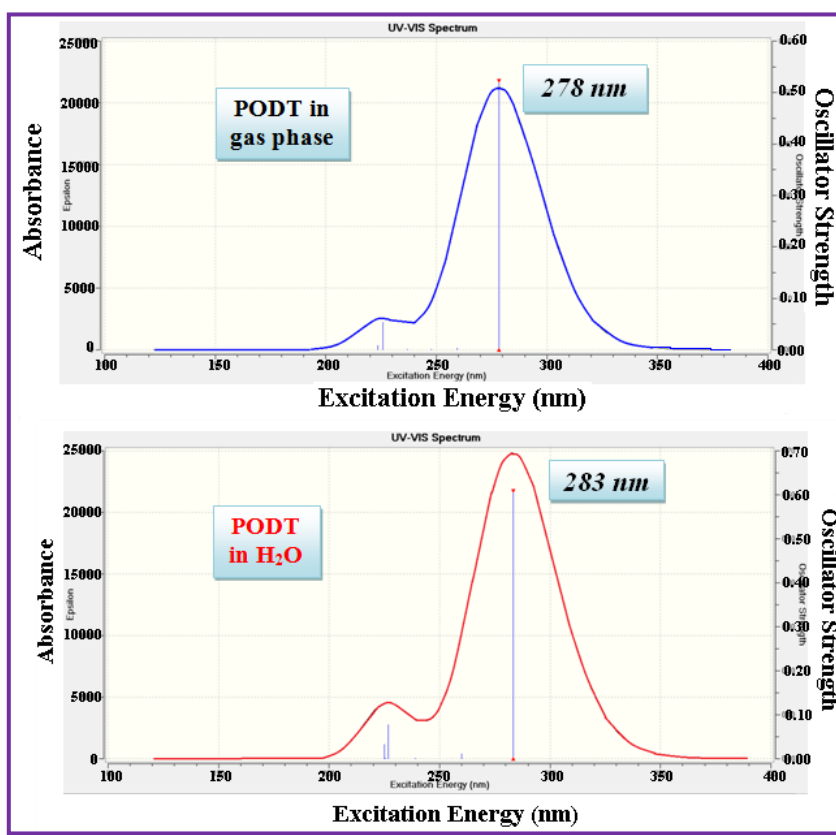


Figure 3.19. Theoretical UV–VIS spectra of **PODT** molecule in gas phase and water solution.

The calculated ΔE_g values in two phases for molecules of this series decreased in the following manner: **POD**, **PODT**, **PODA**, **CPODA**, and **DPOD**, figures 3.23 and 3.24. This sequence is inversely proportional with the of λ max sequence.

Table 3.28. The absorption wavelength, energies, and oscillator strengths of the **PODA** molecule.

TD-DFT/(B3LYP)/6-311++G(2d,2p)							
Gas			Major contribution(%)	Water			Major contribution(%)
$\lambda(\text{nm})$	$E(\text{eV})$	f		$\lambda(\text{nm})$	$E(\text{eV})$	f	
279.54	4.4353	0.4815	H→L (70%)	285.42	4.3439	0.5532	H→L (70%)
261.91	4.7339	0.0020	H-1→L(44%),H→L+1(56%)	260.86	4.7529	0.0039	H-2→L+1(9%) H-1→L(44%),H→L+1(46%)
249.77	4.9639	0.0029	H→L+2(69%)	229.81	5.3950	0.0015	H→L+2 (86%),H→L+3(14%)
238.78	5.1923	0.0027	H-2→L (69%)	228.29	5.4310	0.1005	H-2→L+1 (-16%) H-1→L(-42%),H→L+1(43%)
226.70	5.4692	0.0710	H-3→L+1 (19%) H-1→L(44%),H→L+1(-36%)	226.68	5.4696	0.0045	H-3→L(83%),H-2→L(-17%)
223.98	5.5356	0.0020	H→L+3 (69%)	216.79	5.7192	0.0234	H-3→L(12%),H-2→L(57%) H-1→L+1(-19%),H→L+5(12%)

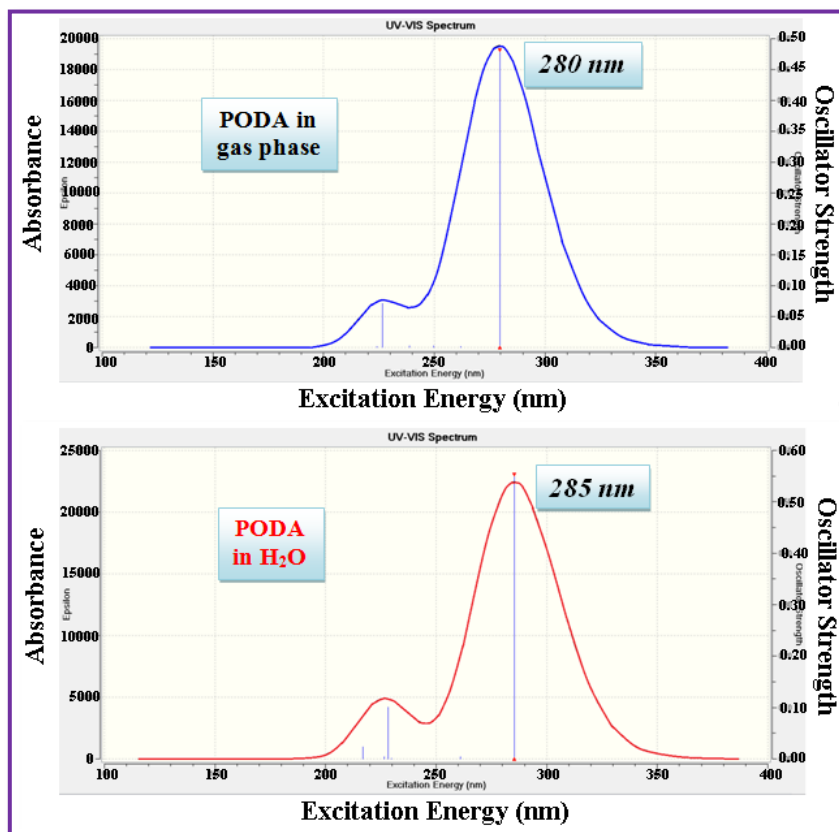


Figure 3.20. The theoretical UV absorption spectra of PODA molecule in gas phase and water phase.

Table 3.29. Calculated absorption wavelengths, energies and oscillator strengths of CPODA molecule.

TD-DFT/(B3LYP)/6-311++G(2d,2p)							
Gas			Major contribution(%)	Water			Major contribution(%)
$\lambda(\text{nm})$	$E(\text{eV})$	f		$\lambda(\text{nm})$	$E(\text{eV})$	f	
288.08	4.3038	0.5842	H→L (70%)	294.61	4.2084	0.6661	H→L (70%)
270.95	4.5758	0.0081	H-2→L(-13%),H-1→L(-28%) H→L+1(60%)	268.36	4.6201	0.0069	H-1→L (-37%),H→L+1(63%)
248.98	4.9796	0.0021	H→L+2 (69%)	230.90	5.3697	0.0366	H-3→L(49%),H-2→L(32%) H-1→L(-19%)
241.86	5.1264	0.0031	H-3→L(84%),H-2→L(16%)	230.16	5.3869	0.0719	H-3→L(14%),H-2→L+1(-15%) H-1→L(32%),H→L+1(20%) H→L+2(-19%)
227.66	5.4461	0.0676	H-2→L+1(-26%) H-1→L(49%),H→L+1(25%)	229.84	5.3943	0.0130	H-2→L(17%),H-2→L+1(-8%) H-1→L(15%),H→L+1(12%) H→L+2(48%)
226.64	5.4704	0.0222	H-3→L(-11%),H-2→L(55%) H-1→L+1(16%),H→L+1(9%) H→L+6(9%)	228.39	5.4286	0.0256	H-3→L(-32%),H-2→L(44%) H-1→L+1(10%),H→L+2(-14%)

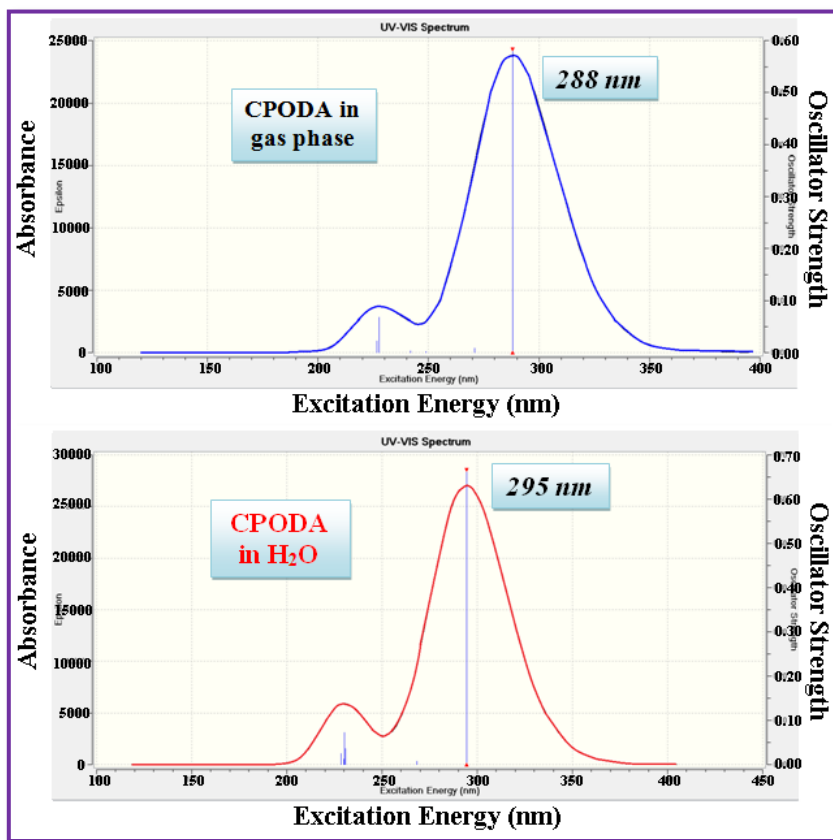


Figure 3.21. UV-visible spectra of CPODA molecule in gas phase and water solvent.

Table 3.30. The absorption wavelength, energies, and oscillator strengths of the DPOD molecule.

TD-DFT/(B3LYP)/6-311++G(2d,2p)							
Gas			Major contribution(%)	Water			Major contribution(%)
λ (nm)	E (eV)	f		λ (nm)	E (eV)	f	
302.96	4.0924	0.8092	H→L (71%)	307.24	4.0354	0.9018	H→L (71%)
265.19	4.6753	0.0117	H-3→L+2(8%), H-2→L+1(-9%) H-1→L(33%), H→L+1(27%) H→L+3(23%)	266.06	4.6601	0.0286	H-3→L+2(-9%), H-2→L+1(10%) H-1→L(38%), H→L+1(-23%) H→L+3(-20%)
262.97	4.7149	0.0004	H-3→L+3(10%), H-2→L(44%) H-1→L+1(-12%), H→L+2(34%)	264.51	4.6873	0.0001	H-3→L+3(11%), H-2→L(50%) H-1→L+1(13%), H→L+2(27%)
257.54	4.8142	0.0000	H-4→L (70%)	257.19	4.8208	0.0015	H-3→L(21%), H-1→L(23%) H→L+1(46%), H→L+3(-10%)
255.78	4.8473	0.0014	H-3→L(21%), H-1→L(-22%) H→L+1(40%), H→L+3(-17%)	241.84	5.1267	0.0000	H-4→L (70%)
235.80	5.2580	0.0152	H-2→L(-38%), H-1→L+1(-20%) H→L+2(43%)	237.42	5.2222	0.0111	H-3→L(61%), H-1→L(-16%) H→L+1(-23)

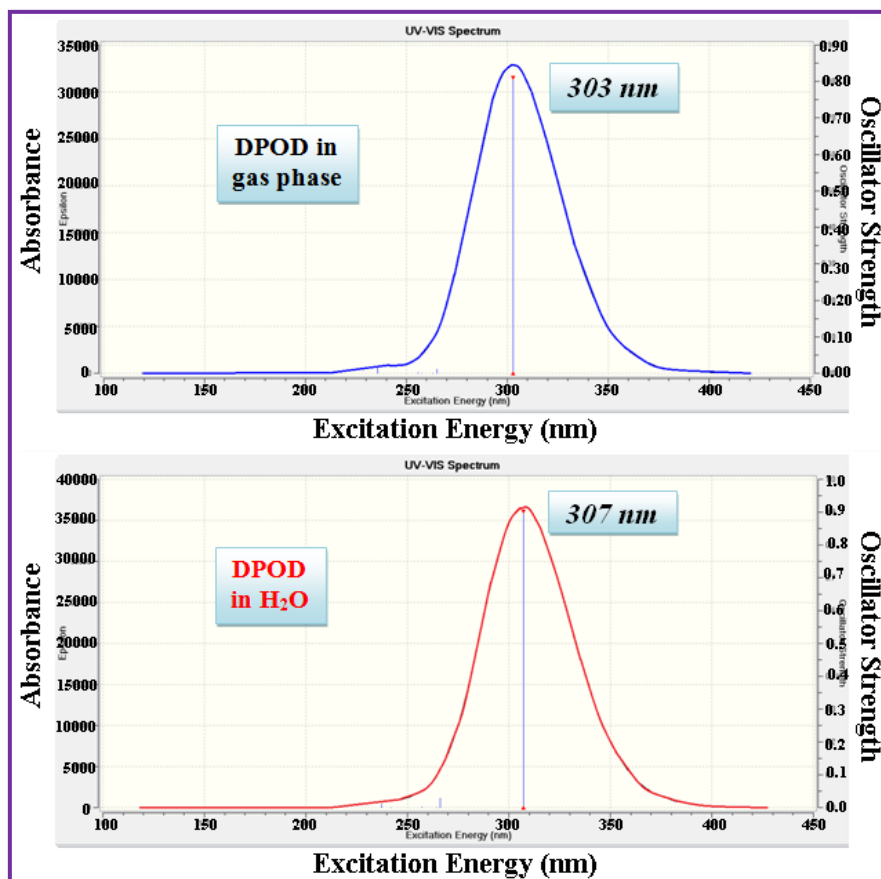


Figure 3.22. Theoretical UV–VIS spectra of DPOD molecule in gas phase and water solution.

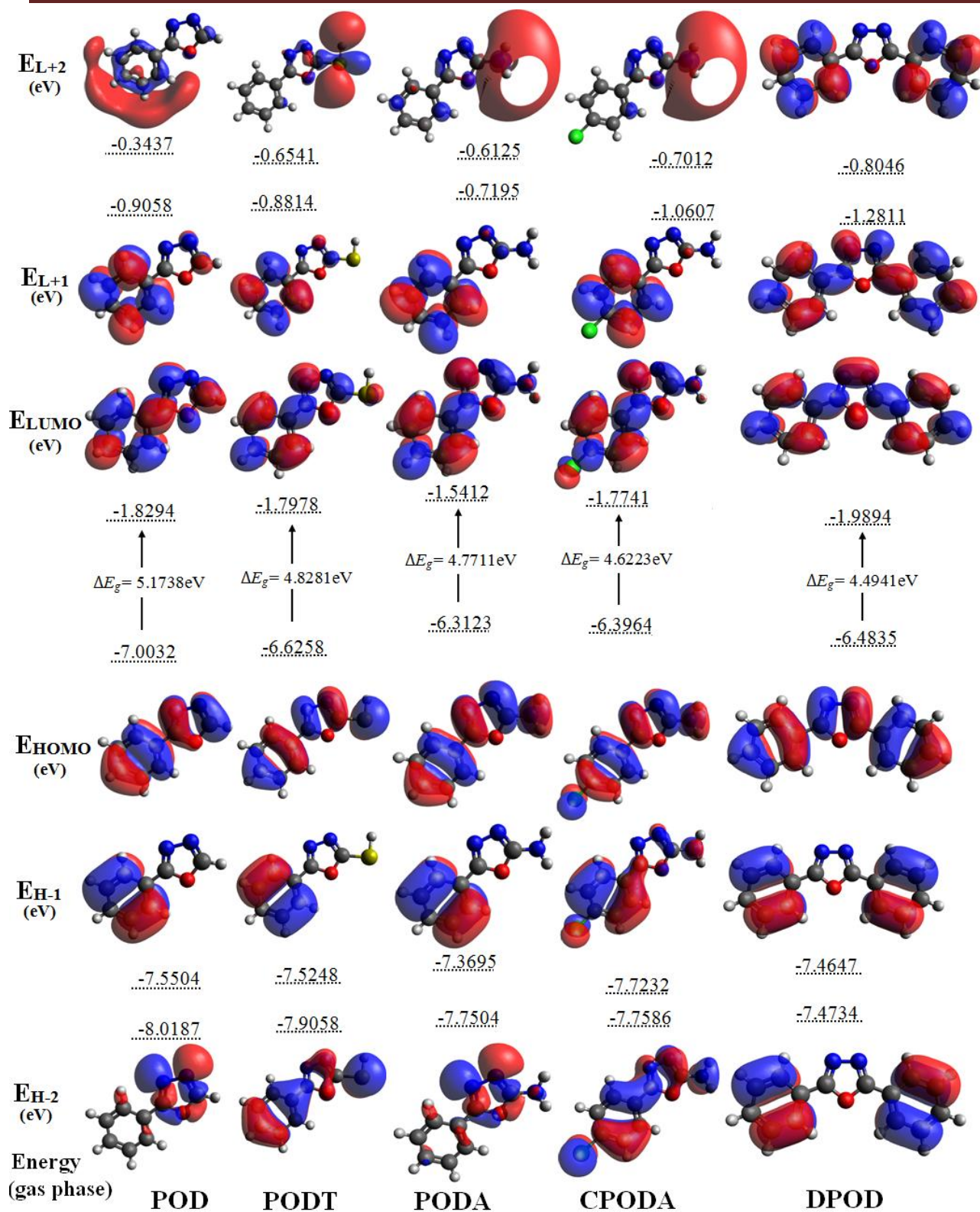


Figure 3.23. The energy with molecular orbital geometry for the POD, PODT, PODA, CPODA, and DPOD molecules in gas phase.

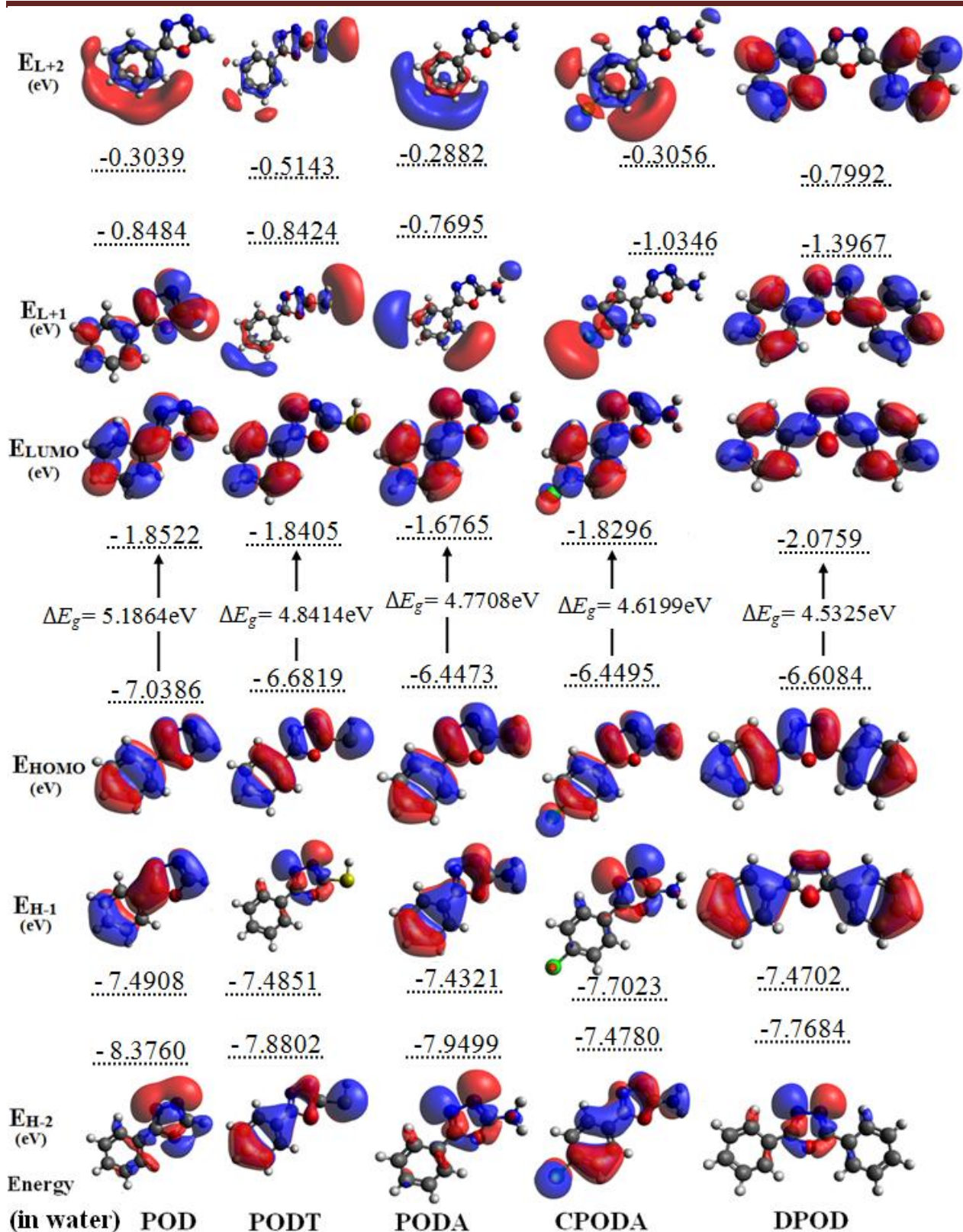


Figure 3.24. The energy with molecular orbital geometry for the **POD**, **PODT**, **PODA**, **CPODA**, and **DPOD** molecules in water.

3.2.3.2- Molecular electrostatic potential

The different values of the electrostatic potential at the surface are represented by different colors; red represents regions of most negative electrostatic potential, blue represents regions of most positive electrostatic potential and green represents regions of zero potential. Potential increases in the order red < orange < yellow < green < blue. While the negative electrostatic potential corresponds to an attraction of the proton by the concentrated electron density in the molecule (and is colored in shades of red), the positive electrostatic potential corresponds to repulsion of the proton by atomic nuclei in regions where low electron density exists and the nuclear charge is incompletely shielded (and is colored in shades of blue).

The MEP surfaces of molecules figure 3.25 shows that the negative potential swings between oxygen and the nitrogen atoms, and phenyl ring, and have access of negative charge (red region). The carbone oxadiazole atoms and hydrogen atoms bear the positive charge (blue region). The predominance of white color on the remaining part of the molecule indicates the presence of neutral potential. The negative (red color) regions of MEP are related to electrophilic reactivity and the positive (blue color) ones to nucleophilic reactivity.

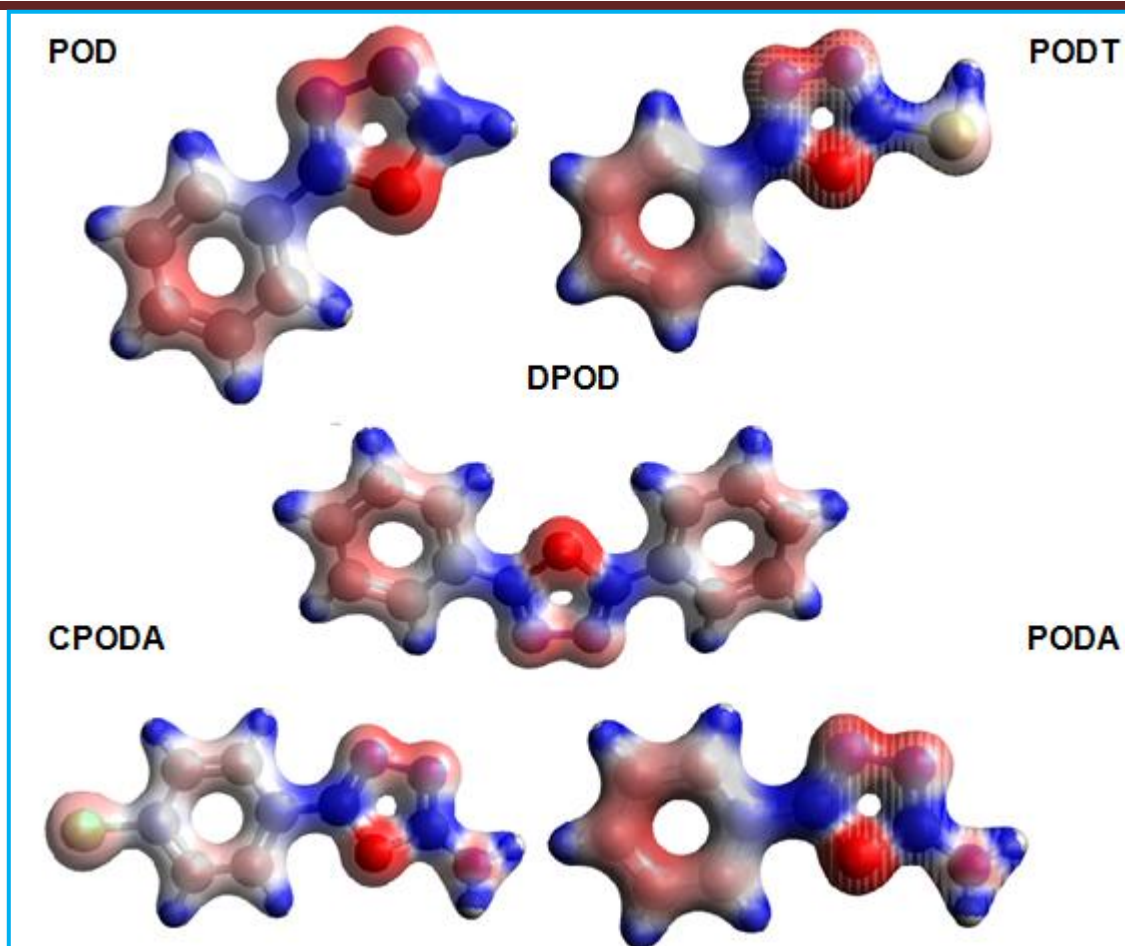


Figure 3.25. The Molecular Electrostatic Potentials (MEP).

3.2.4- NMR Spectroscopy

The theoretical NMR results of series two compounds in gas phase, and DMSO are described in **tables 3.31 - 3.35**, and figures 3.26 – 3.30.

In **POD** molecule the chemical shift value for the proton bonding with C₅ oxadiazole ring is 3.33 ppm, similar to **OD** molecule, series one. The δ value of aromatic protons in **DPOD** are in the range of 5.25 – 8.74 ppm. The hydrogen atoms located in ortho positions (from the oxadiazole ring) showing a little more deshielding than meta and para aromatic hydrogen atoms, the same thing are shown in the **POD**, **CPODA**, **PODT**, and **PODA** compounds.

Table 3.31. The calculated NMR chemical shifts in ppm of all atoms for **POD** molecule in (gas phase, and DMSO solvent).

Atom	GIAO(B3LYP)/6-311++G (2d,2p)	
	Gas phase	DMSO
O(1)	221.28	229.18
C(2)	93.66	96.15
N(3)	354.80	331.49
N(4)	363.92	340.46
C(5)	94.08	100.40
C(6)	170.57	168.91
C(7)	181.30	184.40
C(8)	186.70	185.25
C(9)	186.56	190.27
H(10)	8.20	8.17
C(11)	187.68	190.19
H(12)	7.41	7.50
C(13)	190.09	194.73
H(14)	5.44	5.44
H(15)	5.40	5.39
H(16)	5.30	5.33
H(17)	3.33	3.16

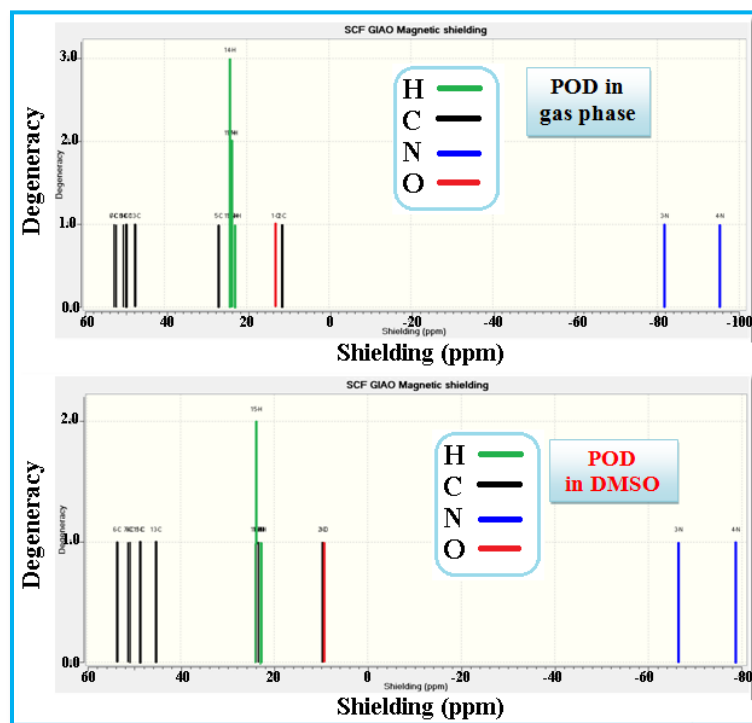


Figure 3.26. NMR spectra of **POD** molecule in gas phase and DMSO solvent.

While the H atoms present in meta and para positions of the oxadiazole ring are bonded with more negative charge carbon atoms (red colour in MEP maps), figure 3.25. Hence the high shielded atoms appear at lower chemical shift (up-field). The hydrogen atoms present in ortho position relative to chlorine atom in **CPODA** molecule showing a larger δ (down-field), when compared to the other compounds in this series.

Table 3.32. The calculated NMR chemical shifts in ppm for **DPOD** molecule in (gas phase, and DMSO solvent).

Atom	GIAO(B3LYP)/6-311++G (2d,2p)	
	Gas phase	DMSO
O(1)	208.40	214.06
C(2)	84.13	86.50
N(3)	350.13	327.66
C(6)	170.28	168.44
C(7)	179.53	183.19
C(8)	186.38	184.95
C(9)	185.83	189.81
H(10)	8.74	8.70
C(11)	187.12	189.74
H(12)	7.75	7.83
C(13)	188.76	193.74
H(14)	5.71	5.71
H(15)	5.42	5.41
H(16)	5.25	5.28

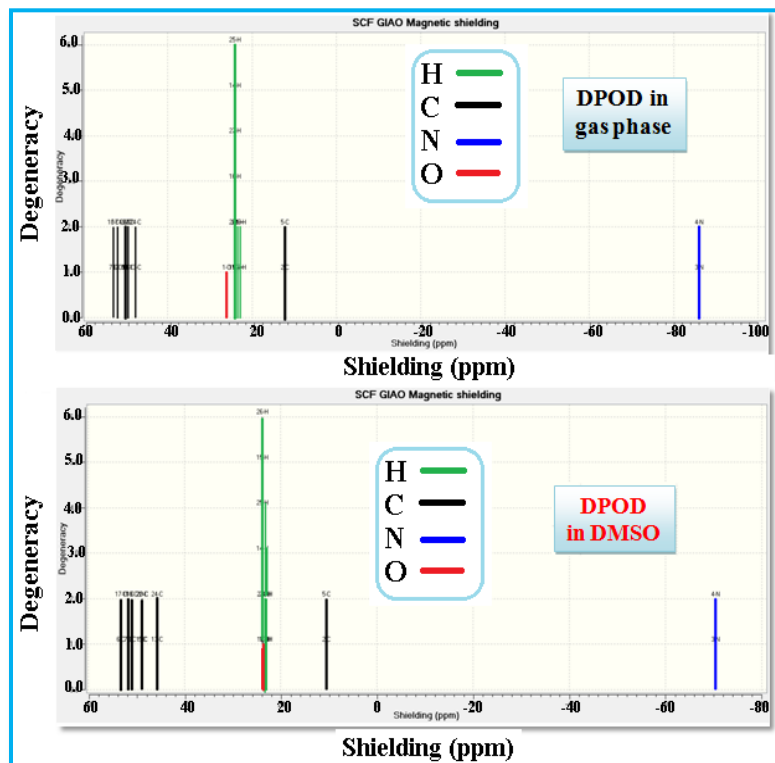


Figure 3.27. NMR spectra of **DPOD** molecule in gas phase and DMSO solvent.

The H₇ (in **PODT** molecule) are directly bonded with sulfur atom (deshielding) demonstrating an increase in the chemical shift 11.50 ppm (down-field). The two protons H₇ and H₈ for amine group in **PODA**, and **CPODA** molecules illustrate down-field at δ values 12.19, 11.95, and 12.26, 11.90 respectively. Similar values of δ are obtained for the corresponding protons of the amine group in series one compounds.

The chemical shift values of C₂ and C₅ in oxadiazole ring for all series two molecules are ranging from 78.75 – 93.66, and 71.94 – 94.08 ppm respectively. The smaller δ value (up-field) of C₂ (in **PODT** molecule) relate to the directly bonding with S atom. The deshielding (down-field) causes a larger chemical shift for C₂ and C₅ atoms in **POD** molecule, when phenyl group directly bonded with C₂ atom.

Table 3.33. The calculated NMR chemical shifts in ppm for **PODA** molecule in (gas phase, and DMSO solvent).

Atom	GIAO(B3LYP)/6-311++G (2d,2p)	
	Gas phase	DMSO
O(1)	146.28	153.67
C(2)	81.09	84.42
N(3)	249.31	226.81
N(4)	333.56	312.63
C(5)	71.94	74.82
N(6)	75.20	74.54
H(7)	12.19	12.29
H(8)	11.95	12.25
C(9)	170.73	169.26
C(10)	178.13	181.69
C(11)	185.46	183.81
C(12)	185.63	189.66
H(13)	8.54	8.50
C(14)	187.08	189.69
H(15)	7.60	7.69
C(16)	187.17	191.88
H(17)	5.46	5.46
H(18)	5.34	5.33
H(19)	5.13	5.15

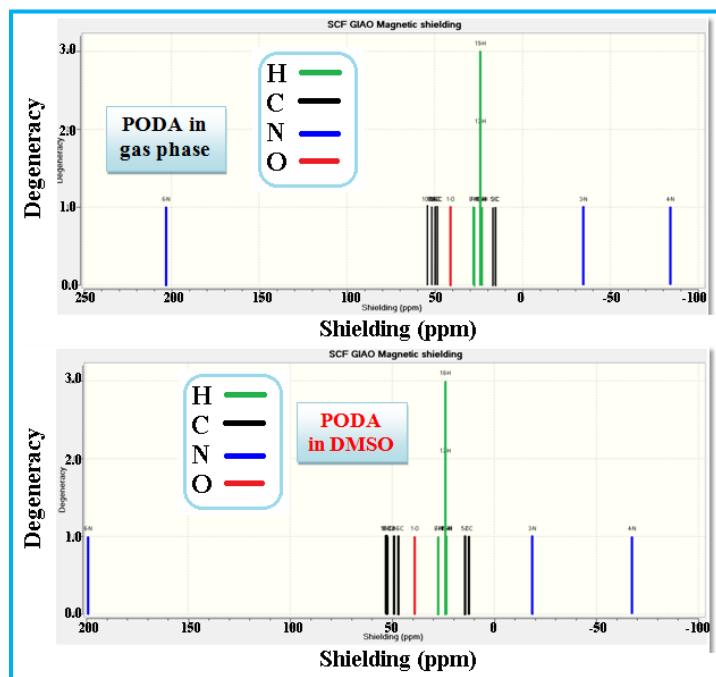


Figure 3.28. NMR spectra of **PODA** molecule in gas phase and DMSO solvent.

Generally, the aromatic C atoms give signals ranging from 100 – 150 ppm of δ values [97]. In this study, the chemical shift values for aromatic carbon atoms (except the carbon atom directly bonded with oxadiazole ring) are ranging between 157 – 190 ppm. The chemical shift of C atoms connected with oxadiazole ring in the range 168.66 -170.73 ppm, which is lower than the other aromatic C atoms. This may be linked to the shielded atoms (up-field). The aromatic C atoms in **CPODA** molecule have lower δ values ranging 123 – 180 ppm. These lower values related to the connection of chlorine with phenyl ring.

Table 3.34. The calculated NMR chemical shifts in ppm for **CPODA** molecule in (gas phase, and DMSO solvent).

Atom	GIAO(B3LYP)/6-311++G (2d,2p)	
	Gas phase	DMSO
O(1)	144.97	152.84
C(2)	80.68	84.05
N(3)	250.00	227.80
N(4)	335.57	315.97
C(5)	72.11	75.01
N(6)	75.07	74.42
H(7)	12.26	12.34
H(8)	11.90	12.19
C(9)	168.66	168.36
C(10)	172.93	177.21
C(11)	180.13	179.43
C(12)	156.98	160.33
H(13)	8.39	8.35
C(14)	158.23	160.22
H(15)	7.44	7.54
C(16)	123.30	120.49
H(17)	8.01	8.01
H(18)	7.90	7.88
Cl(19)	487.71	483.57

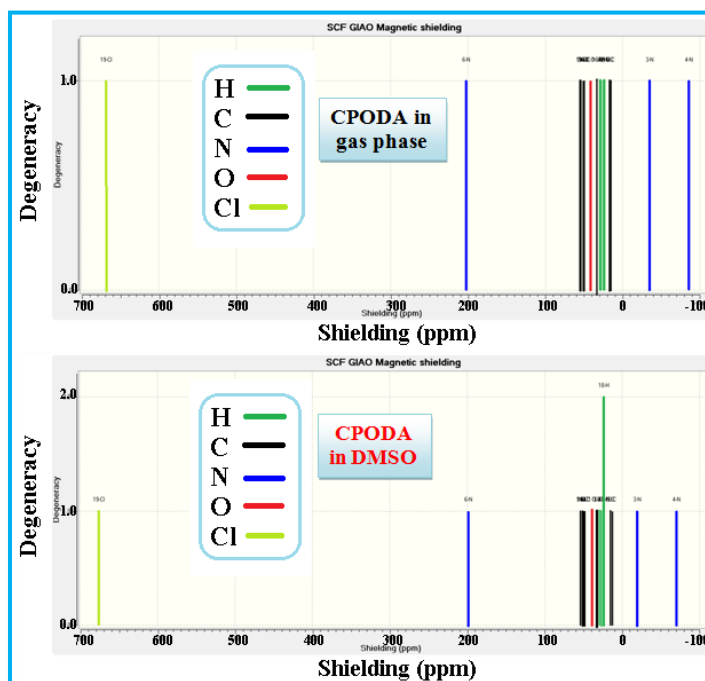


Figure 3.29. NMR spectra of **CPODA** molecule in gas phase and DMSO solvent.

Table 3.35. The calculated NMR chemical shifts in ppm for **PODT** molecule in (gas phase, and DMSO solvent).

Atom	GIAO(B3LYP)/6-311++G (2d,2p)	
	Gas phase	DMSO
O(1)	186.46	192.54
C(2)	78.75	84.89
N(3)	287.07	270.14
N(4)	335.70	316.01
C(5)	82.70	85.03
S(6)	438.39	437.84
H(7)	11.50	11.75
C(8)	169.53	167.95
C(9)	180.55	183.52
C(10)	186.59	190.21
C(11)	189.39	194.04
C(12)	187.61	190.20
C(13)	185.79	184.60
H(14)	8.74	8.70
H(15)	5.57	5.57
H(16)	5.18	5.21
H(17)	5.36	5.35
H(18)	7.68	7.76

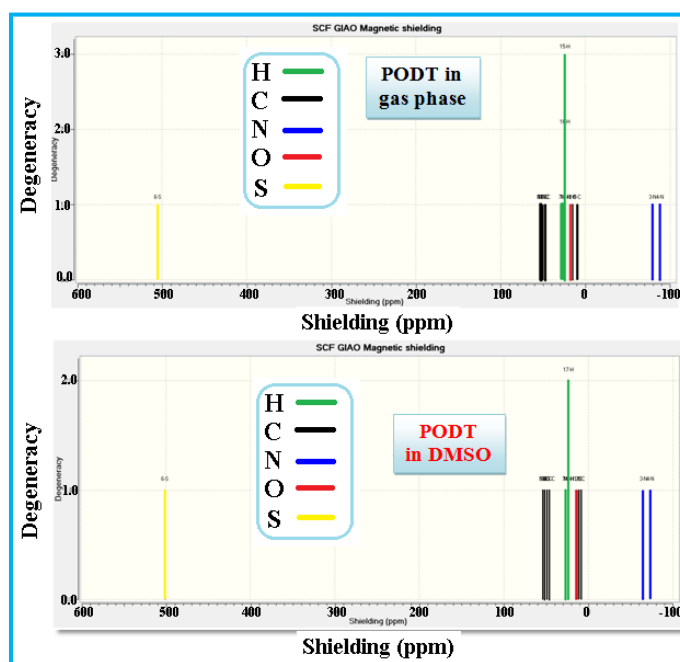
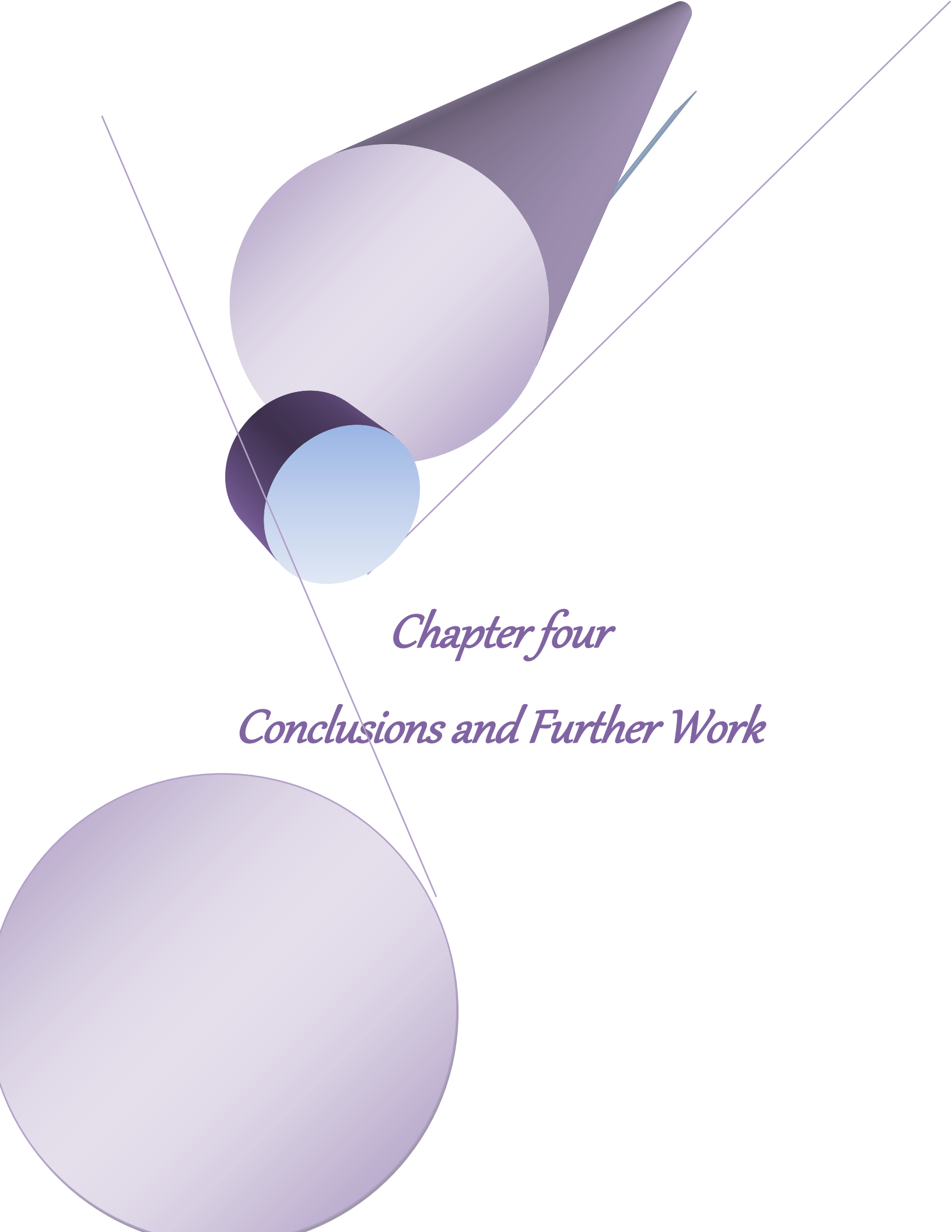


Figure 3.30. NMR spectra of **PODT** molecule in gas phase and DMSO solvent.



Chapter four

Conclusions and Further Work

4.1- Conclusions

The presented work focus on the use of the density functional theory **DFT** to provide theoretical calculations for the equilibrium optimize geometry, vibrational frequency, energy of molecular orbitals, electronic properties (absorption electronic spectra, molecular orbital, molecular electrostatic potential [in gas phase and in water solution]), and nuclear magnetic resonance spectra [in gas phase and in Dimethyl sulfoxide solution] for the oxadiazole derivatives.

The following points summaries the important findings:-

I- From the optimize geometry of **ODDA** molecule, the C₂-N₆ bond (between C₂ atom in oxadiazole ring and -NH₂ group) is (1.372 Å). In the other molecules, the C₂-N₆ bond changing in the following sequence **PODA > ODA = CPODA > CODA > AODCN > NODA**. This may be due to the replacement of the electron donating group by electron withdrawing group or phenyl ring in C₅ position.

II-The calculated electronic spectra of series one molecules are predicted one absorption peaks in gas phase, and two absorption peaks (one of them is strong, while the second one weak or appear as a shoulder) in water solution. The calculated λ max values in the gas phase for the compounds is changed in the order **OD < ODA < CODA < ODDA < AODCN < NODA** are 179, 207, 211, 213, 248, and 306 nm respectively. While the λ max in water solution is changed in following configuration **OD < ODA < ODDA < CODA < AODCN < NODA** are 178, 210, 213, 218, 264, and 342 nm respectively. The greater λ max value for **NODA** may be related to extra conjugation. Red shift appeared during the transfer from gas phase to polar solvent (water). This mean that λ max is related to $\pi \rightarrow \pi^*$ transition. The λ max for **ODDA** molecule is unchanged in both phases (213 nm). This confirmed that the transition is $\pi \rightarrow \pi^*$, Appendix 1.

The results of electronic spectra for series two compounds demonstrate two absorption peaks in each phase (water, and gas) except the **DPOD** molecule which has only one peak. The λ max (nm) for strongest peak in gas phase is changed according following configuration: **DPOD (303) > CPODA (288) > PODA (280) > PODT (278) > POD (254)**. In water solvent, λ max of strongest peak changed in the same order: **DPOD (307) > CPODA (295) > PODA (285) > PODT (283) > POD (259)**. According to these results it can be concluded that this transition is $\pi \rightarrow \pi^*$. So the red and *hyperchromism* shifts occurs during the transferring from the gas phase to the polar solvent (water).

Comparing the calculated UV spectrum results for both series, it can be concluded that series two have longer λ max than series one molecules. This may be due to the increase or elongation in the conjugation. Since series two molecules consist phenyl ring, Appendix 1.

III- The molecular electrostatic potential maps for the oxadiazole derivatives in series one show a negative potential over the nitrogen ring atoms, and a positive potential over the carbon and hydrogen atoms. From these results, it can be concluded that the carbon atoms indicate the strongest attraction and the nitrogen ring atoms associated with the strongest repulsion. Change H atom by NH_2 groups in compounds **ODA**, and **ODDA** show a blue color on NH_2 , this mean that NH_2 have positive potential. But in substitute electron withdrawing groups such as Cl, NO_2 , and CN the color on the nitrogen ring atoms approach to yellow, this represent moderate negative potential. The molecular electrostatic potential surfaces of series two molecules show a negative potential swings between oxygen and nitrogen atoms, and phenyl ring, which accessing for negative charge (red region). The negative regions of MEP are related to electrophilic reactivity. The

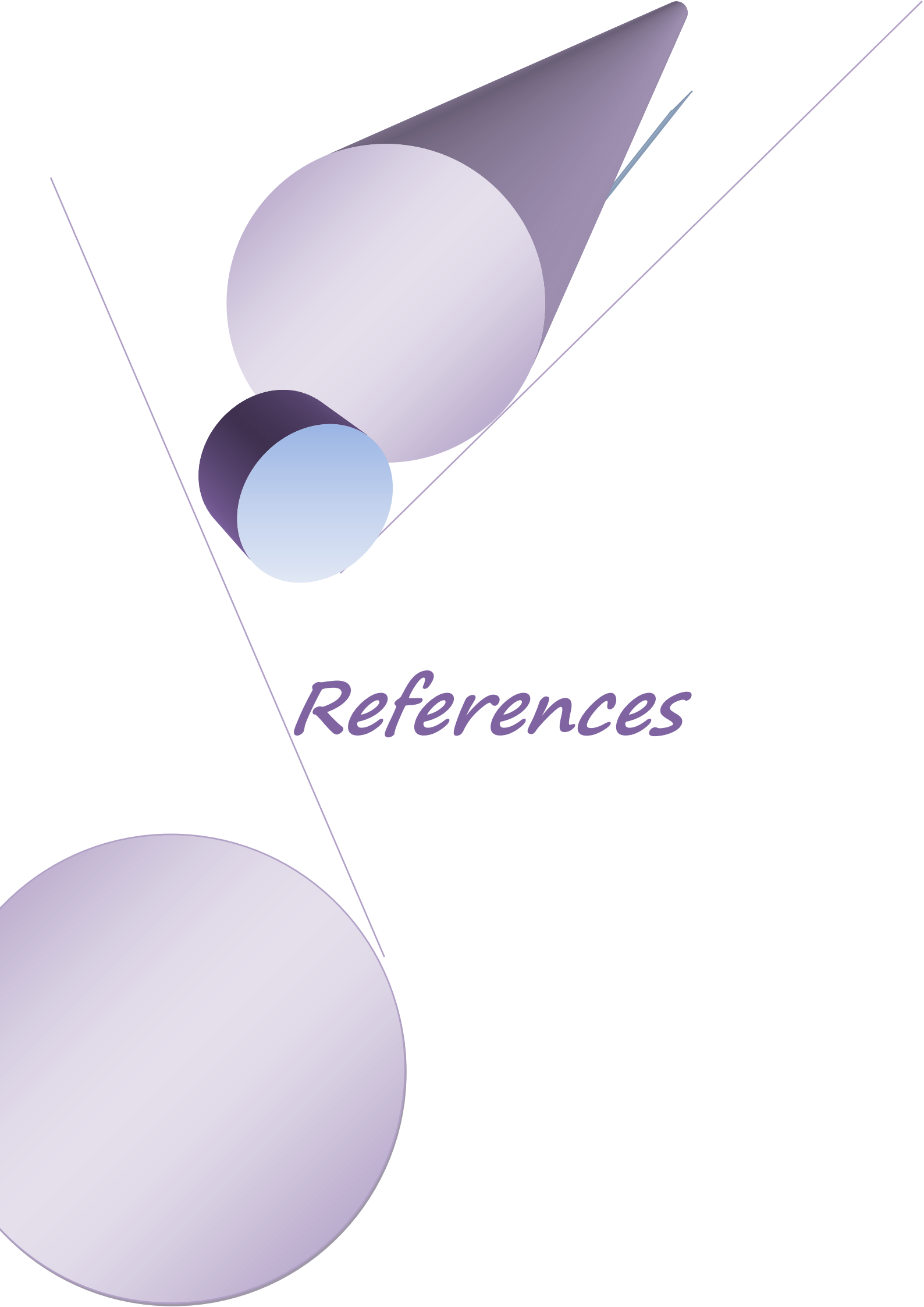
carbonyl oxadiazole atoms and hydrogen atoms bear a positive charge (blue color) which indicates nucleophilic reactivity.

IV- In NMR study a high changes in the **chemical shift** values are noticed when transferred from gas to the solution (in DMSO) phase, in both series compounds :-

- Increase for O atom in oxadiazole ring.
- Decrease for both N atoms (in oxadiazole ring), and O atoms in $-\text{NO}_2$ group.

4.2. Further work

- 1-The present work is concentrated on theoretical study for optimized molecular geometry, plus IR, Raman, UV-Visible, and NMR spectra. But it is necessary to evaluate these parameters experimentally.
- 2- Calculation the thermodynamic properties such as heat capacity, Gibbs free energy, change in enthalpy, and entropy.
- 3- It can be design theoretically new oligomers by connect two or three different oxadiazole derivatives (in different way), and calculate theoretically its chemical properties.
- 4- From the HOMO and LUMO results, the softness or hardness can be evaluated for the oxadiazole derivatives.



References

REFERENCES

1. R. Gupta, M. Kumar and V. Gupta, " *Heterocyclic Chemistry: Five members Heterocyclic* ", 1st ed., Springer, 203 (2005).
2. S. Sharma, A-Review: Oxadiazole Their Chemistry and Pharmacological Potentials, *Der Pharma Chemica.*, 2: 253-263 (2010).
3. N. Demirbas, Synthesis and characterization of new tri hetrocyclic compounds consisting of 1,2,4-triazol-3-one, 1,3,4-thiadiazole and 1,3,4-Oxadiazole rings, *Turk. J. Chem.*, 29, 125-133 (2005).
4. C. S. de Oliveira, B. F. Lira, J. M. Barbosa-Filho, G. F. Lorenzo and P.F. de Athayde-Filho, Synthetic approaches and pharmacological activity of 1,3,4-oxadiazoles: A-Review of the literature from 2000–2012, *Molecules*, 17(9): 10192-10231 (2012).
5. K. C. Nagaraj, M. S. Niranjana and S. Kiran, 1,3,4-oxadiazole:a potent drug candidate with various pharmacological activities., *Int. J. Pharm. Pharm. Sci.*, 3: 9-16 (2011).
6. T. Eicher and S. Hauptmann," *The Chemistry of Heterocycles* ", 2nd ed., Wiley-VSH, Germany (2003).
7. R. Sharma, N. Kumar and R. Yadav, A-Review: Chemistry and Pharmacological Importance of 1,3,4-Oxadiazole Derivatives, *J. Chem.*, 4(2): 1-27 (2015).
8. Z. Jakopin, R. Roškar and M. S. Dolenc, Synthesis of 3,5-disubstituted 1,2,4-oxadiazoles as peptidomimetic building block, *Elsevier*, 48(8): 1465-1468 (2007).
9. A. H. Shridhar, J. Keshavayya and Joy H. Hoskeri, Synthesis of 1,3,4-Oxadiazole Incorporated Azo Dye Derivatives as a Potent Biological Activity Molecules, *Int. J. Pharm. Pharm. Sci.*, 4(2): 386-390 (2012).

References

10. L. D. Namera, B. J. Rathod, H. R. Maheta and C. U. Bhoya, Microwave Assisted Synthesis of 2,5-Distyryl-1,3,4-Oxadiazole Derivatives as Anti Microbial Agents, *ILCPA*, 10, 46-54 (2014).
11. R. Iqbal, M. Zareef, S. Ahmed, J. H. Zaidi, M. Arfan, M. Shafique and N. A. Al-Masoudi, Synthesis, Antimicrobial and Anti-HIV Activity of Some Novel Benzenesulfonamides Bearing 2,5-Disubstituted-1,3,4-Oxadiazole Moiety, *J. Chin. Chem. Soc.* 53(3): 689-696 (2006).
12. M. Shailaja, M. Anitha, A. Manjula and B. V. Rao, Synthesis and biological activity of novel 2,5-disubstituted-1,3,4-oxadiazoles, *Indian J. Chem.* 49B(8): 1088-1097 (2010).
13. S. Bondock, S. Adel, H. A. Etman and F. A. Badria, Synthesis and antitumor evaluation of some new 1, 3, 4-oxadiazole-based heterocycles *Eur. J. Med. Chem.*, 48, 192-199 (2012).
14. K. Gudasi, M. Patil, R. Vadavi, R. Shenoy and S. Patil, Transition metal complexes with a new tridentate ligand, 5-[6-(5-mercapto-1, 3, 4-oxadiazol-2-yl) pyridin-2-yl]-1, 3, 4-oxadiazole-2-thiol, *J. Serb. Chem. Soc.*, 72(4): 357-366 (2007).
15. W. J. Goodby, J. P. Collings, T. Kato, C. Tschierske, H. Gleeson and P. Raynes, " *Handbook of Liquid Crystals* ", 2nd ed., Wiley (2014).
16. O. Lehman, Solution propagation in liquid crystals, *Z. Phys. Chem.*, 4, 462 (1889).
17. K. T. Kamtekar, C. S. Wang, S. Bettington, A. S. Batsanov, I.F. Perepichka, M.R. Bryce, J.H. Ahnabinal and M.C. Petty, New electroluminescent bipolar compounds for balanced charge-transport and tuneable colour in organic light emitting diodes: triphenylamine oxadiazole-fluorene triad molecules. *J. Mat. Chem.*, 16(39): 3823-3835 (2006).

References

18. C. Wang, L. Palsson, A. Batsanov and M. Bryce, Molecular Wires Comprising π -Extended Ethynyl- and Butadiynyl-2,5-Diphenyl-1,3,4-Oxadiazole Derivatives: Synthesis, Redox, Structural, and Optoelectronic Properties, *J. Am. Chem. Soc.*, 128, 3789-3799 (2006).
19. S. Bala, S. Kamboj and A. Kumar, " Heterocyclic 1, 3, 4-oxadiazole compounds with diverse biological activities ", *J. Pharm. Res.*, 3(12): 2993-2997 (2010).
20. a) P. J. Mohr, B. N. Taylor, and D. B. Newell " *CODATA Recommended values of the fundamental physical constants : 2006*, " *Rev. Mod. Phys.*, 80: 633-730 (2008).
b) E. J. McMurry, " *Organic Chemistry with Biological Applications* ", 2nd ed., Macmillan Learning, Canada (2011).
21. A. B. F. Duncan and F. A. Matsen, " *Chemical Application of Spectroscopy* ", 1st ed., Wiley, New York (1956).
22. S. Wartewig, " *IR and Raman Spectroscopy* " , Wiley-VCH Verlag, Germany (2003).
23. M. J. Chalmers and R. P. Griffiths, " *Handbook of Vibrational Spectroscopy* ", John Wiley and Sons Ltd., UK Chichester (2002).
24. http://images.slideplayer.com/26/8335494/slides/slide_10.jpg.
25. P. Atkins and R. Friedman, " *Molecular quantum mechanics* ", 5th ed., Oxford, New York (2005).
26. G. Placzek, " *Rayleigh-Streuung und Raman-Effekt:Handbuch der Radiologie* ", 1st ed., Akad. Verlag,Leipzig, VI:205-374 (1934).
27. D. A. Long " *Raman Spectroscopy* ", 1st ed., 4:74-110, UK, London (1977).
28. S. K. Freeman, " *Application of Laser Raman Spectroscopy* ", Wiley, New York (1974).

References

29. L. Taegweon, L. A. Chad, D. M. Bal, J. Jun Byung, S. Jia, S. Amy, L. Ho-Jin, and K. E. Howard, Synthesis, Structural Characterization, and Unusual Field-Effect Behavior of Organic Transistor Semiconductor Oligomers: Inferiority of Oxadiazole Compared with Other Electron-Withdrawing Subunits, *J. AM. CHEM. SOC.*, *131*(5): 1692–1705 (2009).
30. S. M. Bachrach, " *Computational organic chemistry* ", 2nd ed., John Wiley and Sons, Inc., Canada (2007).
31. R. Chang, " *Physical Chemistry for the Chemical and Biological Sciences* ", 3rd ed., University science books, Sausalito, CA (2001).
32. L. Piela, " *Ideas of quantum chemistry* ", 1st ed., Elsevier, Amsterdam, London, New York (2007).
33. J. H. Moore and N. D. Spencer, " *Encyclopedia of Chemical Physics and Physical Chemistry* ", London (2001).
34. C. N. R. Rao, " *Ultra-violet and visible Spectroscopy. Chemical Applications* ", 1st ed., Butterworth and Co. Ltd., London (1961).
35. A. E. Gillam and E. S. Stern, " *An Introduction to Electronic Absorption Spectroscopy* ", Edward Arnold Ltd., London (1957).
36. P. Atkins, " *Concepts in physical chemistry* ", 3rd ed., Oxford, New York (1995).
37. P. Atkins and J. de Paula, " *Physical chemistry* ", 9th ed., Oxford, New York (2010).
38. J. W. Moore, " *Physical chemistry* ", 5th ed., Longman Publishing group, London (1999).
39. R. J. Sabin, " *Advances in Quantum Chemistry* ", 3rd ed., Elsevier, London (2007).
40. C. Dykstra, G. Frenking, K. Kim and G. E. Scuseri, " *Theory and Applications of Computational Chemistry* ", 3rd ed., Elsevier, London (2005).

References

41. M. Kasha, Characterization of electronic transitions in complex molecules, *Disc. Faraday Soc.*, 9, 14-19 (1950).
42. H. McConnel, Effect of Polar Solvents on the Absorption Frequency of $n \rightarrow \pi$ Electronic Transitions, *J. Chem. Phys.*, 20(4): 12-21 (2004).
43. N. S. Bayliss and E. G. McRae, Solvent Effects in the Spectra of Acetone, Crotonaldehyde, Nitromethane and Nitrobenzene, *J. Phys. Chem.*, 58(11): 1006-1011(1954).
44. L. Nagaard, R. L. Hansen, J.T. Nielsen, J. Rastrup-Andersen, G.O. Sorensen and P. A. Steinr, Microwave spectra of isotopic 1, 3, 4-oxadiazoles: Molecular structure, 14-N quadrupole coupling constants, and centrifugal distortion constants of 1,3,4-oxadiazole *J. Molec. Struct.*, 12, 59-69 (1972).
45. J. Demaison, M. K. Jahn, E. J. Cocinero, A. Lesarri, J. U. Grabow, J. C. Guillemin and H. D. Rudolph, The accurate semi-experimental structure of 1,3,4-oxadiazole by the mixed estimation method, *J. Phys. Chem.*, 117, 2278–2284 (2013).
46. D. H. Christensen, J. T. Nielsen and O. F. Nielsen, Infrared spectra of 1,3,4-oxadiazole and 2,5,-dimethyl-1,3,4-oxadiazole. Vibrational assignment of 1,3,4-oxadiazole, *J Mol. Spectrosc*, 24, 225-234 (1967).
47. A. El-Azhary, Vibrational Analysis of the Spectra of 1,3,4-Oxadiazole, 1,3,4-Thiadiazole, 1,2,5-Oxadiazole and 1,2,5-Thiadiazole: Comparison between DFT, MP2 and HF Force Fields. *Spectro. Chim. Acta.*, 52, 33-44 (1996).
48. J. S. Kwiatkowski, J. Leszczynski and I. Teca, Molecular structure and infrared spectra of furan, thiophene, selenophene and their 2,5-N and 3,4-N derivatives: density functional theory and conventional post-Hartree-Fock MP2 studies, *J. Mol. Struct.*, 436-437: 451-480 (1997).

References

49. F. Hegelund, R. W. Larsen, R. A. Aitken, K. M. Aitken and M. H. Palmer, High-resolution infrared and theoretical study of four fundamental bands of gaseous 1,3,4-oxadiazole between 800 and 1600 cm^{-1} , *J. Mol. Spectr.*, 246(2): 198-212 (2007).
50. M. H. Palmer, Comparison of theoretical and experimental studies of infrared spectral data for the 5-membered ring heterocycles, *J. Mol. Struc.*, 834-36: 113-128 (2007).
51. D. Avci and Y. Atalay, Theoretical analysis of vibrational spectra and scaling-factor of 2-aryl-1,3,4-oxadiazole derivatives, *Int. J. Quantum Chem.*, 109, 328-341 (2009).
52. R. J. Lakowicz, I. Gryczynski, H. Malak, and Z. Gryczynski, Effect of Fluorescence Quenching by Stimulated Emission on the Spectral Properties of a Solvent-Sensitive Fluorophore, *J. Phys. Chem.*, 100, 19406-19411 (1996).
53. V. A. Gaenko, A. Devarajan, E. R. Trifonov, and A. V. Ostrovskii, Spectral and Density Functional Studies on the Absorbance and Fluorescence Spectra of 2-R-5-Phenyl-1,3,4-oxadiazoles and Their Conjugate Acids, *J. Phys. Chem.*, 110(28): 8750-8757 (2006).
54. M. Song, K. Li Wu, L. Zhu, J. Zheng and Y. Xu, 5-Phenyl-1,3,4-oxadiazol-2-amine, *Acta Cryst.*, E68, o3058 (2012).
55. E. Romano, J. N. Soria, R. Rudyk and A. S. Branda'n, Theoretical study of the infrared spectrum of 5-phenyl-1,3,4-oxadiazole-2-thiol by using DFT calculations, *Mol. Simu.*, 38(7): 561-566 (2012).
56. E. G. Lewars, " *Computational Chemistry: Introduction to the Theory and Applications of Molecular and Quantum Mechanics* ", 2nd ed., springer (2011).

References

57. M. J. T. Frisch, G. W. Schlegel, H. B. Scuseria, G. E. Robb, M. A. Cheeseman, J. B. Ortiz, J.V. Cioslowski, J. Fox, and D. J. Gaussian 09, Revision C. 01, Gaussian, Inc.: Wallingford, CT, (2009).
58. <https://sourceforge.net/projects/avogadro/files/latest/download>.
59. D. Young, " *Computational Chemistry: A Practical Guide for Applying Techniques to Real World Problems* ", 3rd ed., John Wiley and Sons Ltd. (2004).
60. K. I. Ramachandran, G. Deepa, and K. Namboori, " *Computational chemistry and molecular modeling* ", 4th ed., Springer, India, (2008).
61. F. Jensen, " *Introduction to Computational Chemistry* ", 2nd ed., Wiley (2006).
62. M. A. L. Marques, C.A. Ullrich, F. Nogueira, A. Rubio, K. Burke, and E.K.U. Gross, " *Time-Dependent Density Functional Theory* ", 1st ed., Springer-Verlag (2006).
63. C. Ullrich, " *Time-Dependent Density-Functional Theory: Concepts and Applications* ", 1st ed., Oxford University Press (2012).
64. Runge, Erich, and E. K. U. Gross, Density-Functional Theory for Time-Dependent Systems. *Phys. Rev. Lett.*, 52(12): 997–1000 (1984).
65. M. Petersilka, U. J. Gossmann and E. K. U. Gross, Excitation Energies from Time-Dependent Density-Functional Theory, *Phys. Rev. Lett.*, 76(8): 1212-1215 (1996).
66. V. R. Leeuwen, Causality and Symmetry in Time-Dependent Density-Functional Theory, *Phys. Rev. Lett.* 80(6): 1280-283 (1998).
67. M. Schindler and W. Kutzelnigg, Theory of Magnetic Susceptibilities and NMR Chemical Shifts in Terms of Localized Quantities. II. Application to Some Simple Molecules, *J. Chem. Phys.*, 76, 1919-1933 (1982).
68. F. London, Quantum Theory of Interatomic Currents in Aromatic Compounds, *J. Phys. Radium*, 8, 397-409 (1937).

References

69. R. Ditchfield, Self-consistent perturbation theory of diamagnetism. I. A gauge-invariant LCAO (linear combination of atomic orbitals) method for NMR chemical shifts, *Mol. Phys.*, 27, 789-807 (1974).
70. P. R. Rablen, S.A. Pearlman and J. Finkbiner, A Comparison of Density Functional Methods for the Estimation of Proton Chemical Shifts with Chemical Accuracy, *J. Phys. Chem.*, 103, 7357-7363 (1999).
71. P. V. R. Schleyer, C. Maerker, A. Dransfeld, H. Jiao and N. Hommes, Nucleus-Independent Chemical Shifts: A Simple and Efficient Aromaticity Probe, *J. Am. Chem. Soc.*, 118, 6317-6318 (1996).
72. F. J. Luque, J. M. López, and M. Orozco, Perspective on Electrostatic interactions of a solute with a continuum. A direct utilization of ab initio molecular potentials for the prevision of solvent effects, *Theor. Chem. Acc*, 103: 343–345 (2000).
73. F. H. Allen, O. Kennard, D. G. Watson, L. Brammer, A. G. Orpen, and R. Taylor, Tables of bond lengths determined by x-ray and neutron diffraction. Part 1. Bond lengths in organic compounds, *J. Chem. Soc., Perkin Trans II*, 12 (1987).
74. P. Udhayakala, A. Jayanthi, T. V. Rajendiran, and S. Gunasekaran, Computation and interpretation of vibrational spectra, thermodynamical and HOMO-LUMO analysis of 2-chloro-4-nitroaniline, *Int.J. ChemTech Res.*, 3(4): 1851-1862 (2011).
75. M. E. Casida, C. Jamorski, K. C. Casida, and D. R. Salahub, Molecular excitation energies to high-lying bound states from time-dependent density-functional response theory: Characterization and correction of the time-dependent local density approximation ionization threshold, *J. Chem. Phys.*, 108, 4439–4449 (1998).

References

76. E. K. U. Gross and W. Kohn, Time-dependent density functional theory, *Adv. Quant. Chem.*, 21, 255–291 (1990).
77. O. J. Wacker, R. Kümmel, and E. K. U. Gross, Time-dependent density-functional theory for superconductors, *Phys. Rev. Lett.*, 73(21): 2915–2918 (1994).
78. M. A. L. Marques and E. K. U. Gross, Time-dependent density functional theory, *Annu. Rev. Phys. Chem.*, 55, 427–455 (2004).
79. T. Kakitani and H. Kakitani, Application of self-consistent HMO theory to heteroconjugated molecules, *Theoret. Chin. Acta*, 46(4): 259-275 (1977).
80. M. Govindarajan, M. Karabacak, V. Udayakumar, and S. Periandy, FT-IR, FT-Raman and UV spectral investigation: Computed frequency estimation analysis and electronic structure calculations on chlorobenzene using HF and DFT, *Spectrochimica Acta Part A*, 88, 37– 48 (2012).
81. S. Gunasekaran, R. A. Balaji, S. Kumeresan, G. Anand, and S. Srinivasan, Experimental and theoretical investigations of spectroscopic properties of N-acetyl-5-methoxytryptamine, *Can. J. Anal. Sci. Spectrosc*, 53, 149-160 (2008).
82. A. M. Asiri, M. Karabacak, M. Kurt, and K. A. Alamry, Synthesis, molecular conformation, vibrational and electronic transition, isometric chemical shift, polarizability and hyperpolarizability analysis of 3-(4-methoxy-phenyl)-2-(4-nitro-phenyl)-acrylonitrile: a combined experimental and theoretical analysis, *Spectrochim. Acta Part A: Molecular and Biomolecular Spectroscopy*, 82(1): 444–455 (2011).
83. B. Kosar and C. Albayrak, Spectroscopic investigations and quantum chemical computational study of (E)-4-methoxy-2-[(p-tolylimino)methyl]phenol, *Spectrochim Acta A: Molecular and Biomolecular Spectroscopy*, 78(1): 160–167 (2011).

References

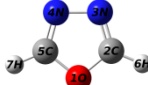




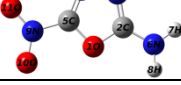
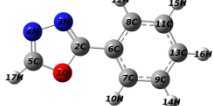

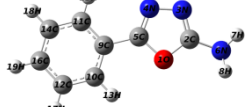
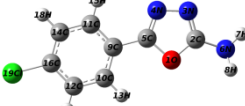

84. J. S. Murray and K. Sen, " *Molecular Electrostatic Potentials : Concepts and Applications* ", 1st ed., Elsevier, Amsterdam, 69-71 (1996).
85. P. Thul, V.P. Gupta, V. J. Ram, and P. Tandon, Structural and spectroscopic studies on 2-pyranones, *Spectrochim. Acta A*, 75(1): 251–260 (2010).
86. I. Alkorta and J. J. Perez, Molecular polarization potential maps of the nucleic acid bases, *Int. J. Quant. Chem.*, 57(1): 123-135 (1996).
87. K. Wolinski, J. F. Hilton, and P. Pulay, Efficient implementation of the gauge-independent atomicorbital method for NMR chemical shift calculations, *J. Am. Chem. Soc.*, 112, 8251–8260 (1990).
88. J. R. Cheeseman, G. W. Trucks, T. A. Keith, and M. J. Frisch, A Comparison of models for calculating nuclear magnetic resonance shielding tensors, *J. Chem. Phys.*, 104, 5497–5509 (1996).
89. A. E. Reed and F. Weinhold, Natural localized molecular orbitals, *J. Chem. Phys.*, 83, 1736–1740 (1985).
90. L. Rai, Synthesis of Quinazoline Analogues of Biological Interest, *Master of Pharmacy in Pharmaceutical Chemistry*, Al-Ameen Collegue of Pharmacy, Bangalore (2010).
91. C. D. Contreras, M. Montejo, J. J. Lo´pez Gonza´lez, J. Zinzuk, and S. Branda´n, Structural and vibrational analices of 2-(2-benzofuranyl)-2-imidazoline, *J. Raman Spect.* 42(1): 108–116 (2011).
92. S. Jeyavijayan and M. Arivazhagan, Study of density functional theory and vibrational spectra of hypoxanthine, *Indian J. Pure Appl. Phys.*, 48, 869-874 (2010).
93. G. Socrates, " *Infrared and Raman Characteristic Group Frequencies e Tables and Charts* ", 3rd ed., John Wiley & Sons, Chichester (2001).

References

94. C. C. Sangeetha, R. Madivanane, and V. Pouchaname, The Vibrational Spectroscopic (FT-IR & FT Raman, NMR, UV) study and HOMO& LUMO analysis of Phthalazine by DFT and HF Studies, *Int. J. Eng. Res. G. Sci.*, 2(6): 222-251 (2014).
95. C. Sridevi, G. Shanthi, and G. Velraj, Structural, vibrational, electronic, NMR and reactivity analyses of 2-amino 4Hchromene-3-carbonitrile (ACC) by ab initio HF and DFT calculations, *Spectrochim. Acta A*, 89: 46-54 (2012).
96. A. Srivastava and V. B. Singh, Theoretical and experimental studies of vibrational spectra of naphthalene and its cation, *Indian J. Pure. Appl. Phys.*, 45, 714–720 (2007).
97. M. Karabacak, Z. Cinar, M. Kurt, S. Sudha, and N. Sundaraganesan, FT-IR, FT-Raman, NMR and UV–vis spectra, vibrational assignments and DFT calculations of 4-butyl benzoic acid, *Spectrochimica Acta Part A*, 85, 179– 189 (2012).

Appendix 1

Table : The results of λ max for the series one and two molecules.

Compound	Structure	λ max (nm)	
		gas	water
Series one			
OD		179	178
ODA		207	210
ODDA		213	213
CODA		211	218
AODCN		248	264
NODA		306	342
Series two			
POD		254	259
PODT		278	283
PODA		280	285
CPODA		288	295
DPOD		303	307

الخلاصة

في السنوات الأخيرة أصبحت الكيمياء النظرية ذات أهمية كبيرة في العديد من المجالات الكيميائية والصيدلانية. أن مشتقات الأوكسادايازول لها تطبيقات واسعة في الأنشطة الدوائية والبيولوجية. لذلك ينطوي هذا العمل على دراسة نظرية لسلسلتين من مشتقات الأوكسادايازول. السلسلة الأولى تحتوي على جزيئة الأوكسادايازول المعوضة بمجاميع واهبة او ساحبة للألكترون [1,3,4]-oxadiazole (OD)، 2-1,3,4 oxadiazole (ODA) -أمين، 2,5,1,3,4 oxadiazole - داي أمين (ODDA)، 5-كلورو-oxadiazole-4,3,1-2-أمين (CODA)، 2-أمينو-oxadiazole-5-carbonitrile-1,3,4 (AODCN)، 5- نيترو-oxadiazole-1,3,4-2-أمين (NODA)]. السلسلة الثانية تحتوي على مشتقات oxadiazole التي تنتج عن طريق تعويض المجاميع المذكورة أعلاه بالإضافة لمجموعة الفينيل [2-فينيل-oxadiazoles (POD)-1,3,4، 5-فينيل-oxadiazole-1,3,4-2-ثيول (PODT)، 5-فينيل-1,3,4-oxadiazole-2-أمين (PODA)، 4,5-(كلوروفينيل-oxadiazole-1,3,4-2-أمين) (CPODA)، 2,5-ثنائي فينيل-oxadiazole (DPOD)-1,3,4].

تمت الدراسة النظرية باستخدام طريقة نظرية دوال الكثافة DFT لعناصر القاعدة 6-311++G(2d,2p) وبأسلوب B3LYP، وذلك باستخدام برنامج كاوس 09. في حالات محدودة، تم استخدام برنامج أفوكادرو للمساعدة في عرض أشكال المدارات الإلكترونية أو الجهود الألكتروستاتيكية الجزيئية.

لجزيئات السلسلتين المذكورتين أعلاه، تم حسابا تقييم العديد من الخصائص الفيزيائية مثل: - الشكل الهندسي المتوازن، أطراف الاهتزاز للجزيئات، والخصائص الإلكترونية (أطراف الأمتصاص الإلكترونية، طاقات المدارات الجزيئية، وخريطة الجهود الألكتروستاتيكية الجزيئية. [في الحالة الغازية وفي المحلول المائي])، وأطراف الرنين النووي المغناطيسي [في الحالة الغازية وفي محلول ثنائي ميثيل سلفوكسايد]. ثم تمت المقارنة بين الحالات المختلفة.

قورنت النتائج للشكل الهندسي المتوازن التي تم الحصول عليها في هذه الدراسة مع البيانات التجريبية والنظرية المتوفرة فقط للجزيئات التالية OD، POD، PODT، وPODA، كشفت المقارنة عن اتفاق جيد بينهم. أشارت النتائج للشكل الهندسي المتوازن لجزيء ODDA أن طول الأصرة C_2-N_6 (بين ذرة C_2 في حلقة الأوكسادايازول ومجموعة $-NH_2$ المرتبطة بها) هو (1.372 \AA) . لوحظ تغير في طول هذه الأصرة للجزيئات المدروسة الأخرى، حسب التسلسل التالي $ODA < CPODA < PODA$

NODA < AODCN < CODA . ويعزى هذا الى استبدال مجموعة واهبة للإلكترون بمجموعة ساحبة للإلكترون أو حلقة فينيل في الموقع C₅ من حلقة الأوكسادايازول.

تم حساب أطياف الأهنزاز للجزيئات المدروسة (ترددات الأهنزاز، وشددها في طيف الأشعة تحت الحمراء و رامان) مع تشخيص دقيق وعالي الجودة لكل الذبذبات الأساس 3N-6. كانت النتائج المحسوبة للجزيئات **OD، POD، وPODT** ذات تطابق عالي مع كل من البيانات التجريبية والنظرية السابقة.

قيمت نظريا الخصائص الإلكترونية [في الحالتين الغازية وفي المحلول المائي] للسلسلة الأولى. بينت النتائج تغير في قيم الأطوال الموجية ذات قمة الأمتصاص العظمى λ_{max} المحسوبة في الحالة الغازية حسب التسلسل التالي **OD > ODA > CODA > ODDA > AODCN > NODA**. وحيث أن أكبر قيمة الى λ_{max} المحسوبة تعود للمركب **NODA** يعزى ذلك الى أستطالة أو أمتداد الأقتران في هذه الجزيئة.

أظهرت الأطياف الإلكترونية المحسوبة لجزيئات السلسلة الثانية عن وجود قمتي أمتصاص الكترونية في حالتي (الغاز والمحلل المائي) لإطيف جزئي **DPOD** الذي يحوي على قمة واحدة فقط. لوحظ من البيانات أن λ_{max} (nm) للقمة ذي الشدة العالية في الحالة الغازية تتغير حسب التسلسل التالي: **DPOD (303) < CPODA (288) < PODA (280) < PODT (278) < POD (254)**. أما في حالة أستخدام الماء كمذيب ، تتغير λ_{max} (nm) بنفس الترتيب السابق للأمتصاص ذي الذروة العالية: **DPOD (307) < CPODA (295) < PODA (285) < PODT (283) < POD (259)**. ووفقا لهذه النتائج يمكن أن نستنتج أن الانحراف للأحمر عند الأنتقال من الطور الغازي الى المذيب القطبي المائي يشير الى أن الأنتقال هو من نوع $\pi \rightarrow \pi^*$. لوحظ أن أعلى قيمة الى λ_{max} تعود للمركب **DPOD**. يرجع ذلك إلى الأقتران العالي بين حلقة الأوكسادايازول وحلقتي الفينيل، حيث أدى إلى تقليل فجوة الطاقة ΔE_g . القيم المحسوبة الى ΔE_g للحالتين لجزيئات السلسلة الثانية تغيرت على النحو التالي: **PODT < POD < DPOD < CPODA < PODA**.

بينت خرائط الجهود الألكتروستاتيكية الجزيئية لمشتقات الأوكسادايازول في السلسلة الأولى مواقع الجهود السالبة المحتملة على الذرات ذي الكهروسلبية العالية (ذرتي النيتروجين في حلقة الأوكسادايازول)، والجهود الموجبة على ذرات الكربون والهيدروجين. من هذه النتائج، فإنه يمكن أن نلخص إلى أن ذرات الكربون تتميز بقوة جذب وذرات النيتروجين في حلقة الأوكسادايازول بقوة تنافر. أن تغيير أو أستبدال ذرة H بمجموعة **NH₂** في المركبين **ODA** و **ODDA** يؤدي الى ظهور اللون الأزرق على **NH₂**، وهذا يعني أن مجموعة

NH₂ تتموضع عليها شحنة موجبة. عند تعويض مجاميع ساحبة للألكترون Cl، NO₂ وCN يتغير لون ذرتي النيتروجين في حلقة الأوكسادايازول إلى الأصفر، وهذا يمثل جهود سالبة معتدلة. أما سطوح الجهود الألكتروستاتيكية الجزيئية إلى مركبات السلسلة الثانية أشارت إلى أن الجهود السالبة (اللون الأحمر) تتمركز على الأكسجين وذرتي النيتروجين في حلقة الأوكسادايازول وحلقة الفينيل. والجدير بالذكر أن المنطقة ذي الشحنة السالبة تعني أنها منطقة تمتلك فعالية ألفة الكترونية electrophilic reactivity. أما ذرات الكربون في حلقة الأوكسادايازول وذرات الهيدروجين تحمل شحنة موجبة (اللون الأزرق) والتي تشير إلى أنها تمتلك صفة محبة للنواة nucleophilic reactivity.



جمهورية العراق
وزارة التعليم العالي والبحث العلمي
جامعة النهريين
كلية العلوم
قسم الكيمياء

دراسة نظرية طيفية لمجموعة من مشتقات 1,3,4- أوكسادايازول

رسالة

مقدمة الى مجلس كلية العلوم / جامعة النهريين

كجزء من متطلبات نيل درجة الماجستير

في علوم الكيمياء

من قبل

حسن فائز حيدر

بكالوريوس 2013

إشراف

الأستاذ المساعد الدكتور

شذى فاضل السعيدي

أيار
2017 م

رمضان
1438 هـ